

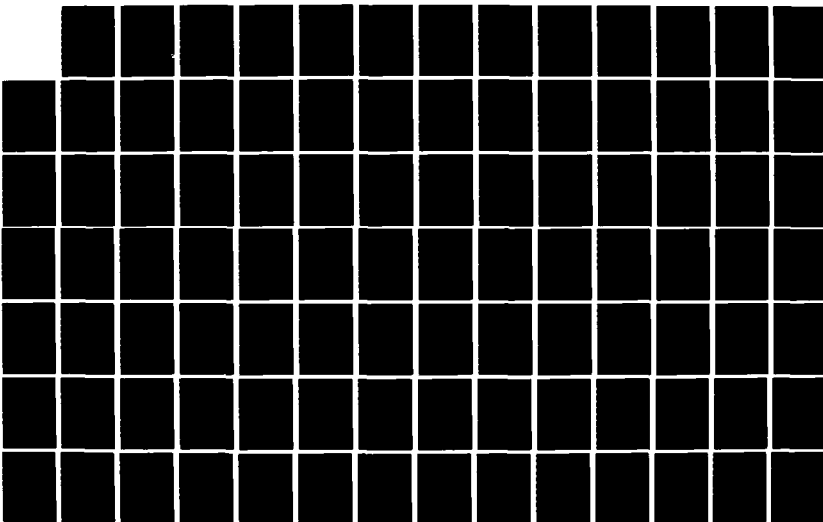
AD-A159 225

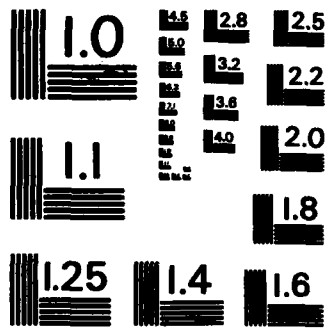
MODAL ANALYSIS OF UNSTABLE RESONATORS(U) AIR FORCE INST 1/3  
OF TECH WRIGHT-PATTERSON AFB OH SCHOOL OF ENGINEERING  
M E ROGERS 03 APR 85 AFIT/D5/PH/85-2

UNCLASSIFIED

F/G 20/5

NL





MICROCOPY RESOLUTION TEST CHART  
NATIONAL BUREAU OF STANDARDS-1963-A

①

AFIT/DS/PH/85-2

AD-A159 225

Modal Analysis of Unstable Resonators

Dissertation

AFIT/DS/PH/85-2

Mark E. Rogers  
Capt USAF

DTIC FILE COPY

DTIC  
ELECTE  
SEP 18 1985  
S D

Approved for publication; distribution unlimited

85 09 17 022

UNCLASSIFIED

SECURITY CLASSIFICATION PAGE

AD-A159 225

## REPORT DOCUMENTATION PAGE

1a. REPORT SECURITY CLASSIFICATION <b>UNCLASSIFIED</b>		1b. RESTRICTIVE MARKINGS <b>NONE</b>			
2a. SECURITY CLASSIFICATION AUTHORITY <b>N/A</b>		3. DISTRIBUTION/AVAILABILITY OF REPORT <b>approved for public release; distribution unlimited.</b>			
2b. DECLASSIFICATION/DOWNGRADING SCHEDULE <b>N/A</b>					
4. PERFORMING ORGANIZATION REPORT NUMBER(S) <b>AFIT/DS/PH/85-2</b>		5. MONITORING ORGANIZATION REPORT NUMBER(S)			
6a. NAME OF PERFORMING ORGANIZATION <b>Air Force Institute of Technology</b>	6b. OFFICE SYMBOL (If applicable) <b>AFIT/ENP</b>	7a. NAME OF MONITORING ORGANIZATION			
6c. ADDRESS (City, State and ZIP Code) <b>Air Force Institute of Technology AFIT/ENP WPAFB, OH 45433</b>		7b. ADDRESS (City, State and ZIP Code)			
8a. NAME OF FUNDING/SPONSORING ORGANIZATION <b>see 6a.</b>	8b. OFFICE SYMBOL (If applicable) <b>see 6b.</b>	9. PROCUREMENT INSTRUMENT IDENTIFICATION NUMBER			
8c. ADDRESS (City, State and ZIP Code) <b>see 6c.</b>		10. SOURCE OF FUNDING NOS.			
11. TITLE (Include Security Classification) <b>Modal Analysis of Unstable Resonators</b>		PROGRAM ELEMENT NO.	PROJECT NO.	TASK NO.	WORK UNIT NO.
12. PERSONAL AUTHOR(S) <b>Rogers, Mark Edward</b>					
13a. TYPE OF REPORT <b>PhD Dissertation</b>	13b. TIME COVERED <b>FROM Mar 81 to Apr 85</b>	14. DATE OF REPORT (Yr., Mo., Day) <b>85, Apr, 03</b>		15. PAGE COUNT <b>247</b>	
16. SUPPLEMENTARY NOTATION  <b>Approved for public release IAW AFI 150-7. L. E. WOLAVER Dean for Research and Professional Development 19 AUG 85</b>					
17. COSATI CODES			18. SUBJECT TERMS (Continue on reverse if necessary and identify by block number)		
FIELD	GROUP	SUB. GR.	<b>laser modes, optical resonators, unstable resonators, complex symmetric kernels, linear prolate functions,</b>		
20	05				
20	06				
19. ABSTRACT (Continue on reverse if necessary and identify by block number)  The analysis of the modes of optical resonators is crucial to understanding how actual laser devices operate. A consistent formulation that treats both the empty and loaded resonator modes is presented in this report. The study centers on unstable resonators and, in particular, strip resonators. The analysis of the bare cavity modes uses a matrix expansion technique with the linear prolate functions as a basis set. These functions form an optimal basis set in that they are related to the Schmidt expansion functions for the integral equation that describes the modes of the bare cavity. As a consequence, the matrix eigenvalue problem is solved using the minimum number of basis functions. The analysis is implemented in a numerical model that generates the linear prolate functions using a finite difference algorithm. The model was used to study the validity of the asymptotic approach at low Fresnel numbers. The results show that the first few lower loss modes predicted by the asymptotic approach are accurate but that the higher loss modes are inaccurately represented by that approach. The linear prolate					
20. DISTRIBUTION/AVAILABILITY OF ABSTRACT <b>UNCLASSIFIED/UNLIMITED <input checked="" type="checkbox"/> SAME AS RPT. <input type="checkbox"/> DTIC USERS <input type="checkbox"/></b>			21. ABSTRACT SECURITY CLASSIFICATION <b>unclassified</b>		
22a. NAME OF RESPONSIBLE INDIVIDUAL <b>Capt Mark E Rogers</b>		22b. TELEPHONE NUMBER (Include Area Code) <b>505-844-0196</b>	22c. OFFICE SYMBOL <b>AFWL/ARDF</b>		

18. (cont) saturable gain, Maxwell's equations, Fredholm integral equations, loaded cavity, bare cavity, gain sheet, matrix eigenvalue problem.

19. (cont) function expansion is also used to numerically demonstrate the orthogonality of the resonator modes.

The analysis of the modes of the loaded cavity begins with Maxwell's equations and ends with a round trip integral equation for the modes of a loaded strip resonator. The gain is included in an additive term instead of a multiplicative term as frequently assumed in other analyses. This result suggests that there is a single loaded cavity mode, as compared to the spectrum of bare cavity modes. The method of stationary phase is used to obtain a geometrical optics approximation to the integral equation, and the results of the approximation showed excellent agreement with past work. A single gain sheet model of the integral equation was developed and solved using an iterative technique. The model was used to study the threshold and saturation behavior of the loaded cavity, and the results were compared to previous studies. A key result was that the power on the feedback mirror retained the same fluctuations with equivalent Fresnel number that was observed for the bare cavity mode eigenvalues in the bare cavity analysis. Other results are discussed in the text. An initial study of the mapping of the loaded cavity mode onto the bare cavity modes was made, showing that the higher loss modes may be significant in this mapping.

Accession For	
NTIS GRA&I	<input checked="" type="checkbox"/>
DTIC TAB	<input type="checkbox"/>
Unannounced	<input type="checkbox"/>
Justification	
by _____	
Distribution/	
Availability Codes	
Dist	Avail and/or Special
A-1	





AFIT/DS/PH/85-2

Modal Analysis of Unstable Resonators

by

Mark E. Rogers, B.S., M.S.

Captain USAF

Approved:

<u>John R. Ehrlich</u> Chairman	<u>April 10, 1985</u>
<u>Norm G. Shantland</u>	<u>April 25, 1985</u>
<u>David A. Lee</u>	<u>May 13, 1985</u>
<u>John Jones Jr.</u>	<u>May 16, 1985</u>

Accepted:

<u>JSPremieriecki</u> Dean, School of Engineering	<u>May 16, 1985</u>
--	---------------------

## Preface

The laser is a device that is used to convert incoherent energy into coherent energy in and near the visible region of the electromagnetic spectrum. The resonator performs a crucial role in the conversion; it is the principal part of the laser that defines the degree of coherence of the output. The study of optical resonators conceptually began with the analysis of waveguides. However, the study is complicated by the fact that optical resonators are multimode devices that are unbounded in the transverse directions. Since about 1960, numerous researchers have considered the problem of modal analysis of resonators and much is known about the natural modes of optical resonators. However, most analyses have oversimplified the problem of including the saturable gain medium. This dissertation is an effort aimed at treating this problem. We begin by looking at the modes of an empty resonator in order to establish a baseline for the study of loaded resonators as well as to examine the utility of the linear prolate functions as a basis set when solving for the modes of a one dimensional "strip" resonator with a kernel expansion. We then include the gain rigorously, beginning with Maxwell's equations and ending with a new integral equation that describes the modes of a loaded resonator. We specialize this equation to the case of a strip resonator and then model the gain medium with a single gainsheet at the feedback mirror of a positive branch, confocal unstable resonator. Although this model is only a first order model, the results shed new light into the area

of loaded cavity analysis. The application of this work is broad, giving better insight into how actual lasers work and how to model such devices.

I owe a debt of gratitude to many people who contributed to this research. My advisor, Dr (Lt Col) John H. Erkkila, spent endless hours with me, discussing everything from abstract concepts to difficult derivations to detailed numerical codes. Without his insights and support, this research could not have been done. The other members of my advisory committee, Dr Donn Shankland and Dr John Jones, were always available to answer my questions. Their direction was very instrumental in the success of this effort. Dr David Lee was also very helpful. He always made time in his busy schedule to consider my questions. His comment that "graduate school is supposed to change the way you think" has stuck in my mind and given me insight into the educational process I might otherwise have missed. Dr Leno Pedrotti frequently encouraged me in dry times, helping me keep a perspective on the research program. The scientists of the the Air Force Weapons Laboratory Resonator Analysis Group help keep this research effort directed at realistic applications. My follow-on assignment with this group has been highly rewarding. This group included Dr W. P. (Pete) Latham, Dr Tom Ferguson, Dr Martin Smithers, Dr Alan Paxton, Dr Tom Gavrielides and Capt Ted Salvi. Of course, I am deeply indebted to my lovely wife Jan for her support and encouragement while she ran our household during my four and

a half years in graduate school. She even managed to give birth to our three daughters, Jennifer, Julie and Gwendolyn. It is to her and my daughters that I dedicate this work. Last but most of all, I thank my Lord and Savior, Jesus Christ, for teaching me the truth of Jeremiah 33:3.

## Contents

	Page
Preface.....	iii
List of Figures.....	ix
List of Tables.....	xi
List of Symbols.....	xii
Abstract.....	xv
I. Introduction.....	1
II. Analysis of the Modes of the Empty Strip Resonator.....	5
A. Introduction.....	5
1. Geometry of Strip Resonator.....	6
2. Basic Assumptions for Strip Resonators.....	10
B. Bare Cavity Round Trip Equation.....	12
C. Methods of Finding the Modes of Empty Resonators.....	16
D. The Linear Prolate Functions (LPF).....	19
1. Defining Equations.....	20
2. Properties of the LPF.....	37
3. Numerical Generation of the LPF.....	40
E. Derivation of the Matrix Eigenvalue Problem.....	42
F. Solution of the Matrix Eigenvalue Problem.....	45
G. Results.....	48
1. Numerical Convergence.....	49
2. Validation of Approach.....	57
3. Studies of Eigenvalues Near a Mode Crossing.....	71
4. Study of the Asymptotic Approach at Low Fresnel Numbers.....	75
5. Demonstration of the Orthogonality of the Modes.....	76
H. Summary.....	79
III. Modal Analysis of Loaded Resonators.....	81
A. Introduction.....	81
B. Derivation of Active Medium Propagator.....	81
C. Round Trip Integral Equation for Loaded Strip Resonator.....	88
D. Summary.....	96
IV. Modelling of Loaded Resonators.....	98
A. Introduction.....	98
B. Review of Past Work in Loaded Resonator Modelling.....	98
C. Geometric Optics Analysis of Loaded Strip Resonators.....	109
D. Single Gains Sheet Diffraction Model.....	114

	Page
E. Numerical Implementation of Loaded Cavity Models.....	121
F. Results of the Numerical Model of the Loaded Cavity.....	125
1. Transverse Grid Size.....	126
2. Convergence as a Function of Number of Points.....	127
3. Convergence as Function of Number of Iterations.....	129
4. Variations in Loaded Cavity Parameters as Function of Small Signal Gain.....	133
5. Intensity/Phase Plots for Small Signal Gain Variations.....	139
6. Loaded Cavity Mode Near a Mode Crossing....	155
7. Trends in Loaded Cavity Eigenvalues and Power on Mirror with Variations in Fresnel Number.....	160
8. Mapping the Loaded Cavity Mode onto the Bare Cavity Modes.....	164
G. Summary.....	173
V. Conclusions and Recommendations.....	176
A. Introduction.....	176
B. Bare Cavity Analysis and Modelling.....	177
C. Loaded Cavity Analysis.....	180
D. Loaded Cavity Modelling.....	182
E. Summary.....	186
Bibliography.....	188
Appendix 1. Orthogonality of the Eigenfunctions of Complex Symmetric Kernels.....	192
Appendix 2. Derivation of Matrix Eigenvalue Problem for Strip Resonator.....	198
Appendix 3. Derivation of Green's Function for Paraxial Wave Equation (2-D).....	202
Appendix 4. Round Trip Equation for Loaded Strip Resonator.....	207
Appendix 5. Method of Stationary Phase Applied to Two Dimensional Propagator.....	213
Appendix 6. Matrix Eigenvalue Problem for Stable Strip Resonator.....	218

	Page
Appendix 7. Matrix Eigenvalue Problem for Resonators with Circular Mirrors.....	222
Appendix 8. Geometrical Optics Approximation to the Loaded Cavity Round Trip Integral Equation.....	226
Vita.....	231

List of Figures

Figure No.	Title	Page
2.1	Basic Geometry for Strip Resonator.....	7
2.2	Stability Diagram.....	9
2.3a-o	LPF 0 - 14.....	22-36
2.4	Differential Equation Eigenvalue for Linear Prolate Function.....	38
2.5	Integral Equation Eigenvalue for Linear Prolate Function.....	39
2.6	Bare Cavity Modes - Intensity.....	52
2.7	Bare Cavity Modes - Phase.....	53
2.8	Behavior of Eigenvalues with Varying Fresnel Number.....	73
2.9	Behavior of Outcoupling with Varying Fresnel Number.....	74
3.1	Single-ended Unstable Resonator (a) resonator geometry (b) equivalent lens train.....	89
4.1	Round Trip in Positive Branch Confocal Unstable Resonator (a) resonator layout (b) equivalent lens train.....	115
4.2	Convergence History - Magnitude of Eigenvalue.....	130
4.3	Convergence History - Phase of Eigenvalue.....	131
4.4	Amplitude of Eigenvalue as Function of Small Signal Gain.....	134
4.5	Phase of Loaded Cavity Eigenvalue as Function of Gain.....	136
4.6	Power on Mirror as Function of Small Signal Gain.....	138
4.7	Outcoupling as a Function of Small Signal Gain.....	140

Figure No.	Title	Page
4.8	Intensity of Loaded Cavity Mode $g_o = 0.0$ .....	142
4.9	Intensity of Loaded Cavity Mode $g_o = 0.4 g_{th}$ .....	143
4.10	Intensity of Loaded Cavity Mode $g_o = 0.8 g_{th}$ .....	145
4.11	Intensity of Loaded Cavity Mode $g_o = g_{th}$ .....	146
4.12	Intensity of Loaded Cavity Mode $g_o = 2.0 g_{th}$ .....	148
4.13	Intensity of Loaded Cavity Mode $g_o = 5.0 g_{th}$ .....	149
4.14	Phase of Loaded Cavity Mode $g_o = 5.0 g_{th}$ .....	151
4.15	Gain Profile.....	153
4.16	Convergence History $g_o = g_{th}$ .....	156
4.17	Convergence History $g_o = 3.0 g_{th}$ .....	158
4.18	Power on Mirror at Mode Crossing.....	159
4.19	Power on Mirror vs Equivalent Fresnel Number.....	161
4.20	Eigenvalue Phase Variations with Fresnel Number.....	163
4.21	Loaded Cavity Mode Expansion.....	167
4.22	Loaded Cavity Mode Expansion.....	171
A4.1	Lens Train Diagram.....	208

## List of Tables

Table No.	Title	Page
II-1	Magnitude of the Mode Eigenvalues.....	51
II-2	Coefficients for $u_0(x)$ as Function of Number of LPF.....	54
II-3	Coefficients for $u_0(x)$ as Function of Number of Points <sup>o</sup> on (-1,1).....	58
II-4	Comparison of Eigenvalues: $M = 10$ , $F_{eff} = 0.225$ .....	60
II-5	Comparison of Eigenvalues: $M = 2.5$ , $F_{eff} = 0.6$ .....	61
II-6	Comparison of Eigenvalues: $M = 3$ , $F_{eff} = 1.8742$ .....	62
II-7	Comparison of Eigenvalues: $M = 2$ , $F_{eff} = 2$ .....	63
II-8	Comparison of Eigenvalues: $M = 10$ , $F_{eff} = 2.7$ .....	64
II-9	Comparison of Eigenvalues: $M = 2$ , $F_{eff} = 2.5$ .....	65
II-10	Comparison of Eigenvalues: $M = 2$ , $F_{eff} = 4$ .....	66
II-11	Demonstration of Orthogonality.....	77
II-12	Demonstration of Orthogonality.....	78
IV-1	Convergence History as Number of Points is Varied.....	128
IV-2	Bare Cavity Mode Expansion Coefficients...	167
IV-3	Bare Cavity Mode Expansion Coefficients...	170

List of Symbols

Symbol	Meaning	Page
$a_i$	$i^{\text{th}}$ mirror halfwidth.....	6
$A_i(x)$	$i^{\text{th}}$ mirror amplitude function.....	116
$b_n$	expansion coefficient.....	17
$B_{nm}$	matrix element.....	45
BCM	acronym for bare cavity modes.....	165
$c$	parameter characterizing the linear prolate functions.....	20
$c$	speed of light in vacuum.....	83
$\bar{D}(\bar{r}, \omega)$	electric displacement vector.....	81
$\bar{E}(\bar{r}, \omega)$	electric field vector.....	81
$F$	Fresnel number for single-ended strip resonator.....	14
$F_i$	Fresnel number for $i^{\text{th}}$ mirror.....	8
$F_{\text{eff}}$	effective Fresnel number.....	43
$g_i$	$g$ parameter for $i^{\text{th}}$ mirror.....	6
$g$	combined $g$ parameter: $g = 2g_1g_2^{-1}$ .....	6
$g_0$	small signal gain coefficient.....	91
$g_{\text{th}}$	threshold gain (Rigrod).....	101
$g'_{\text{th}}$	threshold gain (based on Eq(4.37)).....	152
$g_s(x, z)$	gain function.....	84
$G(x, z, x', z')$	Green's function for two dimensions.....	87
$h(x)$	eigenfunctions for Horwitz standard form integral equation.....	43
$\bar{H}(\bar{r}, \omega)$	magnetic field vector.....	81
$i$	imaginary unit, $\sqrt{-1}$ .....	10

Symbol	Meaning	Page
$I(x,y,z)$	intensity function.....	100
$I_{sat}$	saturation intensity.....	100
$J_n(r)$	Bessel function of first kind of order n.....	222
$k$	wave number for free space.....	83
$K(x,y)$	kernel of integral equation.....	13
$K_{nm}$	matrix element.....	17
$L$	resonator length.....	7
$L_e(z)$	shorthand notation used in Eq(3.28).....	90
LCM	acronym for loaded cavity mode.....	166
LPF	acronym for linear prolate function.....	20
MEVP	acronym for matrix eigenvalue problem....	5
$M_{pn}$	matrix element.....	17
$M$	resonator magnification.....	43
$n(\bar{r})$	index of refraction.....	85
$R_i$	radius of curvature for $i^{th}$ mirror.....	6
$S(x,y;\lambda)$	resolvent kernel.....	193
$t$	parameter used in Horwitz standard form for round trip integral equation....	43
$t$	time.....	10
$u(x)$	bare cavity mode.....	13
$v(x)$	function used in kernel expansion.....	16
$x,y,z$	spatial coordinates.....	7
$\alpha(x)$	loaded cavity mode.....	93
$\beta(x)$	shorthand for terms containing gain.....	93
$\gamma_i$	linear prolate function eigenvalue from defining integral equation.....	22

Symbol	Meaning	Page
$\Gamma_\lambda$	linear prolate function eigenvalue from defining differential equation.....	21
$\delta_{nm}$	Kronecker delta function.....	15
$\delta(x)$	Dirac delta function.....	203
$\epsilon_0$	electric field permittivity.....	82
$\eta_{ext}$	extraction efficiency.....	101
$\Theta(x)$	step function.....	205
$\lambda$	wavelength.....	13
$\lambda$	parameter for inhomogeneous Fredholm integral equation of second kind.....	192
$\mu$	eigenvalue for Horwitz standard form of round trip integral equation.....	43
$\mu_0$	magnetic permittivity.....	81
$\nu$	parameter for loaded cavity mode integral equation.....	92
$\pi$	pi ( = 3.1415926... ).....	14
$\sigma$	bare cavity mode eigenvalue.....	13
$\phi(x)$	solution function for inhomogeneous Fredholm integral equation of second kind.....	192
$\Phi_{m,n}(r)$	circular prolate function.....	222
$\chi(\bar{r}, \omega)$	susceptibility (complex: $\chi = \chi' + i\chi''$ )...	82
$\Psi_\lambda(x)$	linear prolate function of order 1 .....	20
$\omega$	frequency.....	10

Abstract

The analysis of the modes of optical resonators is crucial to understanding how actual laser devices operate. A consistent formulation that treats both the empty and loaded resonator modes is presented in this report. The study centers on unstable resonators and, in particular, strip resonators. The analysis of the bare cavity modes uses a matrix expansion technique with the linear prolate functions as a basis set. These functions form an optimal basis set in that they are related to the Schmidt expansion functions for the integral equation that describes the modes of the bare cavity. As a consequence, the matrix eigenvalue problem is solved using the minimum number of basis functions. The analysis is implemented in a numerical model that generates the linear prolate functions using a finite difference algorithm. The model is used to study the validity of asymptotic technique at low Fresnel numbers. The results show that the first few lower loss modes predicted by the asymptotic approach are accurate but that the higher loss modes are inaccurately represented by that approach. The linear prolate function expansion is also used to numerically demonstrate the orthogonality of the resonator modes.

The analysis of the modes of the loaded cavity begins with Maxwell's equations and ends with a round trip integral equation for the modes of a loaded strip resonator. The gain is included in an additive term instead of a multiplicative

term as frequently assumed in other analyses. This result suggests that there is a single loaded cavity mode, as compared to the spectrum of bare cavity modes. The method of stationary phase is used to obtain a geometrical optics approximation to the integral equation, and the results of the approximation show excellent agreement with past work. A single gain sheet model of the integral equation is developed and solved using an iterative technique. The model is used to study the threshold and saturation behavior of the loaded cavity, and the results are compared to previous studies. A key result is that the power on the feedback mirror retains the same fluctuations with equivalent Fresnel number that is observed for the bare cavity mode eigenvalues in the bare cavity analysis. Other results are discussed in the text. An initial study of the mapping of the loaded cavity mode onto the bare cavity modes is presented, showing that the higher loss modes may be significant in this mapping.

## I. Introduction

The laser (an acronym for 'light amplification through stimulated emission of radiation') can conceptually be broken into three major components: the pump, the gain medium and the resonator. This dissertation is concerned with the resonator. The resonator is an optical configuration that allows for efficient, coherent extraction of the energy stored in the gain medium by the pump. However, the resonator is an optical analog to the microwave waveguide, exhibiting a complex longitudinal and transverse mode structure. This analysis is aimed at an increased understanding of the transverse mode structure of empty and loaded resonators. The applications of the analysis will be focused on strip resonators. By strip resonators, one means a resonator composed of two cylindrical mirrors of infinite length, allowing one transverse dimension to be ignored in the analysis. An empty resonator does not contain any intervening medium, allowing an understanding of its inherent modal properties, while a loaded resonator does contain a gain medium that will alter the actual mode that would be sustained in the laser.

Physically, the transverse modes of the resonator (hereafter referred to as the modes) can be defined as any field distribution that reproduces itself to within a complex constant after a round trip through the resonator. A typical two-mirror resonator is shown in Figure 2.1. A round trip in this resonator consists of a reflection off mirror 1, a

propagation to mirror 2, reflection off mirror 2 and a return propagation to mirror 1. If one uses scalar diffraction theory to analyze this round trip, the modes are found to be the eigenvalues of a homogeneous Fredholm integral equation of the second kind, where the kernel characterizes the round trip. This kernel is more fully discussed in Chapter 2. The eigenvalue that is associated with each eigenmode accounts for the outcoupling loss and the phase (and corresponding frequency) shift of the mode. Several review articles are available on the general theory of optical resonators. (Ref 1-4) Also, most textbooks on laser physics discuss the basic properties of laser resonators, although these texts frequently limit the discussion to stable resonators while this work will mainly deal with unstable resonators. (Ref 5,6) The difference between the two classes of resonators will be made clear in Chapter 2.

This report is a summary of the research conducted in the area of laser resonators. The goal is to develop a consistent formulation of the modes of optical resonators, thus increasing the understanding of the properties of resonators. To accomplish this goal, two areas are investigated.

The first area is a study of empty strip resonators using a kernel expansion technique. The strip resonator is a useful abstraction of the optical resonator that has mirrors with cylindrical curvature in one dimension and infinite extent in the other dimension. Since the round trip integral

equation separates in rectangular coordinates, the two transverse modes can be treated independently, each acting like a strip resonator in the absence of a saturable gain medium. The kernel expansion technique is chosen because it allows the calculation of higher order modes while minimizing the approximations required to make such calculations.

The effects of including a saturable, distributed gain medium that depends nonlinearly on the electromagnetic field in the resonator is the second area to be investigated. The derivation of the loaded cavity integral equation is valid for a three dimensional resonator, although the strip resonator is used for detailed examination of the resultant integral equation. The integral formulation is chosen to blend the earlier analysis of the empty resonator into the analysis of the loaded resonator. A study of the empty and loaded strip resonator modes will give new understanding of how laser resonators behave.

This report is divided into four parts. Chapter II is an analysis of the empty resonator. The chapter begins with a discussion of the basic geometry and underlying assumptions for the strip resonator. Then the round trip integral equation that describes the modes is derived using scalar diffraction theory. A discussion of several solution techniques follows this derivation. The kernel expansion technique is then applied to find the bare cavity modes, using the linear prolate functions as a basis set. The analysis is used to (1) examine the validity of the asymptotic technique at low equivalent Fresnel numbers and

(2) demonstrate the orthogonality of the strip resonator modes. Chapter III begins the analysis of the loaded resonators. The analysis begins with Maxwell's equations and ends with an integral equation that describes the modes of a general two mirror resonator. The results are specialized to the strip resonator. The resultant equation suggests that the loaded cavity mode can be expanded in the modes of an empty strip resonator. In Chapter IV, we model the loaded strip resonator equation with a single gainsheet and examine the behavior of the modes for several cases. The idea of the bare cavity mode expansion is investigated for this special case. The final chapter of this dissertation summarizes the main conclusions and makes recommendations for future work.

## II. Analysis of the Modes of the Empty Strip Resonator

### A. Introduction

In this chapter, we discuss an analysis of the modes of a single-ended, aligned strip resonator that does not contain a gain medium. The chapter begins with a review of the geometry of the strip resonator and the assumptions inherent in this configuration. Then the integral equation that describes the modes is derived and discussed. A variety of solution techniques are available to solve this equation and they are reviewed briefly. The method that will be used in this chapter is the kernel expansion. The basis set that is used is the set of linear prolate functions, which have several properties that make this set highly suited to resonator analysis. After discussing this set of functions, the modes of the strip resonator are found by solving a matrix eigenvalue problem (MEVP). Several cases are studied with the technique, and it is used to explore two areas of interest not yet discussed in the literature. The first is a check of the validity of the asymptotic analysis of the modes at low equivalent Fresnel numbers. The second is a numerical demonstration of the orthogonality of the modes, a property that will be shown to be true analytically in Appendix 1. The chapter concludes with a summary of the empty strip resonator analysis. Some of the work discussed in this chapter has been published in Applied Optics (Ref 21) and Laser Digest (Ref 22).

## 1. Geometry of Strip Resonators

The general strip resonator is shown in Figure 2.1. (Many of the introductory comments and definitions in this section also apply to resonators with two transverse dimensions. However, the analysis that follows applies to strip resonators and it is less confusing to restrict the discussion to this class.) The two mirrors have radii of curvature denoted by  $R_i$ . (The subscript 'i' takes on the values 1 and 2 for the two mirrors.) The mirrors are assumed in this analysis to be aligned on an optical axis such that the centers of curvature lie on the same line and the mirrors extend an equal distance above and below this axis. The half-width of the mirrors is denoted by  $a_i$ . The mirrors are separated by a distance  $L$  and frequently the two mirror resonator is characterized in part by "g parameters" that are defined by

$$g_i = 1 - \frac{L}{R_i} \quad (2.1)$$

A combination of the g parameters that is also useful is

$$g = 2g_1g_2 - 1 \quad (2.2)$$

If one envisions a ray of light bouncing between the mirrors, some combinations of g parameters tends to confine all rays within the mirrors while other combinations allow the rays to leave the resonator. (One can verify these ideas

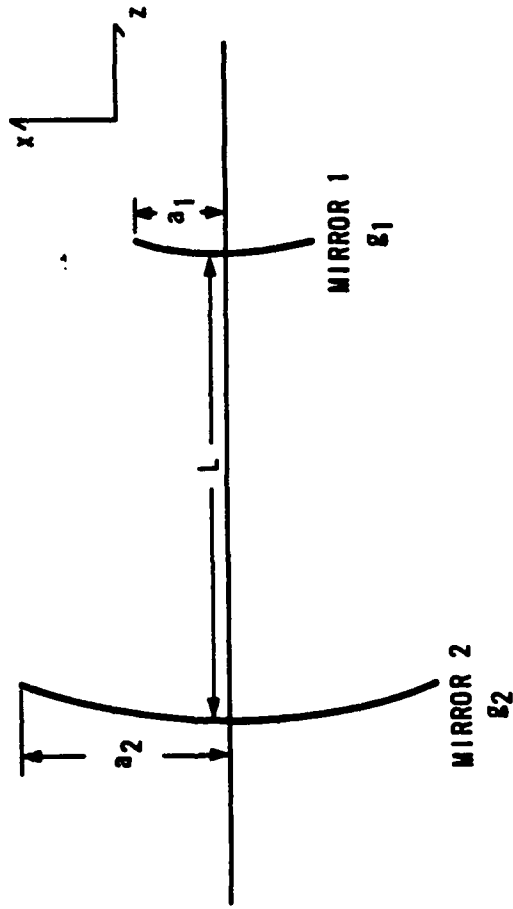


Figure 2.1 Basic Geometry for Strip Resonators.

by simply sketching a few resonators with different curvatures on the mirrors.) Resonators that tend to confine the rays are called "stable" while those that do not confine the rays are called "unstable". The stable region is defined by

$$-1 < g_1 g_2 < 1 \quad (2.3)$$

and the unstable region is any combination of  $g$  parameters that do not meet this condition. Figure 2.2 shows the stable and unstable regions. Stable resonators have many applications to lasers with low output power since the outcoupling is usually done with partially transmissive mirrors.

Unstable resonators are more appropriate for high energy lasers since these lasers have a large gain volume which matches the large mode volume of the unstable resonators and the energy can be outcoupled around the mirrors in unstable resonators, allowing the mirrors to be cooled.

In addition, a useful dimensionless number called the Fresnel number is defined for each mirror as

$$F_i = \frac{a_i^2}{\lambda L} \quad (2.4)$$

The Fresnel number can be interpreted as the number of plane wave Fresnel zones on one mirror as seen from the center of the other mirror. The number is important in diffraction analysis. At low Fresnel numbers, the effects of diffraction

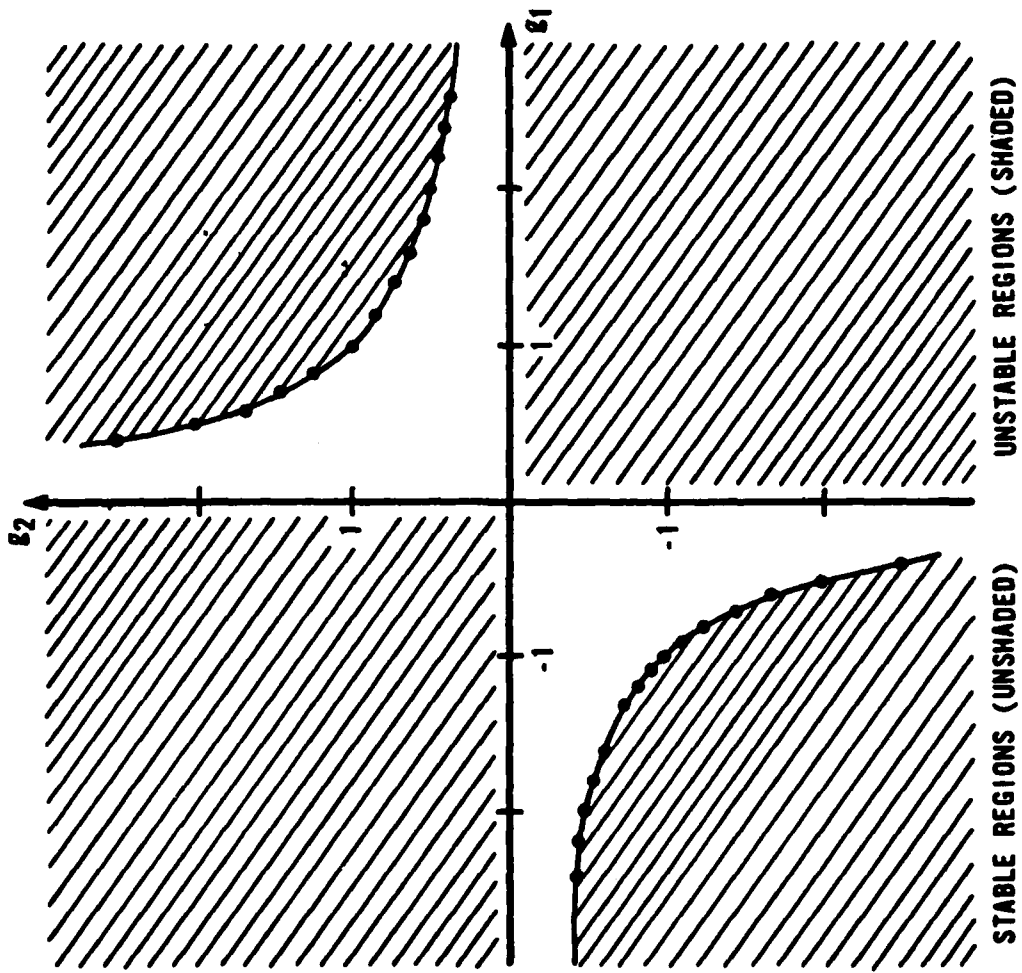


Figure 2.2 Stability Diagram.

strongly affect the beam profile predicted by geometric optics while the effect is less at higher Fresnel numbers. This impact is seen on the modes of the resonator. At low Fresnel numbers, the intensity profiles of the resonator modes are very different from the profiles predicted by geometric optics, while at high Fresnel numbers, the mode profiles appear close to the geometric optics profiles except for high spatial frequency, low amplitude ripples called appropriately 'Fresnel ripples'. Other variations of 'Fresnel numbers' are defined as needed, but they are all related to this basic definition.

## 2. Basic Assumptions for Strip Resonators

A rigorous analysis of the electromagnetic fields that are the modes of an open resonator at optical frequencies should begin with Maxwell's equations. We will use this approach in the next chapter, but in the bare cavity analysis that follows, we use a number of assumptions that are frequently made in the literature. Here we discuss these approximations qualitatively. A detailed quantitative derivation is shown in Chapter III, where the loaded cavity analysis is done. In this chapter, we use the following discussion to give some background on the well-known Fresnel approximation. First, the "bare cavity" is assumed to be filled with a homogeneous, isotropic medium. The medium effects will be addressed in the next chapter. Second, the fields are assumed to have an  $\exp(i(\omega t - kz))$  dependence. Under these assumptions, the spatial variations of the fields

are described by the vector Helmholtz equation. In Cartesian coordinates, the equation separates for each field component. Since we expect a beam-like behavior (as characterized by the dependence chosen above), we further assume the field is predominantly TEM and linearly polarized in the  $x$  direction. Thus the scalar Helmholtz equation is appropriate. Now, to further simplify the analysis, we make the paraxial approximation. If the mirrors are separated by many wavelengths (as they usually are at optical frequencies), then this is a good approximation. The resultant paraxial wave equation is equivalent to the two-dimensional Fresnel diffraction analysis. In Cartesian coordinates, this integral analysis of the bare cavity separates for each transverse coordinate, i.e., the resonator can be analyzed as two orthogonal strip resonators. In Chapter III, this separation will no longer be valid when a gain medium is included unless restrictions are placed on the medium.

While these assumptions seem to be plentiful, they are the usual string of assumptions made in most optical analyses. Their validity is usually supported by having good agreement with experiments, but in the cases of inhomogeneous, nonlinear or active medium, such agreement is not as clear. Indeed, for high energy lasers, the agreement between the bare cavity modes and the actual laser fields has not been well established. These issues are more appropriate to the next chapter. What we want to analyze here is the natural or normal modes of the open resonator which are

analogous to the modes of microwave waveguides. Indeed, Vainstein analyzed the resonator as a highly lossy waveguide. (Ref 9) A final note: the resonator mode is characterized by a longitudinal index that is defined by the number of half integer wavelengths can be fit into the cavity and a pair of transverse indices that denote differing transverse structure on the basic longitudinal mode. (For a strip resonator there would only be one transverse index.) Frequently one calls the mode a "longitudinal mode" when the transverse structure is ignored. Here we assume that we are studying the transverse structure of a single longitudinal mode. The actual laser might have a lasing transition that covers several longitudinal modes with none of the modes exactly on the line-center of the lasing transition. Each of these possibilities complicates the analysis. In Chapter III, we will assume the existence of one longitudinal mode that lies at the same frequency as the line-center of the lasing transition. With all these assumptions in mind, we proceed with the analysis of the bare cavity modes.

#### B. Bare Cavity Round Trip Equation

As mentioned in Chapter 1, the transverse modes of the resonator are frequently defined as the eigenfunctions of a homogeneous Fredholm integral equation of the second kind (FIE II). The associated eigenvalues are related to the outcoupling and phase shifts of the eigenmodes. The general form of the homogeneous FIE II is

$$\sigma u(x) = \int_a^b K(x,y) u(y) dy \quad (2.5)$$

(Appendix 1 contains a brief discussion of the properties of Fredholm integral equations of the second kind that are required for the discussion of resonator modes in this chapter and the next chapter.) The exact expression for the kernel,  $K(x,y)$ , depends both on the nature of the resonator (mirror separation, mirror reflectivities, etc) and the sophistication of the analysis. For the strip resonator, the kernel is given by

$$K(x,y) = \frac{i}{\lambda L} e^{-\frac{ikg_2(x^2+y^2)}{2L}} \int_{-a_2}^{a_2} d\eta e^{-\frac{ik}{L}[g_2\eta^2 - \eta(x+y)]} \quad (2.6)$$

This kernel is derived in Appendix 4, which deals with the derivation of the loaded cavity round trip equation. The bare cavity round trip equation is obtained by simply setting the gain function to zero. The eigenfunction,  $u(x)$ , is the scalar field at mirror 1 as shown in Figure 2.1. The variables  $x$  and  $y$  are limited to the range  $(-a_1, a_1)$ . It is important to bear this restriction in mind when using this and other kernels related to resonator problems. The Fresnel or paraxial approximation is made in this derivation. This is valid as long as  $a^4/(2\lambda z^3) \ll 1$ . This approximation is usually good for realistic optical resonators. For the analysis that follows, the strip resonator will be assumed to be single-ended. This means that the half-width of mirror 2 is assumed to be great enough

that any transverse mode is essentially zero before the edge of the mirror. This doesn't violate the Fresnel approximation since we have restricted the types of field that we will allow as valid modes and it allows us to let  $a_2$  tend to infinity. Then the integral in the kernel can be evaluated analytically and the resulting kernel is

$$K(x,y) = \sqrt{iF} e^{-i\pi F[g(x^2+y^2) - 2xy]} \quad (2.7)$$

where  $F = \frac{a_1^2}{2\lambda L g_2}$  and the transverse coordinates have been normalized by  $a_1$ .

Let us examine the two kernels shown above in more detail. Eq(2.6) shows the kernel for a double-ended strip resonator, while Eq(2.7) shows the kernel for a single-ended strip resonator. Notice that no assumptions have been made as to whether the resonator is stable or unstable. The kernels describe both cases. Note that the kernels are both complex-symmetric but not hermitian. This property means that the eigenvalues, if they exist, are complex. Also, the eigenfunctions do not form a complete set on the interval of the integration, namely  $(-a_1, a_1)$ . This fact is well documented in the literature although a recent paper attempted to show otherwise. (Ref 10,11) The lack of completeness will affect the analysis of the eigenfunctions discussed in a later section. Further, the eigenfunctions, if they exist, obey an "orthogonality" relation different from the usual "power" relation used for the eigenfunctions

of hermitian kernels. (This property has been called "biorthogonality" in some papers. (Ref 55)) Here, the relation is

$$\int_{-a_1}^{a_1} dx u_i(x) u_j(x) = \delta_{ij} \quad (2.8)$$

(See Appendix 1 for a proof of this relationship. A similar proof shows the eigenvectors of a complex-symmetric matrix are also orthogonal in the sense that the inner product satisfies  $(u_i, u_j) = \delta_{ij}$ .) The existence of solutions to the integral equation that describes the resonator modes has been fully established in the literature. (Ref 10,12-14) However, no proof has been shown that an infinite number of solutions exists for unstable resonators, although the modes of a stable strip resonator can be accurately approximated by the infinite, complete set of hermite-gaussian polynomials.

The amplitude of the eigenvalue is related to the loss of the particular mode. The phase of the eigenvalue is interpreted as a frequency shift for the particular mode from the input frequency of the kernel. (Ref 5) Thus the eigenvalues contain a great deal of information about each mode. Plots of the amplitude of the eigenvalues reveal trends that are useful in designing resonators. We will use such plots later in this chapter as the means to verify numerical models of bare resonators.

This concludes the discussion of the integral equation that describes the modes of the strip resonator. Many of the comments made concerning the complex-symmetric kernel apply

to more general configurations. We next discuss various techniques that have been used to solve the integral equation for the modes. This review is necessarily brief. The transformation of the integral equation to a matrix eigenvalue problem (MEVP) is used as the common thread between the various techniques.

### C. Methods of Finding the Modes of Empty Resonators

A number of ingenious techniques have been employed in the past to solve the resonator integral equation. These techniques include the iterative scheme used by Fox and Li (Ref 15), the various matrix methods (Ref 16-18, 53) and the asymptotic techniques (Ref 19-21). As Sanderson and Streifer pointed out (Ref 22), most of the techniques transform the integral equation that describes the modes into a matrix eigenvalue problem. It is this formalism that we will use to review some of these techniques. (One technique that does not readily fit this formalism is the waveguide analysis done by Vainstein (Ref 9) but this approach will not be reviewed here.)

The general transformation from the integral equation to a matrix eigenvalue problem is reviewed here. Our treatment follows that of Sanderson and Streifer. Consider two sets of complete and orthonormal functions,  $v_n(x)$  and  $w_n(x)$ , defined on the interval of interest. Here the interval is  $(-a, a)$ . (Note that a complete and orthonormal set of functions can always be constructed from a complete set by

the Gram-Schmidt orthogonalization process.) Then the kernel of Eq(2.5) is expanded in a convergent infinite series:

$$K(x,y) = \sum_{n,m=0}^{\infty} K_{nm} v_n(x) w_m(y) \quad (2.9)$$

(Note that the kernel is not assumed to be separable. The coefficients in the expansion are matrix elements. By properly choosing the basis functions, one might be able to make this matrix of coefficients diagonal, thus finding a basis set in which the kernel is separable.) The eigenfunction is similarly expanded:

$$u(x) = \sum_{p=0}^{\infty} b_p w_p(x) \quad (2.10)$$

Substituting these equations into Eq(2.5) and then multiplying both sides by  $w_p(x)$  and integrating over  $x$ , one obtains a matrix eigenvalue problem:

$$\lambda b_p = M_{pn} b_n \quad (2.11)$$

where

$$M_{pn} = \sum_{m=0}^{\infty} K_{nm} \int_a^a dx w_p(x) v_m(x) \quad (2.12)$$

The difficulty lies in evaluating these matrix elements for a particular basis set. Since the kernel is symmetric in  $x$  and  $y$ , some simplification results from choosing  $w_n = v_n$ . Then the coefficient matrix  $K_{nm}$  retains the symmetry of the

kernel, namely  $K_{nm} = K_{mn}$ . The difficulty now is the choice of the basis set. If Dirac delta functions are used, one obtains the Fox and Li formulation. Other authors have used the Hermite-gaussian functions (Ref 16), power series (Ref 23) and other functions to evaluate the matrix elements. The asymptotic method is a method where an incomplete set is used. This set is generated by applying the method of stationary phase to a form of the integral equation, Eq(2.5). (Ref 19, 24) Even though this set has not been shown to be complete, the analysis leads to a polynomial equation for the eigenvalues and the expansion coefficients. Thus this method diagonalizes the matrix whose eigenfunctions we seek to find. A considerable savings in computational time results. However, use of this basis set may lead to inaccurate higher order eigenfunctions and eigenvalues. This will be one area investigated in this chapter.

As Sanderson and Streifer point out, the optimal basis set is one that approximates the modes of the resonator as closely as possible. (Ref 22) (We require the basis set to be a complete, orthonormal set of functions on the finite interval  $(-a, a)$ . The modes of the resonator do not meet either of these conditions, being neither complete nor orthogonal in the usual sense.) Since this requires knowledge of the modes before they are calculated, the basis set can be chosen instead to provide the best approximation to the kernel when the series in Eq(2.9) and Eq(2.10) are truncated at some value, say  $N$ . Streifer has shown (Ref 25) that the Schmidt expansion functions are this optimal basis

set. If this basis set is used, the coefficient matrix in Eq(2.9) becomes diagonal and the truncated series is the best N-term approximation (in the mean square sense) for a given value of N . For the strip resonator, this basis set is related to the linear prolate functions. Since this basis set leads to integrals in the matrix elements that cannot be evaluated analytically, it has not yet been used in evaluating the modes of strip resonators. However, the linear prolate functions will be used in this investigation as a basis set to find the strip resonator modes. The analysis is found to be straightforward and the solutions are as accurate as other methods.

We now pause to review the linear prolate functions, their properties, and the numerical method used to calculate them. Following this discussion, the specific matrix eigenvalue problem using this basis set will be derived. After verifying that the implementation is correct by comparing results with other work, two areas will be studied. The first area is the study of the validity of the asymptotic approach at low equivalent Fresnel numbers. The second area is the demonstration of the orthogonality of the strip resonator modes as discussed earlier in this chapter. (See Eq(2.8).)

#### D. The Linear Prolate Functions

This section is broken into three parts. The first part

discusses the defining equations for the linear prolate functions (LPF). The second part covers the properties that will be used in the modal analysis that follows this section. The third part is a discussion of how the linear prolate functions are calculated numerically.

The linear prolate functions are related to the prolate spheroidal wave functions that arise when the wave equation is separated in prolate spheroidal coordinates. However, there is no advantage to examining this connection and it is entirely adequate to consider the LPF as a set of special functions defined by the equations given below. Although the following discussion is fairly detailed, the interested reader is referred to the literature where a number of excellent references go into far greater detail. (Ref 26-33) The book by Flammer (Ref 26) is an excellent work on the prolate spheroidal functions. The chapter by Freiden in Progress in Optics (Ref 27) is very complete summary of the linear prolate functions and much of what follows is based upon this reference.

### 1. Defining Equations

The linear prolate functions can be considered as solutions to a Sturm-Liouville differential equation,

$$(1-x^2) \frac{d^2 \Psi_\lambda(x,c)}{dx^2} - 2x \frac{d \Psi_\lambda(x,c)}{dx} + (\lambda^2 - c^2 x^2) \Psi_\lambda(x,c) = 0 \quad (2.13)$$

where the boundary conditions are chosen such that the LPF remain finite at  $\pm 1$ . A family of LPF is characterized by the

parameter  $c$ , and each LPF within the family is characterized by the eigenvalue of the differential equation,  $\Gamma_2$ . The dependence of each LPF on the parameter  $c$  is implicit in every application of the LPF and the subsequent notation may not explicitly show this dependence.

The LPF can also be defined as the eigenfunctions of the finite Fourier transform: (Ref 27,29)

$$i^2 \sqrt{\frac{2\pi\gamma_2}{c}} \Psi_2(x) = \int_{-1}^1 dy e^{icxy} \Psi_2(y) \quad (2.14)$$

Here, the LPF are characterized by a second eigenvalue,  $\gamma_2$ .

A third equation that could be used to define the LPF is the first iterate of Eq(2.14). This equation is found by multiplying Eq(2.14) by  $\exp(-icxz)$  and integrating over  $x$ :

$$\gamma_2 \Psi_2(z) = \int_{-1}^1 dy \frac{\sin c(y-z)}{\pi(y-z)} \Psi_2(y) \quad (2.15)$$

The intimate connection between the LPF and the modal analysis of resonators is highlighted by the fact that Eq(2.15) is the equation for the modes of the stable, confocal resonator. In this case the LPF actually are the modes of the resonator. We will later find another class of resonators that have LPF as exact solutions.

Figure 2.3(a-o) show the first fifteen LPF for the case where  $c = 3.5903916$ . Notice that each LPF is characterized by a large peak on the semi-infinite interval and lower amplitude oscillations elsewhere. Also note that this peak

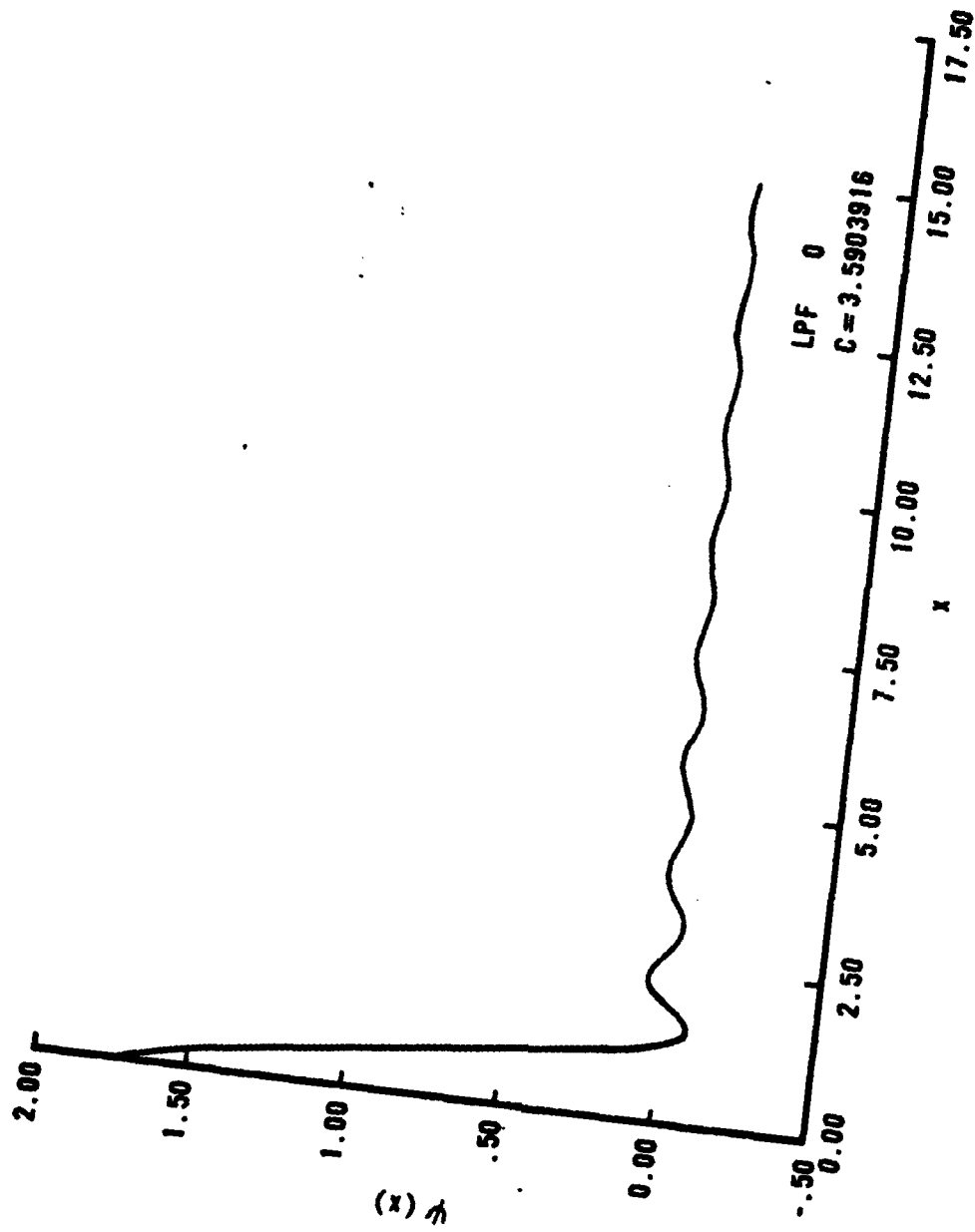


Figure 2.3a LPF 0.

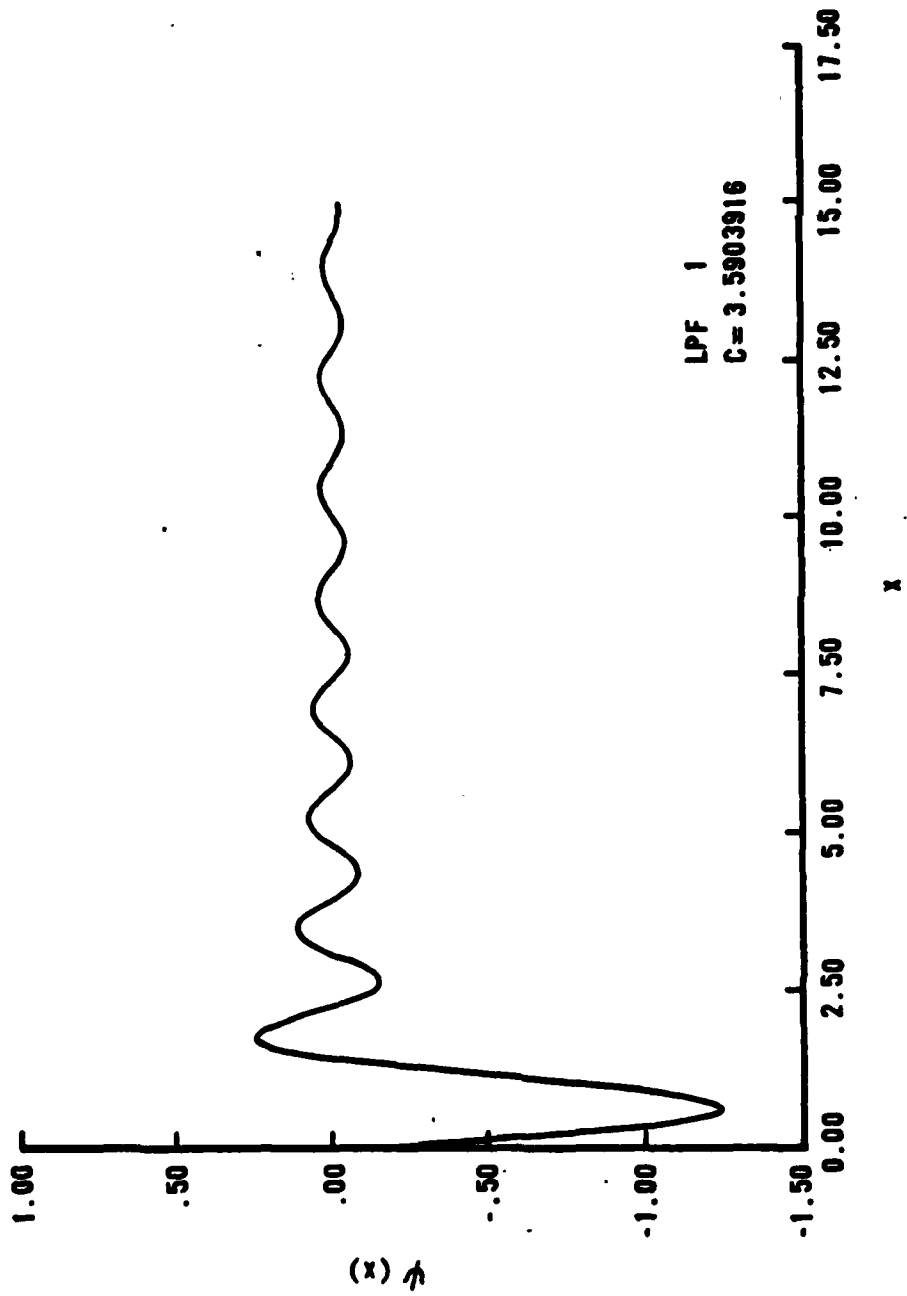


Figure 2.3b LPF 1.

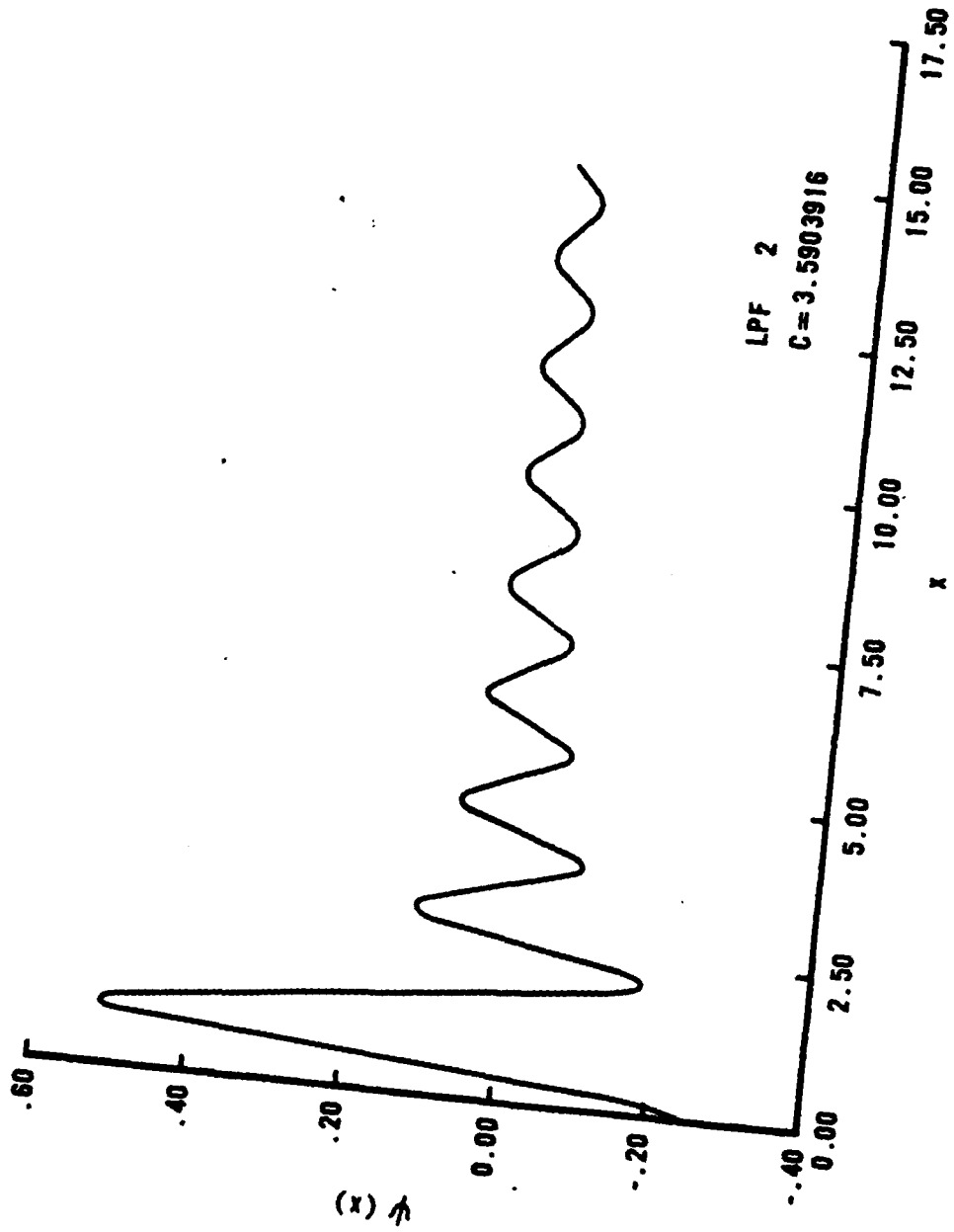


Figure 2.3c LPF 2.

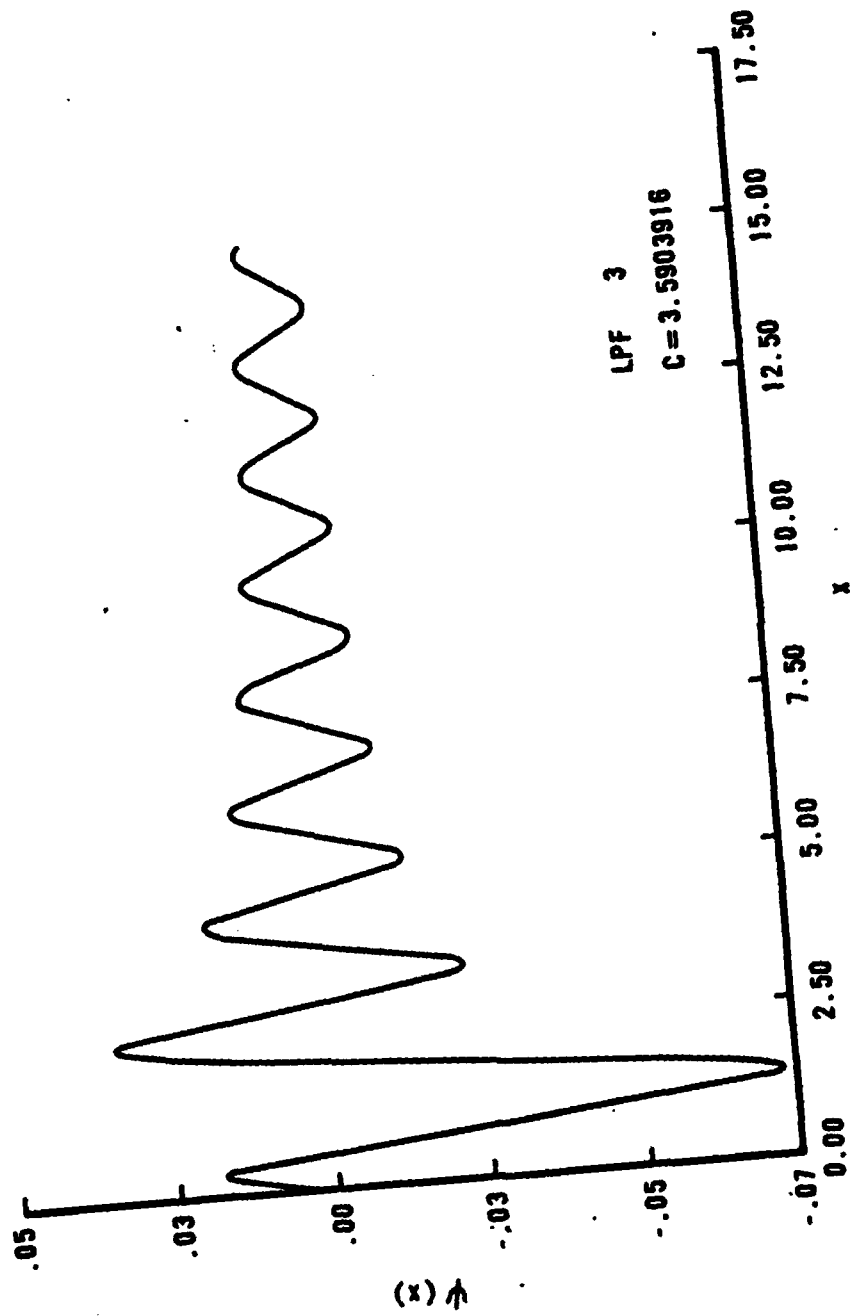


Figure 2.3d LPF 3.

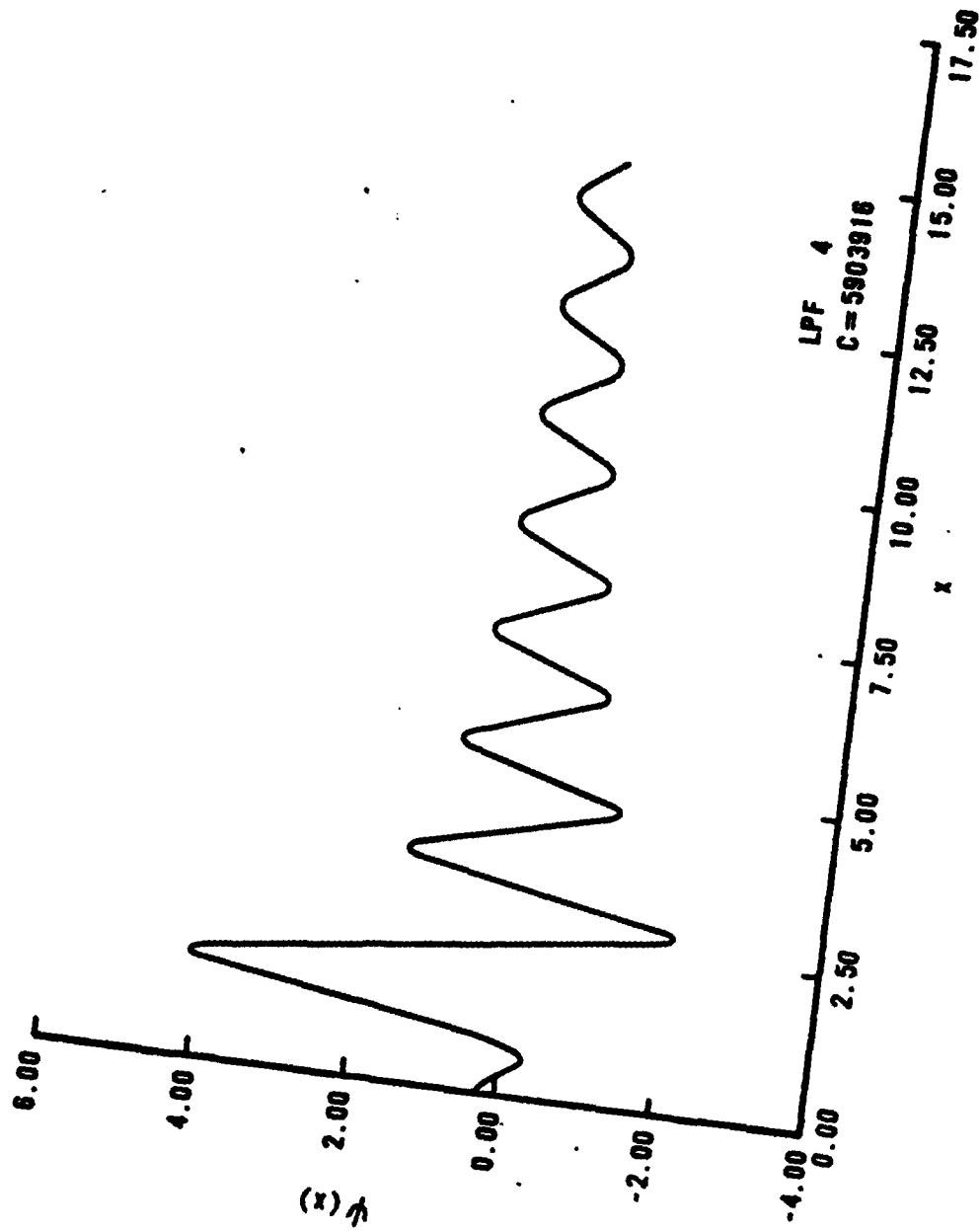


Figure 2.3e LPF 4.

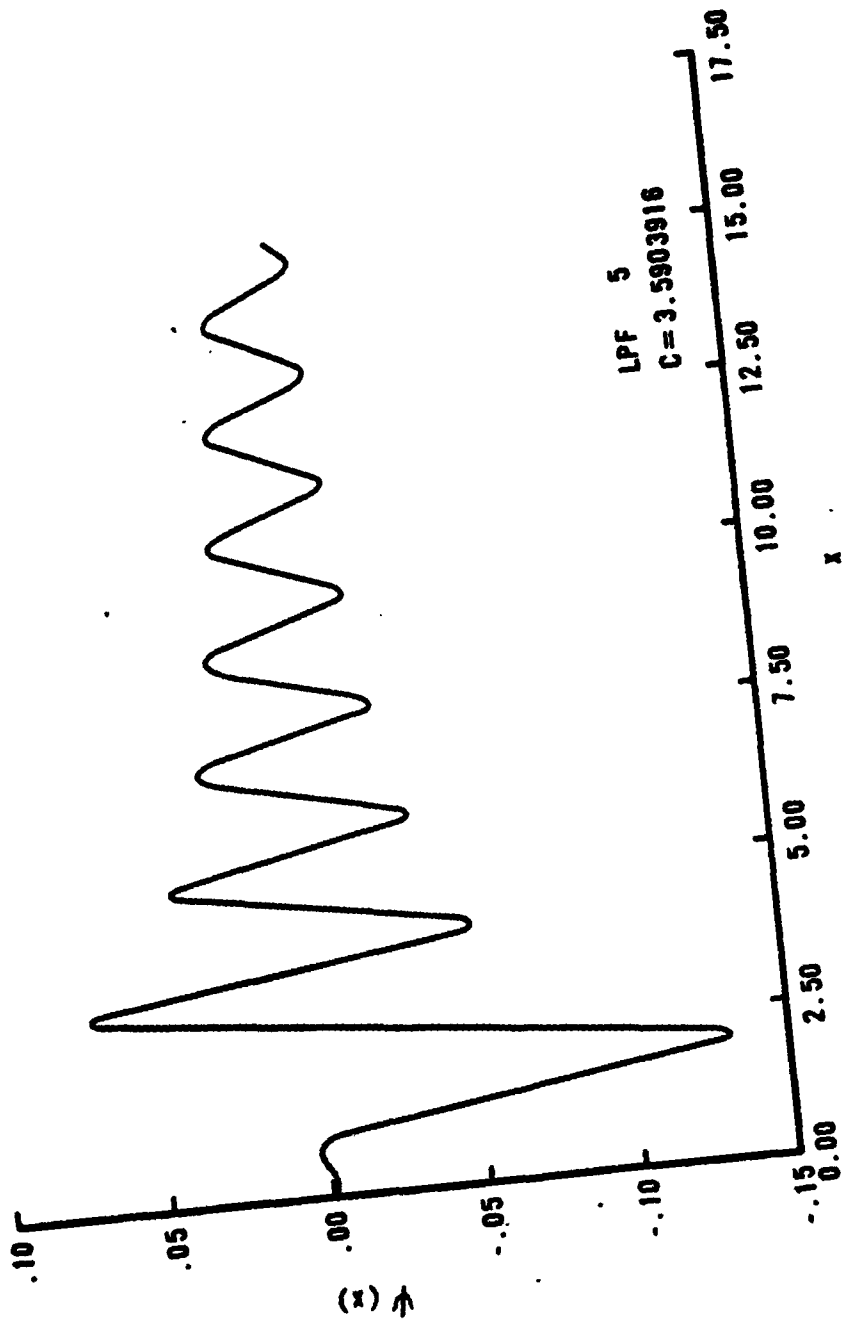


Figure 2.3f LPF 5.

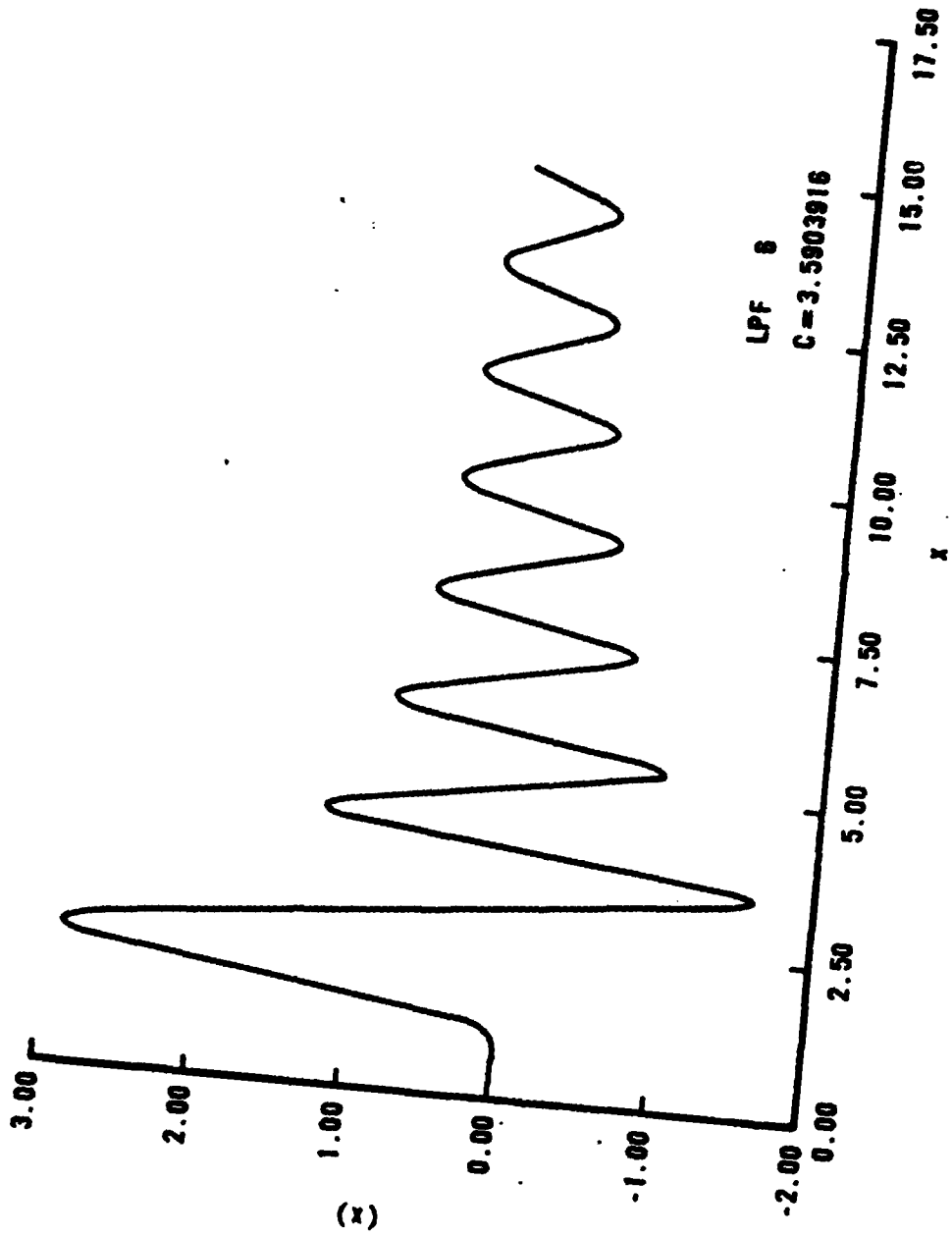


Figure 2.38 LPF 6.

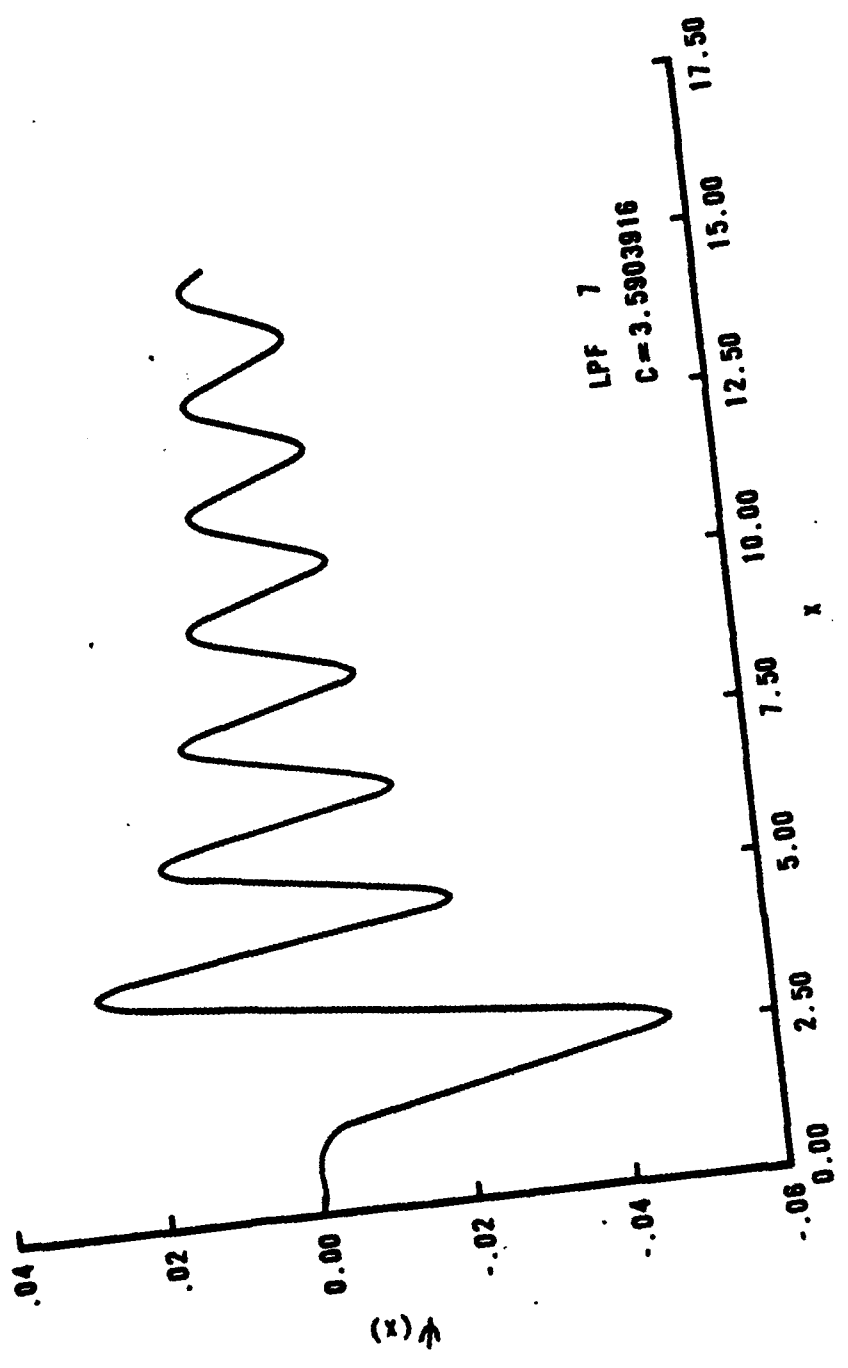


Figure 2.3h LPF 7.

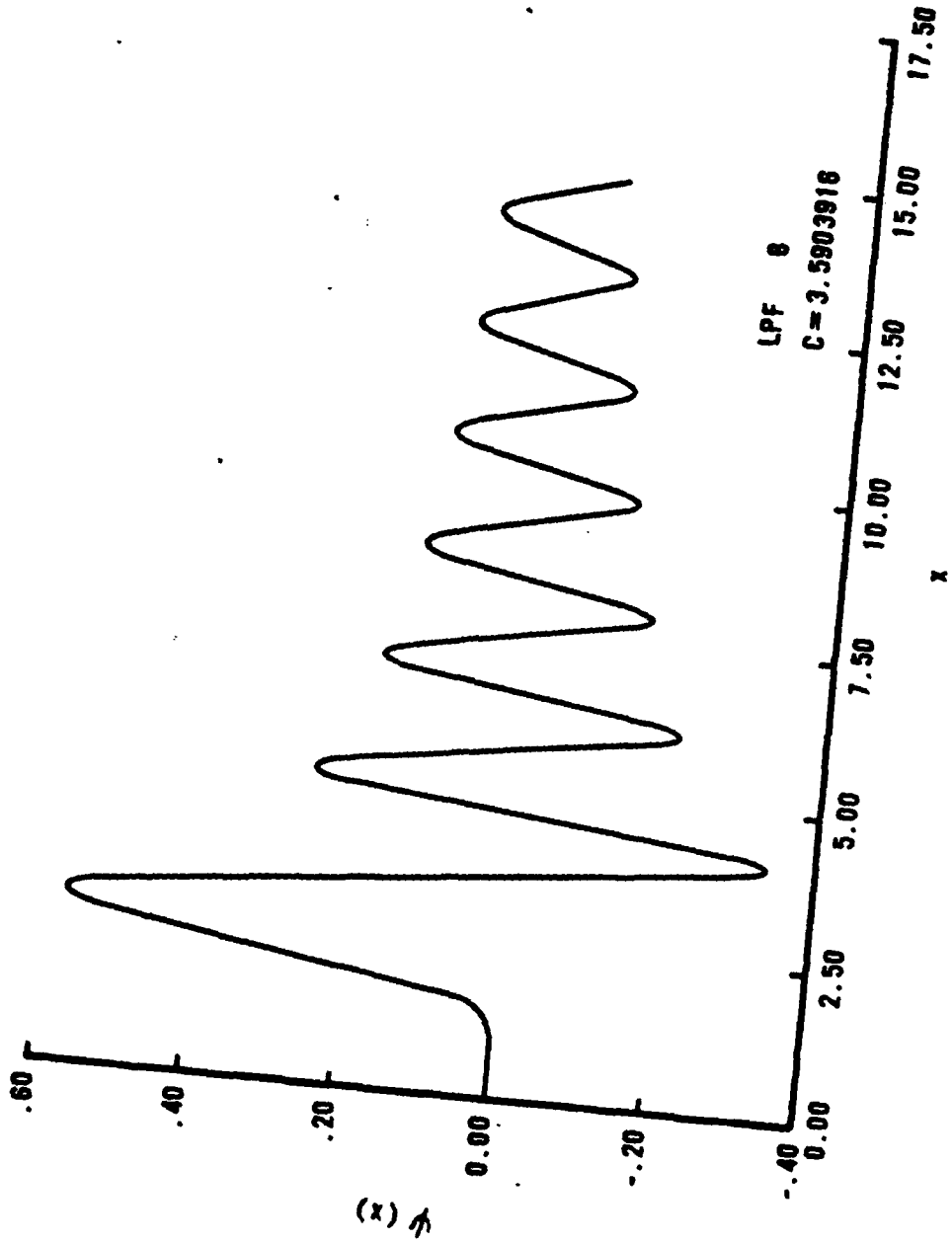


Figure 2.31 LPF 8.

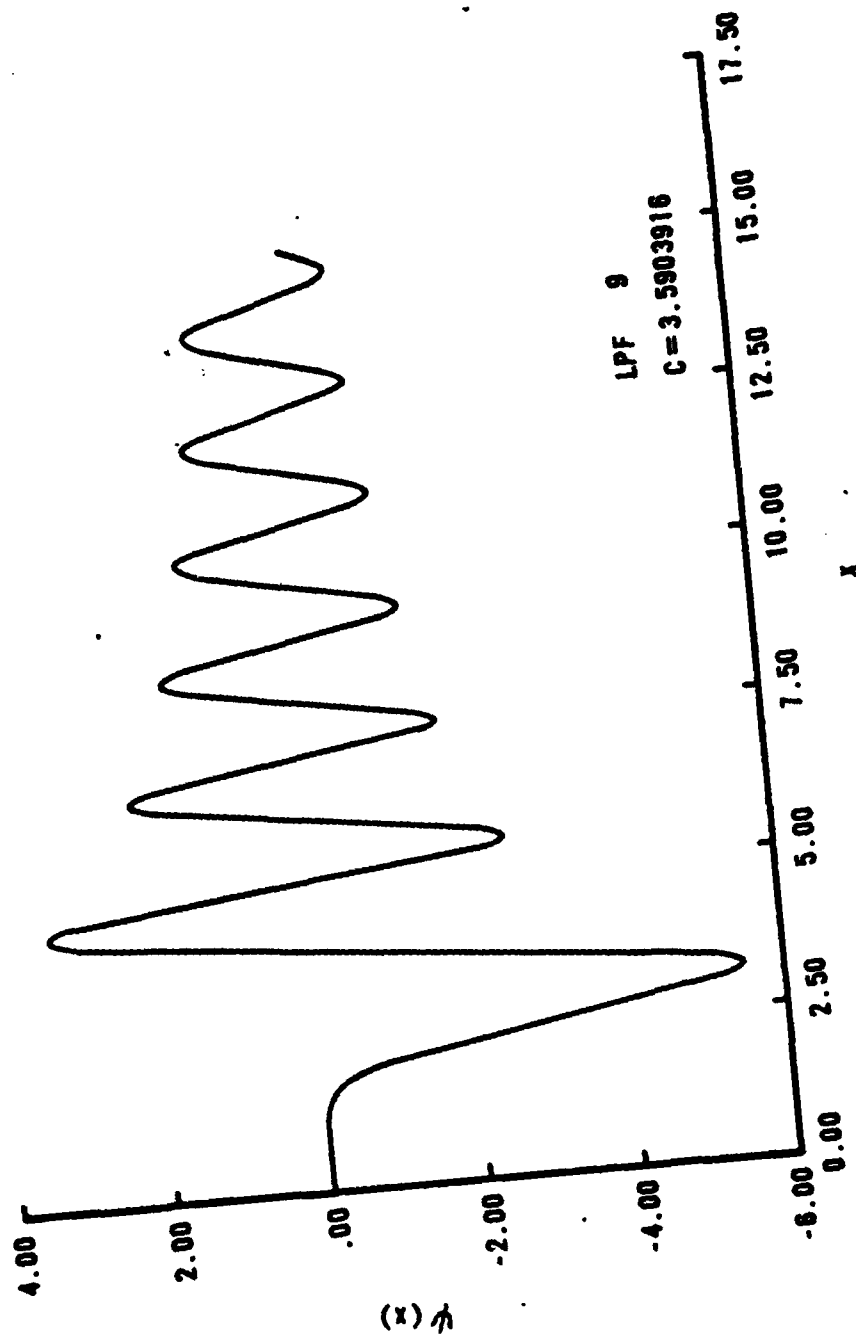


Figure 2.3j LPF 9.

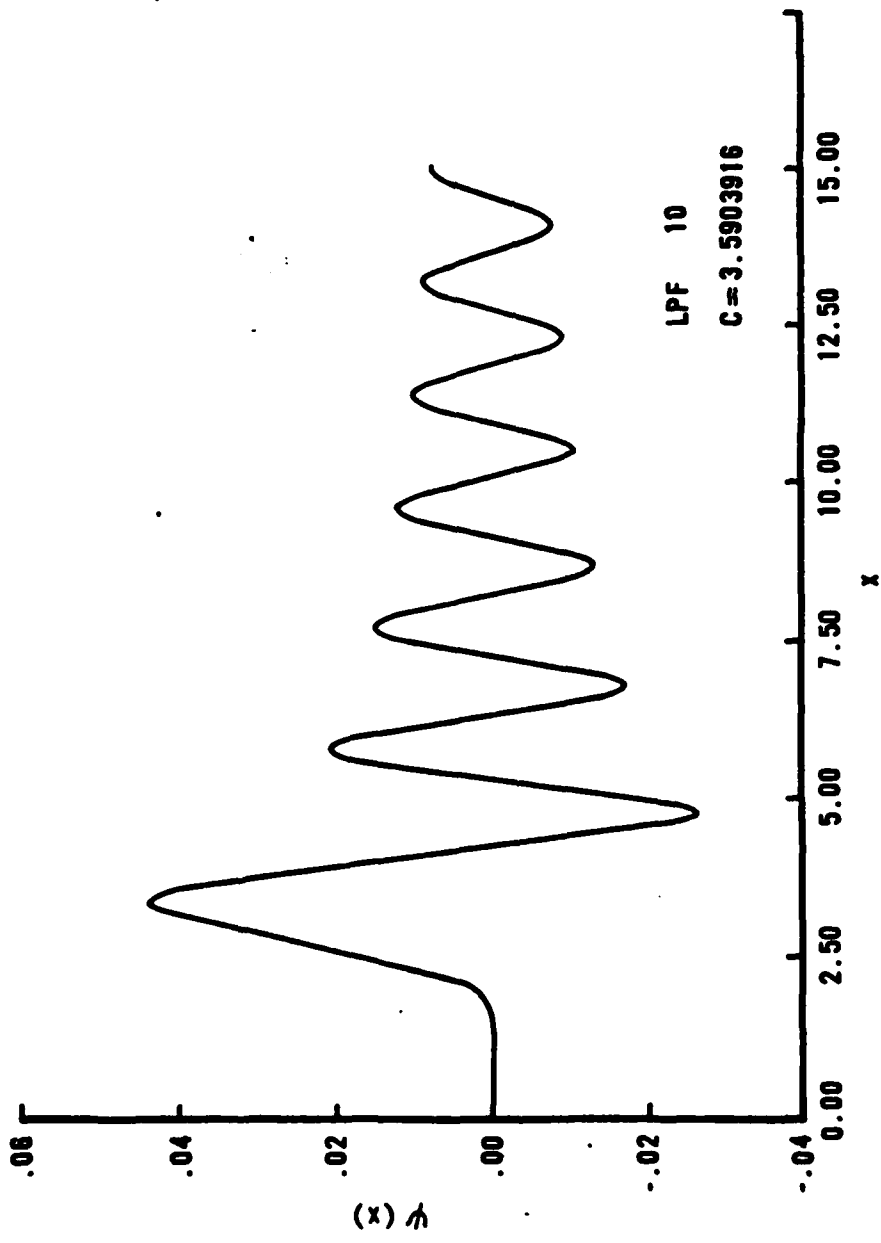


Figure 2.3k LPF 10.

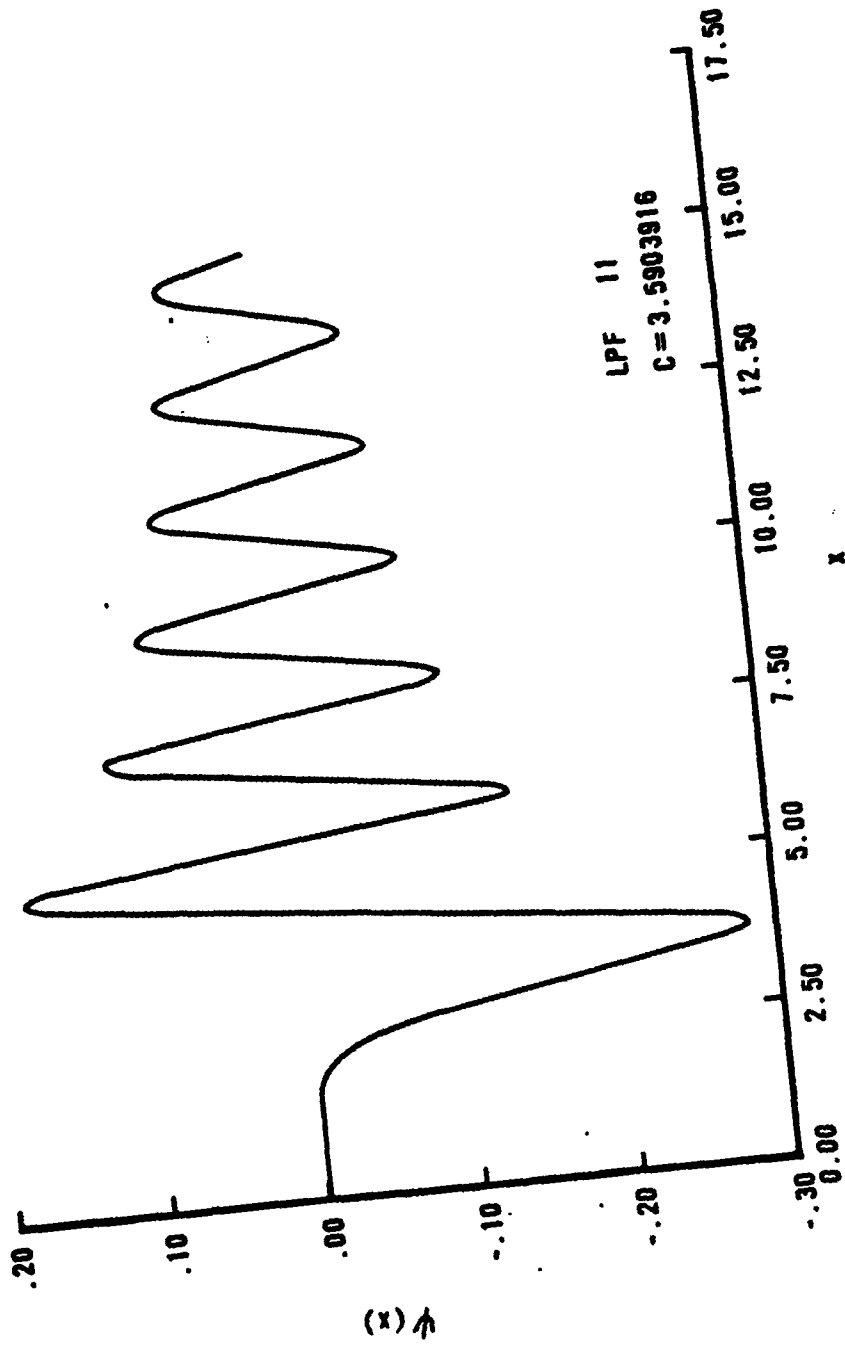


Figure 2.31 LPF 11.

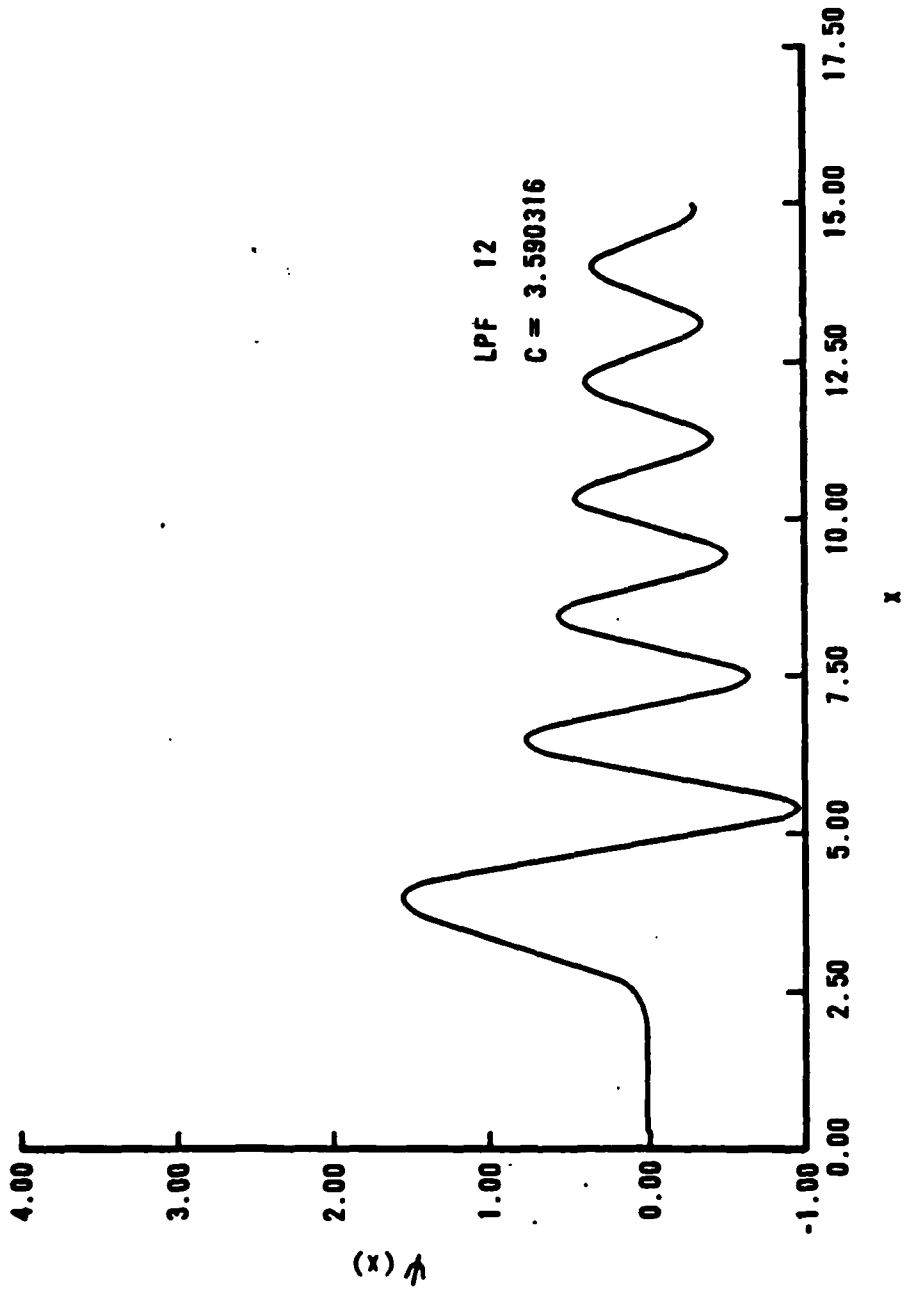


Figure 2.3m LPF 12.

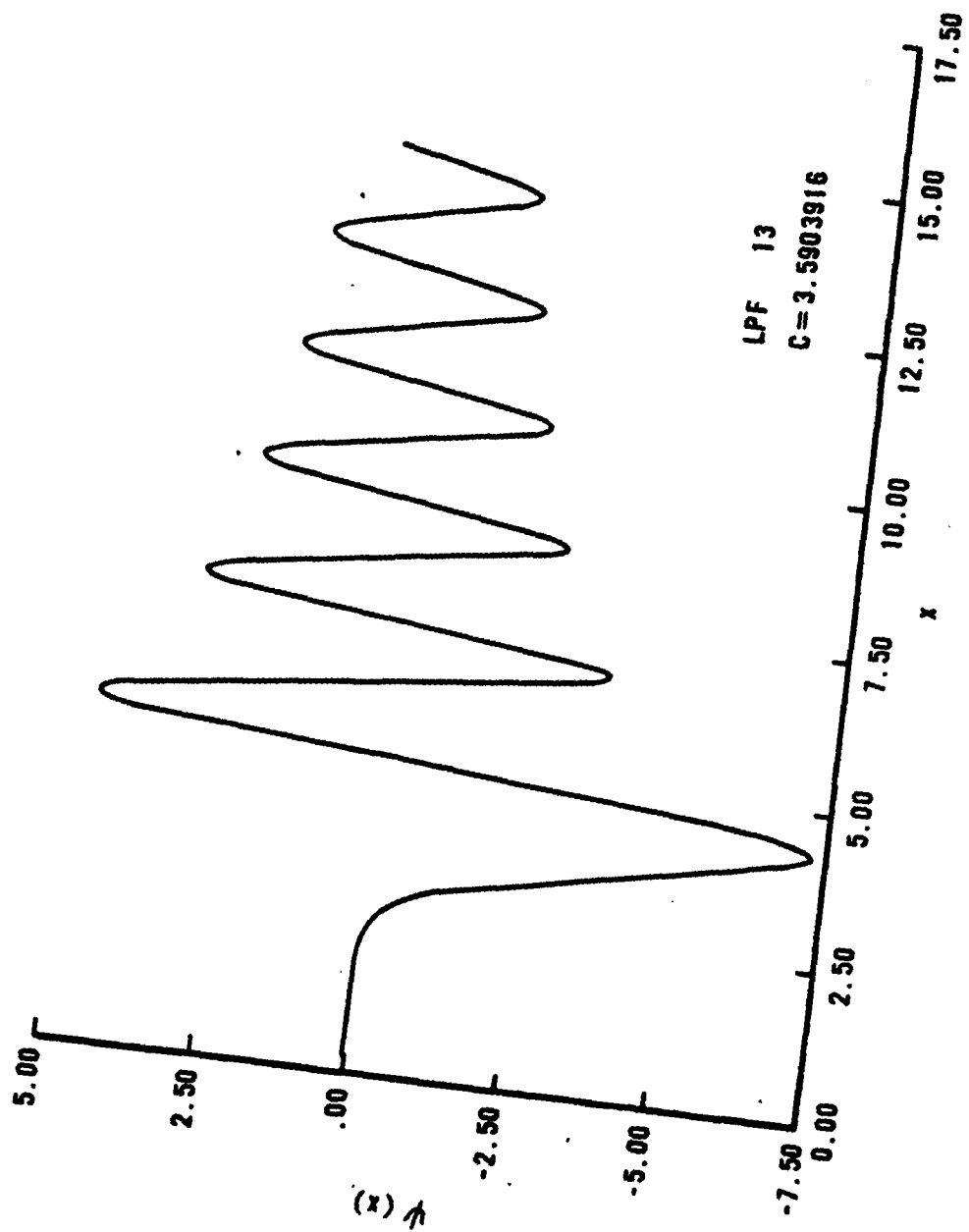


Figure 2.3n LPF 13.

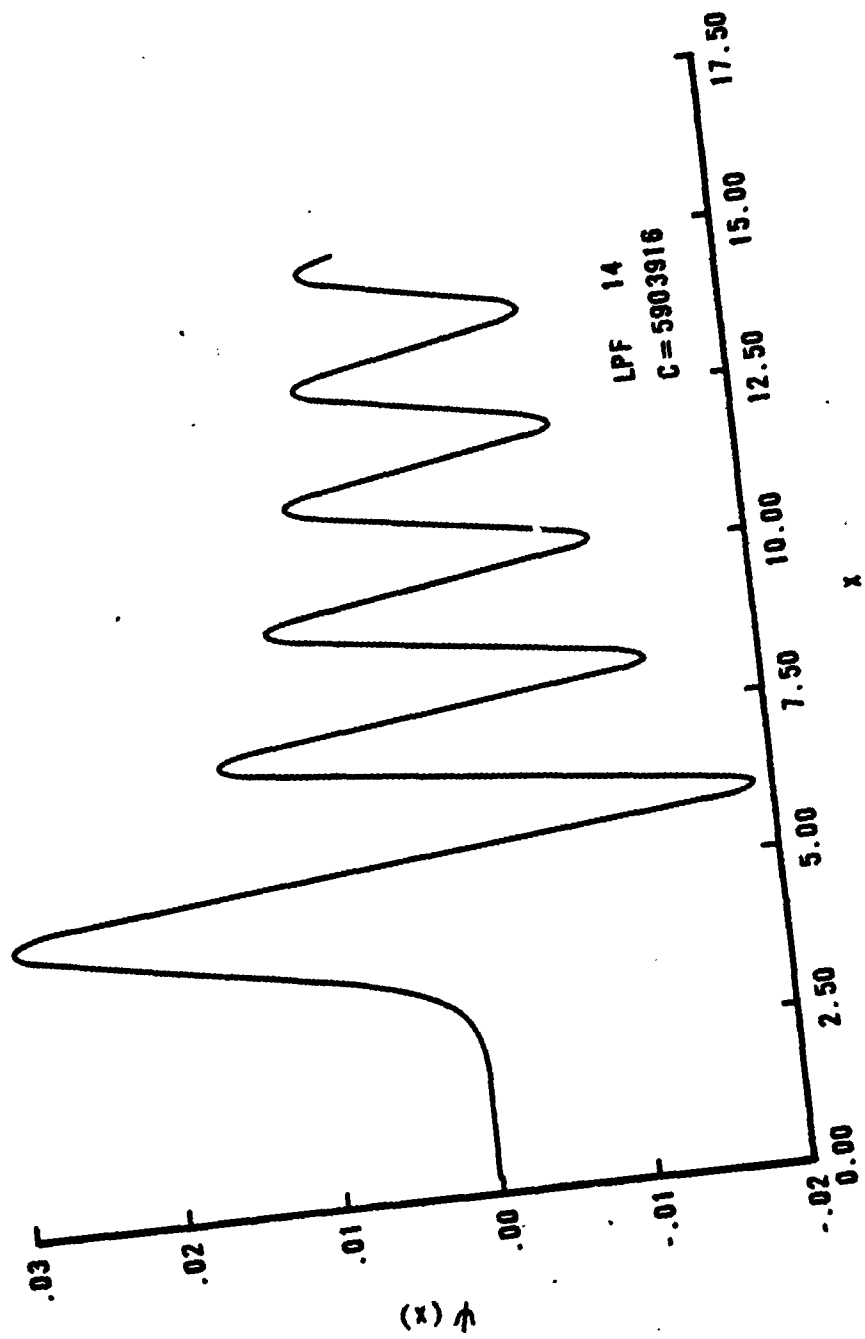


Figure 2.30 LPF 14.

moves out to larger values of  $x$  as the index of the LPF increases. For some value of the index, the LPF will be nearly zero in the interval  $(-1,1)$  and one expects LPF of this index or larger to contribute little to the mode of the resonator. We will find this to be supported by later results. Finally, note that the LPF are even for even index and odd for odd index.

## 2. Properties of the LPF

We now consider the properties of the LPF. The functions are real-valued functions and the two eigenvalues associated with them are real. The eigenvalue of the differential equation increases with increasing index:

$$0 < \Gamma_0 < \Gamma_1 < \Gamma_2 < \dots \quad (2.16)$$

Figure 2.4 is a plot of this eigenvalue as a function of increasing index. The integral equation eigenvalue exhibits a markedly different behavior. Figure 2.5 shows this behavior. A good approximation to this sharp cutoff is

$$\gamma_n \approx \begin{cases} 1 & \text{for } n \leq n_c \\ 0 & \text{for } n > n_c \end{cases} \quad (2.17)$$

where  $n_c = \frac{2c}{\pi}$ . This steplike behavior is very useful in many applications of the LPF. Another property that will be used is the orthogonality of the LPF over the finite interval.

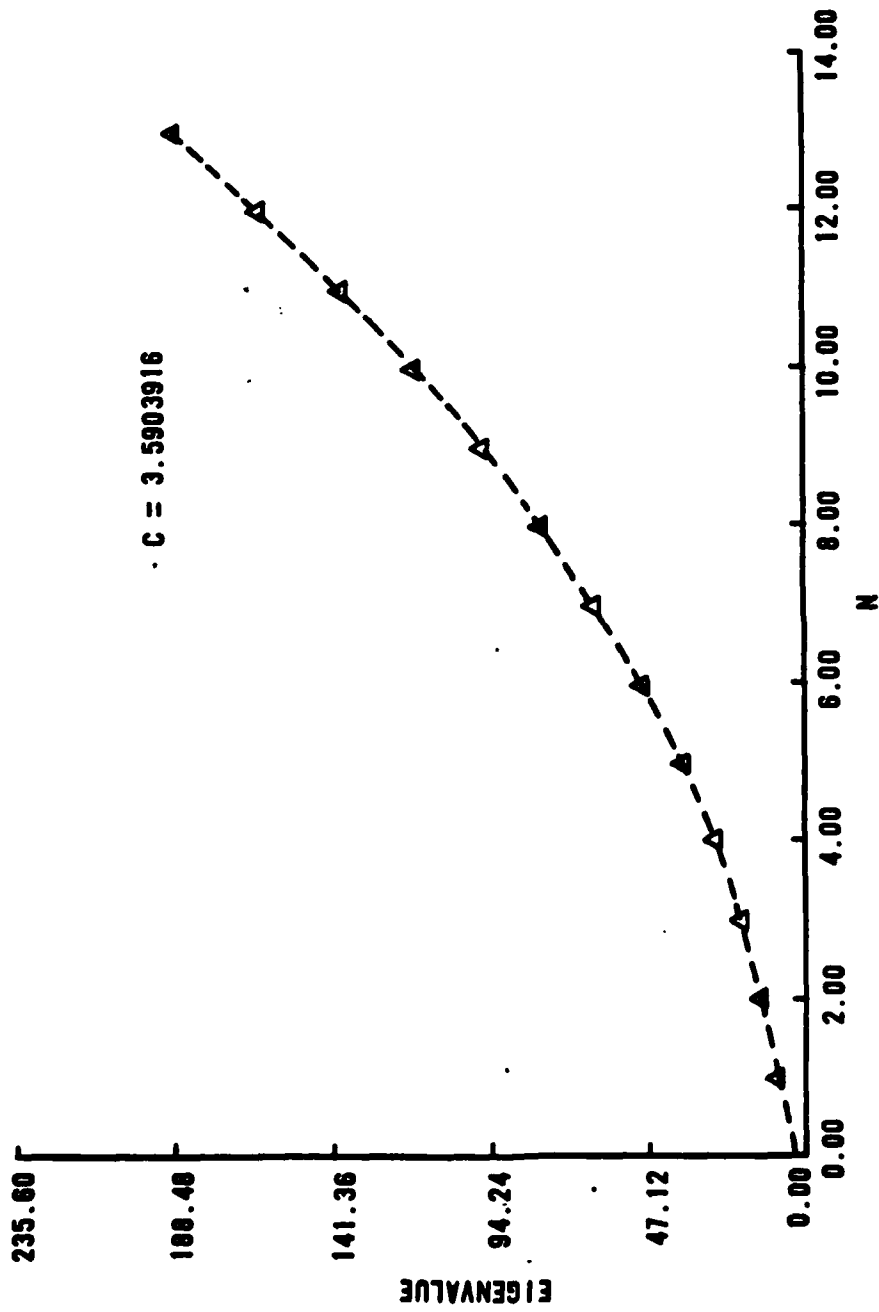


Figure 2.4 Differential Equation Eigenvalue for Linear Prolate Function.

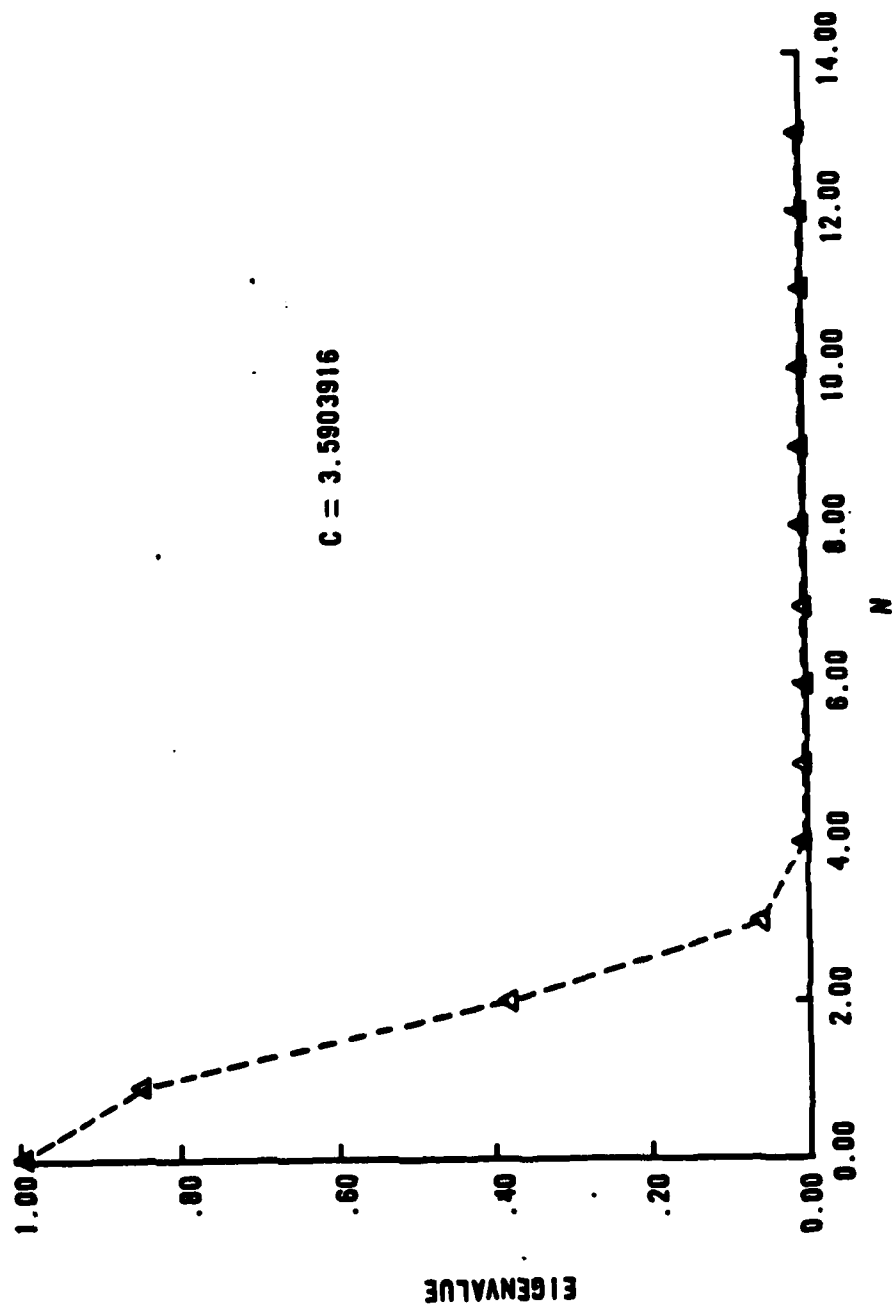


Figure 2.5 Integral Equation Eigenvalue for Linear Prolate Function.

$$\int_{-1}^1 dx \Psi_n(x) \Psi_m(x) = \gamma_n \delta_{nm} \quad (2.18)$$

The LPF also are orthonormal on the infinite interval.

Since the LPF satisfy a Sturm-Liouville problem, they are a complete set on the finite interval. (The LPF are square-integrable functions in the space  $L_2$  with the norm shown above.) This completeness shows that the kernel expansion and expansion of the eigenfunction discussed in Eq(2.9) and Eq(2.10) are convergent series (and converge to the desired functions) when the LPF are used as a basis set. Frieden also shows that the LPF are complete on the infinite interval. (Ref 27)

A property that will be very useful in the analysis of the strip resonator modes is the expansion of the kernel of the finite Fourier transform in LPF:

$$e^{icxy} = \sum_{\lambda=0}^{\infty} i^{\lambda} \sqrt{\frac{2\pi}{c\gamma_{\lambda}}} \Psi_{\lambda}(x) \Psi_{\lambda}(y) \quad (2.19)$$

This expansion is easily obtained from the defining integral equation, Eq(2.14), and the orthogonality property, Eq(2.18). This concludes the review of the properties of the LPF relevant to the analysis of the strip resonator. We now turn our attention to how the LPF are generated numerically.

### 3. Numerical Generation of the LPF

One disadvantage that has plagued the LPF is that they

have been difficult to generate numerically. One must evaluate an infinite series expansion for the eigenvalues as well as the eigenfunctions in order to obtain highly accurate values for the LPF. Van Buren has written a code that does precisely this. (Ref 34) However, if one desires knowledge of several LPF over a wide range of arguments, such an approach requires too much computer time and memory to be practical. We have developed a method that produces a large set of LPF on the interval  $(-1,1)$  with good speed and accuracy. This method should be of use to other researchers using the LPF. The approach taken is first to use the Van Buren code to generate the two eigenvalues and two endpoints. For even LPF, the values at  $x = 0$  and  $x = 1$  were used; for odd LPF the slope at  $x = 0$  and the value at  $x = 1$  were used. Then these values were used in a finite difference code that generated the LPF over the interval  $(-1,1)$  by solving the differential equation, Eq(2.13). A nonuniform grid was required when generating the LPF because of the large peak discussed earlier. The requirement for a nonuniform grid is more clearly seen by considering the differential equation Eq(2.13) when  $x \approx x_0 \equiv \frac{\sqrt{1-\epsilon}}{\epsilon}$ . Then a differential equation for the derivative of the LPF can be written.

$$(1 - x_0^2) \frac{d}{dx} (\psi'_x) - 2x_0 \psi'_x \approx 0 \quad (2.20)$$

The solution is

$$\Psi'_r(x) \approx e^{\left(\frac{2x_0}{1-x_0}\right)x} \quad (2.21)$$

When  $x_0 \approx 1$ , the LPF has a steep slope. Thus a nonuniform grid was required to follow this variation accurately. Finally, the required number of points in the grid was determined by requiring accurate representation of the LPF. The orthogonality relation was used as the accuracy requirement. The numerically generated LPF were squared and integrated on the interval  $(-1,1)$ . The result was compared to the integral equation eigenvalue. As long as these values agreed to within one percent for the range of LPF of interest, the basis set was found to be accurate enough for the strip resonator modelling.

We now return to the problem of finding the modes of a strip resonator. The next section deals with the derivation of the matrix eigenvalue problem. Following this section, the matrix eigenvalue problem is solved and several useful results are discussed.

#### E. Derivation of the Matrix Eigenvalue Problem

Consider the application of the kernel expansion using the LPF as a basis set to solve the round trip equation for an aligned, single-ended, strip resonator. Recall that this equation is

$$\sigma u(x) = \sqrt{iF} \int_{-1}^1 dy e^{-i\pi F[g(x^2+y^2)-2xy]} u(y) \quad (2.22)$$

Note that when  $g = 0$  this equation is identical in form to the defining integral equation for the linear prolate functions, Eq(2.14). This case occurs when, for a single-ended resonator, the feedback mirror (mirror 1) is confocal with its image in the back mirror (mirror 2). This family of resonators lies on two hyperbolae in the stable region of the  $g_1 - g_2$  stability diagram. (See Figure 2.2) This special class of resonators which have the LPF as exact solutions has not been noted previously in the literature.

We now transform Eq(2.22) into the Horwitz standard form. (Ref 19) The details are contained in Appendix 2. The resultant integral equation is

$$\mu h(x) = \sqrt{\frac{it}{\pi}} \int_{-1}^1 dy e^{-it(y - \frac{x}{M})^2} h(y) \quad (2.23)$$

where the eigenfunctions are related by

$$u(x) = h(x) e^{-i\pi F_{eff} x^2} \quad (2.24)$$

and where the effective Fresnel number is defined as

$$F_{eff} = \frac{F}{2} \left( M - \frac{1}{M} \right) \quad (2.25)$$

The magnification is defined by

$$M = g + \sqrt{g^2 - 1} \quad (2.26)$$

with  $t = \pi MF$  and  $\mu = \sigma \sqrt{M}$ .

Note that Eq(2.23) is most applicable to unstable resonators because of the definition of magnification, and the discussion that follows assumes the strip resonator is unstable. However, note that in the stable region,  $g < 1$ , and the magnification becomes a complex number of magnitude one and the effective Fresnel number becomes pure imaginary. The exponential factor in Eq(2.24) is then gaussian, and the notion of Hermite-gaussian functions for the stable resonator modes arises naturally. (In Appendix 6, we derive a MEVP from Eq(2.22) directly. This MEVP is more applicable to stable strip resonators. In Appendix 7, we derive a MEVP for a resonator with cylindrical symmetry using the circular prolate functions (CPF) as a basis set.)

Next, we expand the exponent in Eq(2.23). Defining  $c = 2t/M$  and using the expansions,

$$e^{icxy} = \sum_{r=0}^{\infty} i^r \sqrt{\frac{2\pi}{c\gamma_r}} \psi_r(x) \psi_r(y) \quad , \quad (2.27)$$

and

$$v(x) = \sum_{r=0}^{\infty} b_r i^{-\frac{r}{2}} \gamma_r^{-\frac{3}{4}} \psi_r(x) \quad , \quad (2.28)$$

one can obtain a matrix eigenvalue problem (MEVP) for the strip resonator modes. (Again, the details are contained in Appendix 2.) The choice of the particular expansion in Eq(2.28) causes the resultant MEVP to have the same complex-symmetric nature that the integral equation had. The MEVP is

$$\mu b_m = \sum_{n=0}^{\infty} B_{mn} b_n \quad (2.29)$$

where

$$B_{mn} = \sqrt{iM} i^{\frac{m+n}{2}} (\gamma_n \gamma_m)^{-\frac{1}{2}} \int_{-1}^1 dx e^{-it(1+\frac{1}{n^2})x^2} \psi_n(x) \psi_m(x) \quad (2.30)$$

Since the complex-symmetric nature is retained, the eigenvectors of this matrix exhibit the same orthogonality property that the eigenfunctions had. The solution of the MEVP gives the eigenvalues of the bare cavity modes and the expansion coefficients  $b_n$ . These coefficients are used to reconstruct the bare cavity modes via this equation:

$$u(x) = e^{i\pi F_{eff} x^2} \sum_{n=0}^{\infty} b_n i^{-\frac{n}{2}} \gamma_n^{-\frac{1}{2}} \psi_n(x) \quad (2.31)$$

Clearly we obtain all the modes only in the case where the MEVP is infinite-dimensional. In practice, the dimensionality is finite, and restricts the number of bare cavity modes that are accurately modelled. We now turn our attention to solving this MEVP and studying a problem of interest, the accuracy of the higher order modes as calculated by the asymptotic approach.

#### F. Solution of the Matrix Eigenvalue Problem

In this section we discuss how the matrix eigenvalue problem derived in the previous section is solved for several cases. The goal is to show the validity of the LPF

expansion, to exhibit its limitations and to obtain a tool to study the modes of a empty strip resonator. The MEVP was solved on a Control Data Corporation Cyber series computer available through the Aeronautical Systems Division at Wright Patterson AFB, Ohio. All computer codes were written in FORTRAN IV and the International Mathematics and Scientific Library (IMSL) subroutines were used whenever possible.

Prior to generating the matrix and finding the eigenvalues and expansion coefficients, it is necessary to generate the LPF as a basis set. This process was described earlier in Section D, Part 3. The LPF were stored on a disk file to be accessed by the MEVP code.

The matrix eigenvalue problem was solved in a straightforward manner. Since the aligned resonator modes can be separated into even and odd parity modes, the size of the matrix can be reduced by calculating only the matrix elements necessary for the parity of interest. In the code developed for this research, the even modes were found first and then the odd modes were computed. An additional advantage to having the symmetric matrix is that only the upper triangle of the matrix needs to be generated. Of the  $N^2$  elements, only  $N(N+1)/2$  need to be calculated. Once the matrix is generated, the IMSL routine "EIGCC" was used to find the eigenvalues and eigenvectors. The eigenvalues are those for the Horwitz standard form and need to be divided by the square root of the magnification to obtain the usual eigenvalues. The eigenvectors were written to a disk file for use by another program to generate the bare cavity modes

and obtain intensity and phase plots.

Clearly, the matrix size must be limited to some dimension,  $N$ . The smaller the value of  $N$ , the faster the MEVP can be solved, but fewer bare cavity modes are accurately modelled. (If  $N$  is too small, none of the modes are accurately modelled. See Eq(2.32) below.) Streifer showed that the linear prolate functions are the basis set that allows the lowest value of  $N$  since these functions are related to the Schmidt expansion functions for the bare cavity kernel. (Ref 25) In practice, we found that to adequately resolve the eigenvalue of the lowest loss mode,  $N$  needed to satisfy the relation

$$N \geq \frac{2c}{\pi} \quad (2.32)$$

In terms of the Fresnel number,  $F = \frac{a_1^2}{2g_2 \lambda L}$ , this relation is  $N \geq 4F$ .

However, in order to obtain the higher order modes and the expansion coefficients,  $N$  needs to be larger than this. No specific criterion was apparent in the studies and each case should be treated separately. By looking at the magnitude of the expansion coefficients of mode of interest, and insuring that the smallest coefficient is at most a ten-thousandth of the largest coefficient, one is reasonably sure that the mode is accurately modelled. Each case studied in the next section used a value of  $N$  that was sufficiently large that the use of additional LPF did not alter the eigenvalues by more than 0.01% or visibly alter the intensity profiles of

the bare cavity modes.

### G. Results

In this section we study a number of topics that utilize the analysis of the previous sections. First, we study the numerical convergence issues for the particular case of  $M = 2.5$  and  $F_{eff} = 0.6$ . This study exercises the codes and exhibits their limitations. This particular case was chosen for two reasons: (1) the value for  $c$  is small, so the matrix was small, allowing many runs for low cost, and (2) the case has been cited in the literature by several authors. (Ref 1, 35, and 36) Second, we validate the analysis and the codes by comparing the results obtained with different solution techniques for several different cases. The techniques used were the iterative approach where the integral equation is solved with the method of successive approximations (MOSA), the asymptotic approaches of Moore and McCarthy (Ref 20) and Horwitz (Ref 19), and the kernel expansion using the LPF. The MOSA approach only yields the lowest loss mode and eigenvalue. Also, for specific cases, comparison could be made with other published data or data provided by Dr. Alan Paxton of the Air Force Weapons Laboratory, Kirtland AFB, NM. Third, we study the behavior of the eigenvalues near a mode crossing where the two lowest loss eigenvalues have nearly the same magnitude. The crossing that was analyzed occurred near  $M = 3$  and  $F_{eff} = 1.8742$ . Fourth, the kernel expansion technique, now thoroughly validated, was applied to examining the validity of the asymptotic approach at low effective

Fresnel numbers. This study is significant because of some of the assumptions made in the asymptotic analysis. The section concludes with a numerical demonstration of the orthogonality of the eigenmodes of the strip resonator. Although this property can be shown analytically (see Appendix 1), it serves as an additional validation of the computer codes and is of some use in the study of loaded cavity modes.

#### 1. Numerical Convergence

We consider the case of  $M=2.5$  and  $F_{eff}=0.6$ . The issue is how many points and how many LPF are needed to obtain accurate results. First, note the parameter  $c$  can be calculated using the equation

$$c = \frac{4\pi M F_{eff}}{M^2 - 1} \quad (2.33)$$

This particular case was chosen because the value of  $c$  is low, namely,  $c = 3.5903914$ . Also, Rensch and Chester have studied this case and their work has been cited by other authors. The cut-off criteria given in Eq(2.32) indicates that  $N$  should be about 3 in order to accurately give the lowest loss eigenvalue. In order to validate the results, we examine the case where  $N$  is much larger than this value. An  $N$  of 14 was found adequate to resolve the first several eigenvalues (by comparison to other methods). Also, one needs to have a suitably fine grid. For this case, we

find that having 250 points or more in a nonuniform grid which is finer near  $z=1$  provides adequate resolution. However, as a baseline, we use 723 points to insure good resolution. Using these parameters, we solve the matrix eigenvalue problem. Table II-1 shows the eigenvalues obtained. We choose the usual convention that the eigenvalues be ordered by magnitude. Higher order eigenvalues were obtained but are not shown because (1) they may not be adequately resolved and (2) they are of such a high loss that they are not of practical interest. Figures 2.6 and 2.7 show the intensity and phase of the lower loss modes. In the next subsection, we compare these results to those obtained from other methods to check the external consistency of the LPF expansion. Here we focus on internal consistency. As noted earlier, these modes are constructed using the linear prolate function expansion. Thus, studying the behavior of the expansion coefficients tells us if convergence has been obtained. Table II-2 contains data for various number of LPF being used in the expansion. The coefficients listed are the first eight coefficients for the expansion of the lowest loss mode. The eigenvalues are also listed. The entries are listed by magnitude and phase. The number of points used in the nonuniform grid was 547. Two facts are readily evident from Table II-2. First, the magnitude of the coefficients decreases for higher order LPF. Second, the addition of more LPF in the expansion does not alter the coefficients of the lower order LPF. Also, note the eigenvalue of the lowest loss mode has converged when

TABLE II-1.

Magnitude of the Mode Eigenvalues  
 $M = 2.5$                        $F_{\text{eff}} = 0.6$

mode index	kernel expansion	asymptotic expansion	iterative technique
0	1.19	1.18	1.19
1	0.83	0.81	--
2	0.60	0.61	--
3	0.30	0.46	--
4	0.09	0.42	--

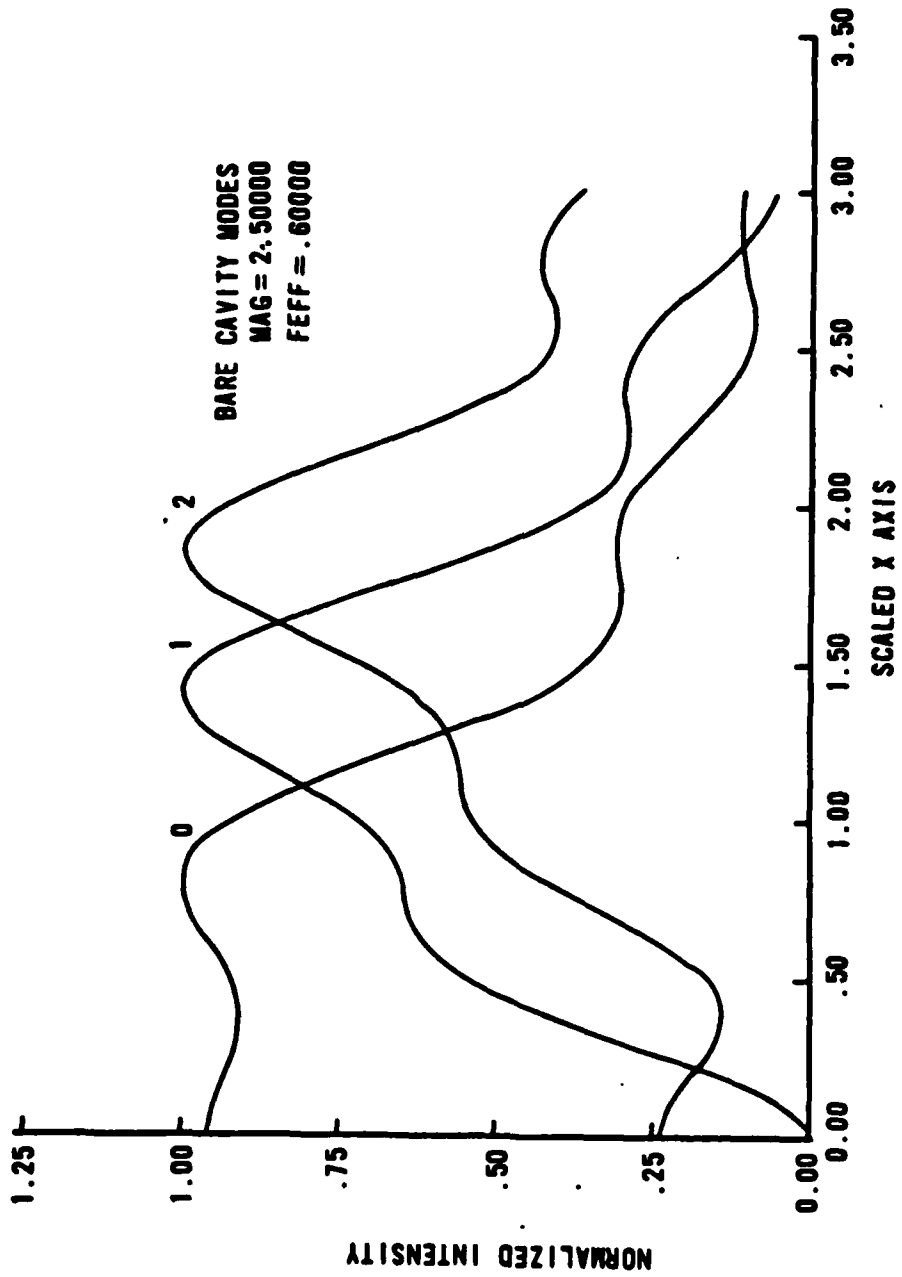


Figure 2.6 Bare Cavity Modes - Intensity.

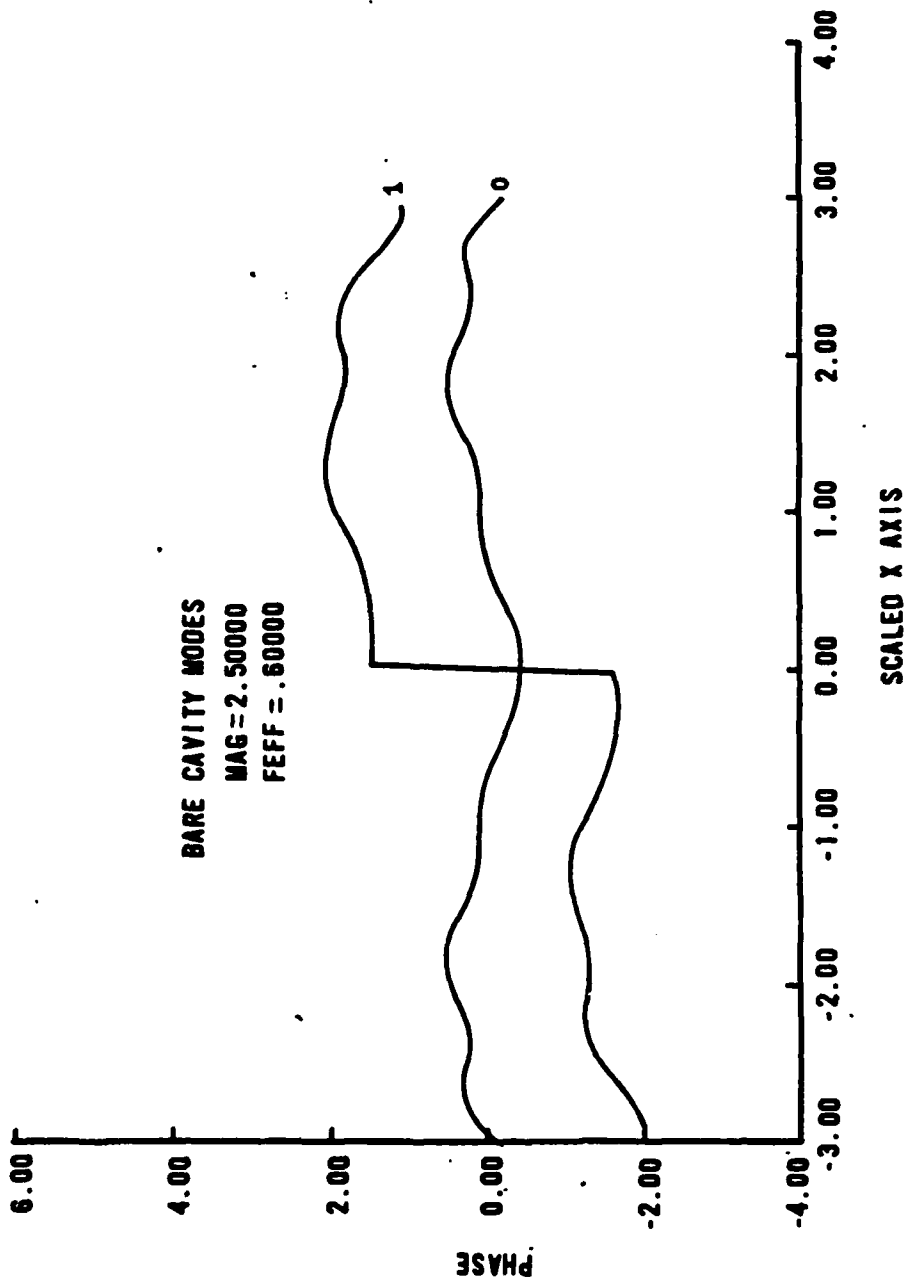


Figure 2.7 Bare Cavity Modes - Phase.

TABLE II-2.

Coefficients for  $u(x)$   
As a Function of Number of LPF  
 $M = 2.5$   $F_{eff} = 0.6$

coeff	Number of LPF					
	2	4	6	8	10	12
$ b_0 $ $\times b_0$	0.807 0.0	0.800 0.0	0.800 0.0	0.800 0.0	0.800 0.0	0.800 0.0
$ b_2 $ $\times b_2$	0.362 -0.650	0.360 -0.592	0.360 -0.591	0.360 -0.591	0.360 -0.591	0.360 -0.591
$ b_4 $ $\times b_4$	---	7.34E-3 -0.607	7.33E-3 -0.607	7.33E-3 -0.607	7.33E-3 -0.607	7.33E-3 -0.607
$ b_6 $ $\times b_6$	---	---	1.42E-5 -0.483	1.42E-5 -0.483	1.42E-5 -0.483	1.42E-5 -0.483
$ b_8 $ $\times b_8$	---	---	---	8.85E-9 -0.309	8.85E-9 -0.309	8.85E-9 -0.309
$ b_{10} $ $\times b_{10}$	---	---	---	---	2.44E-12 -0.239	2.44E-12 -0.239
$ b_{12} $ $\times b_{12}$	---	---	---	---	---	3.26E-16 -0.280
$ A_0 $ $\times A_0$	1.1721 -0.1278	1.1873 -0.1427	1.1874 -0.1428	1.1874 -0.1428	1.1874 -0.1428	1.1874 -0.1428

Number of points in the grid = 547 .

THIS PAGE INTENTIONALLY LEFT BLANK

four LPF have been included in the expansion. This is in good agreement with the criteria established in Eq(2.32). Similar behavior in the coefficients and the eigenvalues are observed for the higher order modes. Although no precise criteria was evident as to when enough LPF have been included for a particular higher order mode (owing to the small number of cases studied), the coefficients exhibit a sharp decrease in magnitude after a certain order of LPF. Table II-3 shows the magnitude of the expansion coefficients of the first eight modes for the case at hand. The sharp decrease is evident. This decrease mirrors the behavior of the integral equation eigenvalue of the LPF and it is the primary reason to consider the LPF as an expansion set. The cases studied to date indicate that the higher order mode has been adequately modeled when the magnitude of the higher order coefficient has decreased four orders of magnitude. This criteria should be treated as a rule of thumb and not a firm cut-off.

We next turn to examining the number of points required to obtain convergence. Here, the major source of error is the numerical generation of the LPF. The errors in the LPF show up in the calculation of the matrix elements and thus in the eigenvalues and eigenvectors. In fact, a very slight deviation from even or odd parity became evident when the LPF expansion was used to confirm numerically the orthogonality relation of the bare cavity modes. This point will be discussed in greater detail later.) In all the mode

calculations discussed in this report, the LPF were calculated so that the eigenvalue,  $\gamma_{\alpha}$ , calculated by numerical quadrature was within one percent of the value obtained from the series expansion for the range of LPF of interest. Table II-3 shows how the expansion coefficients and eigenvalue of the lowest loss mode varied as more points were taken. From this table, we conclude that 375 points appears to be adequate for the calculation of both the eigenvalue and the expansion coefficients. All the calculations made to date indicate that the numerical convergence is well-behaved and that the matrix eigenvalue problem can be readily solved. However, one is forced to concede that the criterion given in Eq(2.32) grows rapidly with increasing Fresnel number. Thus, the kernel expansion is limited inevitably by the size of the matrix required to adequately model the modes of interest. When the matrix gets very large, alternate techniques of extracting the dominant modes and eigenvalues may become more useful. Such techniques include the Krylov or Prony technique used by Siegman and Miller. (Ref 17) As an aside, it is noted that this behavior is not unique to kernel expansion techniques.

## 2. Validation of Approach

The kernel expansion technique using the linear prolate functions as a basis set can be validated by comparison to solutions obtained by other authors or other approaches. We study here the cases of  $( M , F_{eff} ) = ( 10.0 , 0.225 )$ ,  $( 2.5 , 0.6 )$ ,  $( 3.0 , 1.8742 )$ ,  $( 2.0 , 2.0 )$ ,

TABLE II-3.  
 Coefficients for  $u(x)$   
 As a Function of Number of Points on  $(-1,1)$   
 $M = 2.5$   $F_{eff} = 0.6$

coeff	Number of Points			
	223	375	623	723
$ b_0 $ $\pm b_0$	0.996 0.0	0.996 0.0	0.996 0.0	0.800 0.0
$ b_2 $ $\pm b_2$	0.448 -0.591	0.448 -0.591	0.448 -0.591	0.448 -0.591
$ b_4 $ $\pm b_4$	9.137E-3 -0.608	9.130E-3 -0.608	9.129E-3 -0.607	9.127E-3 -0.607
$ b_6 $ $\pm b_6$	1.772E-5 -0.483	1.772E-5 -0.483	1.772E-5 -0.483	1.772E-5 -0.483
$ b_8 $ $\pm b_8$	1.082E-8 -0.308	1.0978E-8 -0.309	1.099E-8 -0.309	1.102E-8 -0.309
$ b_{10} $ $\pm b_{10}$	3.156E-12 -0.345	3.058E-12 -0.264	3.043E-12 -0.249	3.029E-12 -0.234
$ b_{12} $ $\pm b_{12}$	4.551E-16 -0.524	4.151E-16 -0.341	4.100E-16 -0.305	4.037E-16 -0.269
$ u_0 $ $\pm u_0$	1.1873 -0.1428	1.1873 -0.1427	1.1874 -0.1428	1.1874 -0.1428

( 10.0 , 2.7 ), ( 2.0 , 2.5 ), and ( 2.0 , 4.0 ). These cases are ordered in increasing  $t$  , where

$$t = \frac{2 \pi M^2 F_{eff}}{M^2 - 1} \quad (2.34)$$

This parameter is used since it is the parameter of the asymptotic expansion used in the evaluation of Eq(2.23). The values of  $t$  for the cases listed above are, respectively, 1.43, 4.49, 13.2479, 16.8, 17.1, 20.9 and 33.5. Tables II-4 to II-10 list the magnitudes of the eigenvalues for these cases. In each table, results are included from an iterative calculation (except in the case of a mode crossing), an asymptotic calculation, and the LPF expansion. In the fourth and sixth cases, results are included from a paper by Henderson and Latham (Ref 18) where they calculate the even parity mode eigenvalues only.

A few general comments apply to most of these cases. The eigenvalues are ordered by decreasing magnitude. No definite pattern existed as to how the parity of the modes was ordered except that the lowest loss mode is always of even parity. The LPF expansion and the results from Henderson and Latham indicate that the eigenvalues will continue to decrease in magnitude without limit. However, the asymptotic approach predicts the eigenvalues decrease to a nonzero limit. This difference seems to be caused by an inherent approximation in the asymptotic approach. (Ref 17) We address this difference in more detail later.

TABLE II-4.

M = 10      Comparison of Eigenvalues       $F_{\text{eff}} = 0.225$        $t = 1.43$

l	approach	magnitude	phase	parity
0	L	1.2238	0.3169	even
	A	1.3336	0.2874	
	P	1.2238	0.3169	
1	L	0.1189	1.4893	odd
	A	0.1648	1.6052	
2	L	0.0050	-3.1235	even
	A	0.0834	-2.5736	
3	L	0.0001	-1.5204	odd
	A	0.0136	-1.7981	

NOTE: L = linear prolate function expansion  
 A = asymptotic approach (Ref 19)  
 P = power method (Ref 15)

TABLE II-5.

Comparison of Eigenvalues  
 $M = 2.5$        $F_{\text{eff}} = 0.600$        $t = 4.49$

l	approach	magnitude	phase	parity
0	L	1.1874	-0.1428	even
	A	1.1829	-0.1791	
	P	1.1875	-0.1428	
1	L	0.8249	0.1080	odd
	A	0.8059	0.0612	
2	L	0.6008	1.0130	even
	A	0.6120	0.9763	
3	L	0.3048	2.4379	odd
	A	0.4551	2.2756	
4	L	0.0887	-2.0817	even
	A	0.2132 *	-1.9724 *	

\* matched by phase

NOTE: L = linear prolate function expansion  
 A = asymptotic approach (Ref 19)  
 P = power method (Ref 15)

TABLE II-6.

Comparison of Eigenvalues  
 $M = 3.0$        $F_{\text{eff}} = 1.8742$        $t = 13.2479$

l	approach	magnitude	phase	parity
0	L	0.7762	-0.2472	even
	A	0.7691	-0.2654	
	P	-- *	-- *	
1	L	0.7758	0.2066	even
	A	0.1648	1.6052	
2	L	0.6155	-0.4191	odd
	A	0.6206	-0.4408	
3	L	0.4981	2.9994	even
	A	0.4799	2.9997	
4	L	0.4502	1.4978	odd
	A	0.4488	1.3443	
5	L	0.3451	-2.8463	odd
	A	0.4024	-2.5378	
6	L	0.0867	3.0994	even
	A	0.2620 **	2.9477 **	

\* no convergence with power method at mode crossing

\*\* mode matched by phase

NOTE: L = linear prolate function expansion  
 A = asymptotic approach (Ref 19)  
 P = power method (Ref 15)

TABLE II-7.

Comparison of Eigenvalues  
 $M = 2.0$        $F_{\text{eff}} = 2.0$        $t = 16.8$

l	approach	magnitude	phase	parity
0	L	1.0171	0.1440	even
	H&L	1.0166	0.1436	
	A	1.0166	0.1475	
	P	1.0169	0.1444	
1	L	0.8655	-0.4050	even
	H&L	0.8648	-0.4053	
	A	0.8611	-0.3896	
2	L	0.8000	-0.4593	odd
	A	0.8003	-0.467	
3	L	0.7249	0.6887	odd
	A	0.7498	0.6891	
4	L	0.6764	-2.0729	odd
	A	0.6250	-1.9121	
5	L	0.6389	-2.3080	even
	H&L	0.6390	-2.3056	
	A	0.5706 *	-2.2367 *	
6	L	0.5631	1.4217	even
	H&L	0.5676	1.4226	
	A	0.5815 *	1.4408 *	
7	L	0.4281	2.3134	odd
	A	0.5309 *	1.9765 *	
8	L	0.2576	-2.7802	even
	H&L	0.2765	-2.8085	
10	L	0.0866	-0.8142	even
	H&L	0.0865	-0.8145	

\* mode matched by phase

NOTE: L = linear prolate function expansion  
 H&L = moment method (Ref 18)  
 A = asymptotic approach (Ref 19)  
 P = power method (Ref 15)

TABLE II-8.

Comparison of Eigenvalues  
 $M = 10$        $F_{\text{eff}} = 2.7$        $t = 17.1$

l	approach	magnitude	phase	parity
0	L	0.9867	-0.1490	even
	A	0.9821	-0.1510	
	P	0.9869	-0.1492	
1	L	0.2863	1.0585	even
	A	0.2887	1.0248	
2	L	0.2620	-0.1299	odd
	A	0.2420	-0.1632	
3	L	0.1856	2.6926	odd
	A	0.1853	2.5633	
4	L	0.0164	-3.0127	even
	A	0.1036	-2.9009	

NOTE: L = linear prolate function expansion  
 A = asymptotic approach (Ref 19)  
 P = power method (Ref 15)

TABLE II-9.

Comparison of Eigenvalues  
 $M = 2.0$        $F_{\text{eff}} = 2.5$        $t = 20.9$

l	approach	magnitude	phase	parity
0	L	1.0770	-0.0437	even
	H&L	1.0762	-0.0434	
	A	1.0800	-0.0449	
	P	1.0771	-0.0436	
1	L	0.7966	0.0993	odd
	A	0.7925	0.1065	
2	L	0.7364	0.6257	even
	H&L	0.7448	0.7936	
	A	0.7545	0.6257	
3	L	0.7286	-1.0775	odd
	A	0.7062	-1.0752	
4	L	0.6780	-1.0873	even
	H&L	0.6753	-1.0829	
	A	0.6666	-1.0727	
5	L	0.6648	-3.1372	odd
	A	0.6525	-3.1400	
6	L	0.5858	1.4153	odd
	A	0.6410	1.4488	
7	L	0.4882	-2.9229	even
	H&L	0.4656	-2.3702	
	A	0.5125 *	-2.584 *	

\* mode matched by phase

NOTE: L = linear prolate function expansion  
 H&L = moment method (Ref 18)  
 A = asymptotic approach (Ref 19)  
 P = power method (Ref 15)

TABLE II-10.

Comparison of Eigenvalues  
 $M = 2.0$   $F_{\text{eff}} = 4.0$   $t = 33.5$

l	approach	magnitude	phase	parity
0	L	1.0103	0.1395	even
	A	1.0041	0.1312	
	P	1.0080	0.1412	
1	L	0.8907	-0.2741	even
	A	0.8745	-0.2798	
2	L	0.8264	-0.3177	odd
	A	0.8208	-0.3408	
3	L	0.8051	0.5725	odd
	A	0.8012	0.5799	
4	L	0.6630	1.0926	even
	A			
5	L	0.6434	-1.5555	even
	A	0.6488	-1.5651	
6	L	0.6158	2.7015	even
	A	0.6291 *	2.6988 *	
7	L	0.6020	-1.4957	odd
	A	0.6361 *	-1.5411 *	
8	L	0.5323	1.7890	odd
	A	0.6023 *	1.7545 *	
9	L	0.5318	-3.0623	odd
	A	0.5788 *	-2.8552 *	

\* mode matched by phase

NOTE: L = linear prolate function expansion  
 A = asymptotic approach (Ref 19)  
 P = power method (Ref 15)

We now briefly examine the various cases listed above. The first case,  $M=10.0$  and  $F_{eff}=0.225$ , has low values of both  $c$  and  $t$ . Thus the size of the matrix required is small and both the matrix and iterative schemes are in good agreement. However, the asymptotic code predicts eigenvalues that generally disagreed with the other approaches. This confirms that the asymptotic approach is not valid at very low Fresnel numbers. The intensity profiles from the iterative code and LPF expansion agreed as well.

The next case,  $M=2.5$  and  $F_{eff}=0.6$ , was the case studied most closely. As Table II-5 shows, all three methods gave the same lowest loss eigenvalue to three significant digits. Even though  $t = 4.49$ , the LPF expansion and the asymptotic code agreed well for the first two lowest loss eigenvalues. The intensity and phase plots of the eigenmodes agreed well for the first three modes. In addition, calculations made by Dr Paxton of the Air Force Weapons Laboratory for this case predicted the same lowest loss mode shape. However, the mode shape doesn't agree well with the same case as calculated by Rensch and Chester. (Ref 35) In Ref 35, an aperture is placed at the back mirror and thus more spatial structure is introduced in the mode. Note that the LPF expansion and the asymptotic method give very different eigenvalues for the higher order modes. In fact, some of the solutions given by the asymptotic method seem to be spurious solutions that do not correspond to any mode predicted by the LPF expansion.

The third case,  $M=3.0$  and  $F_{eff}=1.8742$ , was chosen

because this case is very near a mode crossing, where the two lowest loss mode eigenvalues have the same magnitude. This case will be discussed separately after this brief review of the various cases. We restrict our examination here to the close match between the LPF expansion and the asymptotic method. Note first that the iterative approach takes an extremely long time to converge near a mode crossing. Near a mode crossing, the outcoupling between the two lowest loss modes is so nearly identical that the code cannot efficiently discriminate between them. (The same problem arises in the study of stable resonators using the iterative method.) Now the LPF expansion and the asymptotic method give good agreement out to the fourth even eigenvalue, but after this eigenvalue, the two codes disagree. The eigenvalues predicted by the LPF expansion continue to decrease toward zero but the asymptotic approach predicts eigenvalues that tend to a finite limit. Note also that the asymptotic approach predicted the mode crossing at  $F_{eff} = 1.8675$  for  $M = 3.0$  while the LPF expansion predicted the mode crossing at  $F_{eff} = 1.8742$ . The difference is most likely due to the low effective Fresnel number which is near the limits of the asymptotic approach.

Let us examine the cases of  $M = 2.0$ ,  $F_{eff} = 2.0$  and  $M = 2.0$ ,  $F_{eff} = 2.5$  at the same time. Here we can use the results given by Henderson and Latham as an additional comparison. (Ref 18) However, note that they only consider even parity modes. In both cases, good agreement is found

between the four methods for the lowest loss mode. The LPF expansion and the matrix method used by Henderson and Latham agree well to the limit of the data available. In the first case, this is at the tenth eigenvalue while the second case is limited to the seventh eigenvalue. The asymptotic code predicted eigenvalues in good agreement with the other two methods, except at the higher order eigenvalues the asymptotic code gave many possible eigenvalues that all have about the same magnitude. In some instances, one could not even match any values to the eigenvalues predicted by the LPF expansion. One should observe that the value of  $t$  is large enough in both cases that the asymptotic method should be valid. We conclude that the first few lower loss eigenvalues predicted by the asymptotic approach are probably accurate, but advise caution if the higher order eigenvalues (and eigenmodes) are to be used.

We examine the case of  $M = 10.0$  and  $F_{eff} = 2.7$  because it allows an examination of eigenvalue behavior at large magnification. Here, the LPF expansion, the asymptotic approach and the iterative approach all agreed well for the lowest loss eigenvalue. The LPF expansion and the asymptotic approach agreed well through the third eigenvalue but for higher loss modes, the eigenvalues did not agree. Those predicted by the asymptotic approach level off and those predicted by the LPF expansion continue to decrease toward zero. Again, this behavior is most likely due to the approximations made in the asymptotic approach, as pointed out by Horwitz. (Ref 19)

Finally, we look at the case of  $M = 2.0$ ,  $F_{eff} = 4.0$ . This case was at the limit of the LPF expansion code due to memory limitations imposed by the computer system. As seen from Table II-10, the lowest loss eigenvalue is predicted to be about 1.01 by the three techniques (LPF expansion, asymptotic approach and iterative approach). Fairly good agreement was found between the LPF expansion and the asymptotic approach up to the fifth eigenvalue. After this value, the asymptotic code predicts eigenvalues with magnitude of about 0.6 to 0.55, while the LPF expansion predicts the eigenvalues continue to decrease.

From the examination of these and other cases, we conclude that the LPF expansion is a valid technique and that the numerical codes used to generate and solve the MEVP gave results that agreed with those given by other methods. Also, the intensity and phase plots of the lower loss eigenmodes agreed between the asymptotic and iterative approaches and the LPF expansion. The advantage of the LPF expansion is that the eigenmodes and their eigenvalues can be computed fairly quickly and with good accuracy. The asymptotic codes are computationally faster but the higher loss modes may not be correct. The iterative scheme is limited to predicting the lowest loss mode only, unless more elaborate techniques (such as Gram-Schmidt orthogonalization) are used. Other matrix approaches such as the one used by Henderson and Latham also give good results for higher order modes. The value of one basis set versus another is determined by the

geometry and computer resources available. While the LPF should give the N-term best expansion, one must still generate the LPF basis set. This requires only a small amount of computer time. Also, the LPF are applicable to rectangular geometries. For cylindrical coordinates, the appropriate basis set is the circular prolate functions.

### 3. Studies of eigenvalues near a mode crossing

Let us now return to the case of the mode crossing. In order to find a mode crossing, one can hold the magnification constant and vary the effective Fresnel number over some range. The mode crossings are usually said to be near integer values of effective Fresnel numbers while the maximum mode separation (in the sense that the two lowest loss eigenvalues are widely separated) usually is said to occur near half-integer Fresnel numbers. (Ref 1) Often one tries to design the resonator so that it has a half-integer Fresnel number to avoid possible mode competition during laser operation. However, the waveguide analysis done by Vainstein indicated that the mode crossings occur at  $n + 7/8$  and the maximum mode separations occur at  $n + 3/8$ . (Ref 9) Numerical studies done with both the asymptotic approach and the LPF expansion support the results from Vainstein. For  $n = 1$ , there should be a mode crossing at approximately 1.875 and such a crossing was found at 1.8742 (via the LPF expansion). The asymptotic code predicted this crossing at 1.8675. This is in good agreement with the LPF expansion results considering the low Fresnel number.

In order to establish the mode crossing precisely, a range of effective Fresnel numbers from 1.3 to 2.4 was examined. Figure 2.8 shows a plot of the four lowest loss eigenvalues in the complex plane. The abscissa is the real part of the eigenvalue while the ordinate is the imaginary part of the eigenvalue. The diagram contains a large amount of information and is fully discussed by Horwitz (Ref 19) and Sanderson and Streifer (Ref 22). Our purpose in showing the diagram is to find the mode crossing but the interested reader is referred to these excellent articles for further insight. The mode crossing is indicated by the arrows. Note that the eigenvalues are nearly complex conjugates. (See Table II-6.) Also, note that only the even parity eigenvalues contribute to the peak near  $\text{Re}(\sigma) = 1$ . In fact, Horwitz's calculations show that for large effective Fresnel numbers, the lowest loss mode splits off in a circle about this value and the higher loss modes circle about the origin. The odd modes always circle about the origin with a radius of less than unity. This splitting off of the lowest loss mode from the other modes is only observed in the strip case. Butts and Avizonis (Ref 21) found that the eigenvalues interleave for all values of effective Fresnel number in the case of circular mirrors. Figure 2.9 shows a plot of the outcoupling versus the effective Fresnel number. The outcoupling is defined as

$$\delta = 1 - \frac{|\lambda|^2}{M} \quad (2.35)$$

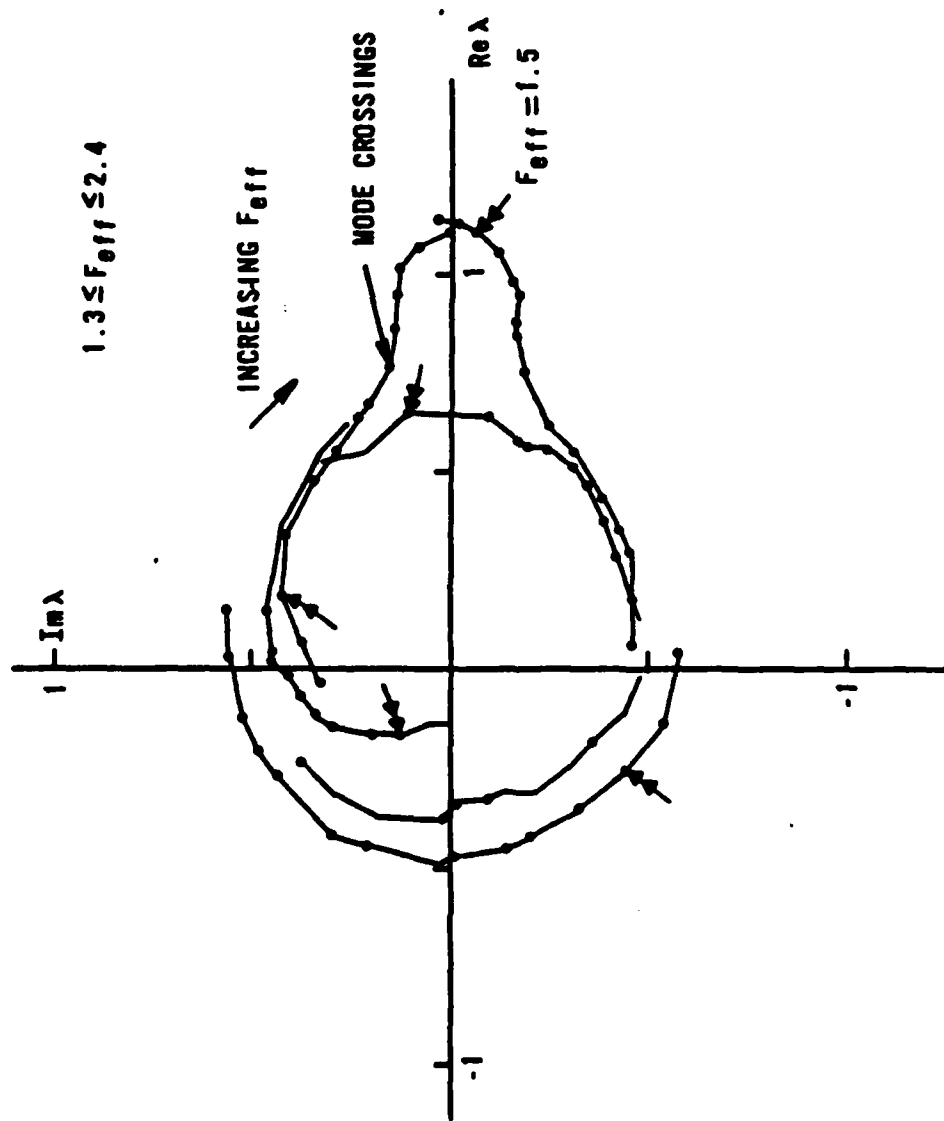


Figure 2.8 Behavior of Eigenvalues with Varying Fresnel Number.

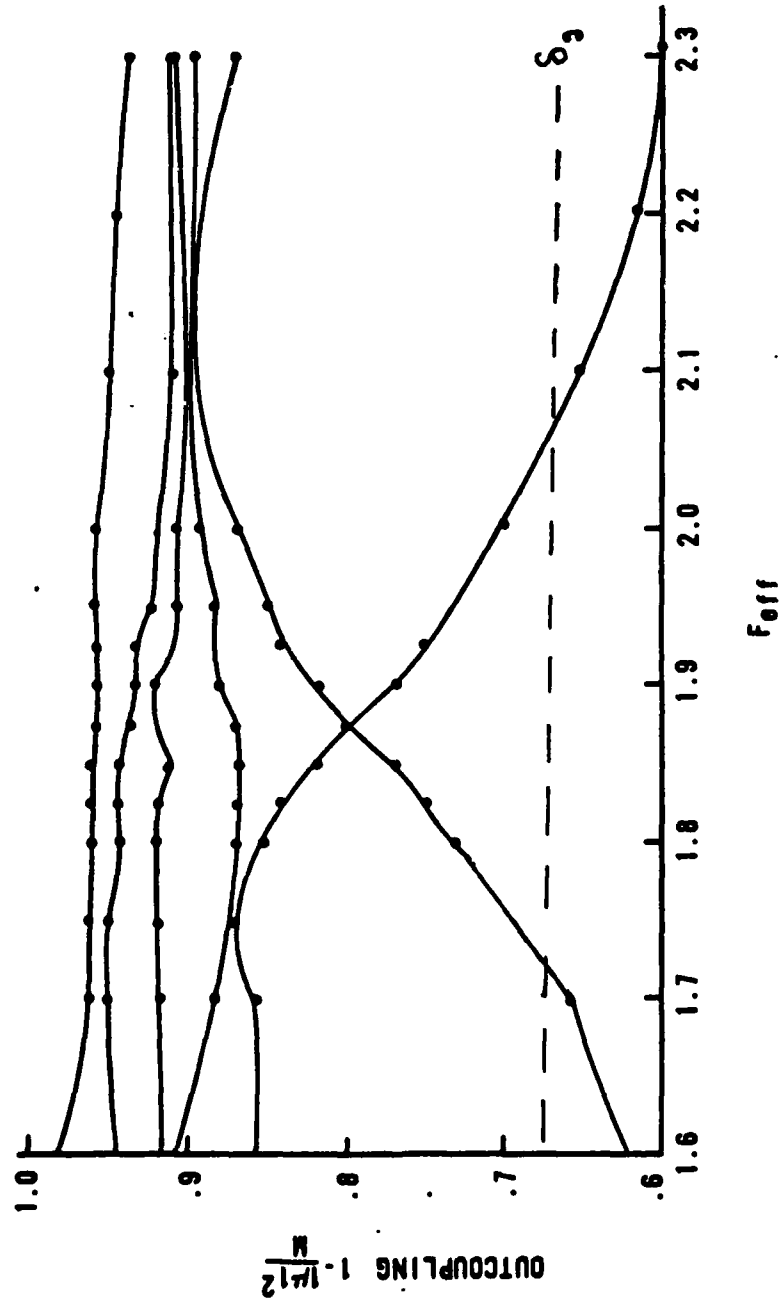


Figure 2.9 Behavior of Outcoupling with Varying Fresnel Number.

The outcoupling is thus related to the magnitude of the eigenvalues and characterizes the loss of a given mode. A line is drawn on this figure for the geometric outcoupling, defined as  $\delta_g = 1 - 1/M$ . (These formulae apply to strip resonators only.) In this figure, the mode crossing is clearly evident. The point of this discussion has been to elaborate on how one finds a mode crossing and to illustrate the behavior of the eigenvalues. The results also serve as an additional validation of the LPF expansion technique.

#### 4. Study of the asymptotic approach at low Fresnel numbers

We now discuss the validity of the asymptotic approach at low effective Fresnel numbers. This discussion uses the results discussed earlier. We found that the first few eigenvalues and eigenmodes were in good agreement with the iterative approach and the LPF approach as long as the asymptotic expansion parameter,  $t$ , was greater than 4. This is rather remarkable, considering the nature of the asymptotic expansion. Smith also found good agreement for the lowest loss mode using the asymptotic technique and comparing to results obtained by Rensch and Chester. (Ref 35) However, as Horwitz suggested, the "leveling off" phenomena observed for the higher loss eigenvalues seems to be due to the approximations inherent in asymptotic approach. (Ref 19, p.1533) In particular, an approximation is made to get the expansion in the form of a set of expansion functions. Without this approximation, the method would not work, for it is here that the diagonalization of the matrix eigenvalue

problem occurs and the reduction of the MEVP to a polynomial problem results. It is also here that the increased computational speed is obtained, but this approximation is the one that causes the higher order modes to be incorrect. It appears from the results obtained to date that some of the higher order modes may even be spurious solutions and not physical modes at all. So we conclude that the asymptotic approach is extremely useful for finding the lower loss bare cavity modes for effective Fresnel numbers larger than 1 and large magnifications. However, caution is advised if the higher loss modes are needed. (For example, one would need these modes if the bare cavity modes are used as a basis set.) Then, more costly but more accurate matrix techniques should be used.

##### 5. Demonstration of the orthogonality of the modes.

The final area in which we apply the LPF expansion is the demonstration of the orthogonality of the modes of the empty strip resonator. The orthogonality is shown in Eq(2.8) and is repeated here:

$$\int_{-a_1}^{a_1} u_i(x) u_j(x) dx = \delta_{ij}$$

This relation also served as a means of normalizing the bare cavity modes. We examine the two cases where  $M = 2.5$  and  $F_{eff} = 0.6$  and  $M = 3.0$  and  $F_{eff} = 1.8742$ . Tables II-11 and II-12 show the inner products for these two cases. In

TABLE II-11.

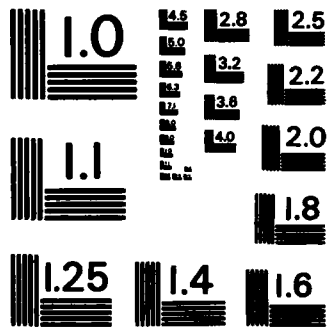
Demonstration of Orthogonality  
 $M = 2.5$                        $F_{\text{eff}} = 0.6$

n	m	$\left  \int_{-1}^1 u_n(x) u_m(x) dx \right $
0	0	1.000 *
0	1	1.045E-07
0	2	1.004E-04
0	3	1.037E-06
0	4	2.680E-04
0	5	2.946E-06
1	2	1.212E-07
1	3	1.989E-04
1	4	9.246E-08
1	5	3.804E-04
2	3	1.203E-06
2	4	3.972E-04
2	5	3.419E-06
3	4	9.174E-07
3	5	1.056E-03
4	5	2.608E-06

\* All inner products with same index are 1.000 .

NOTE: Fourteen LPF were used for generating the bare cavity modes. The grid had 523 points between  $x = -1$  and  $x = 1$  .





MICROCOPY RESOLUTION TEST CHART  
NATIONAL BUREAU OF STANDARDS-1963-A

TABLE II-12.

Demonstration of Orthogonality  
 $M = 3.0$        $F_{eff} = 1.8742$

$n$	$m$	$ \int_{-1}^1 u_n(x) u_m(x) dx $
0	0	1.000 *
0	1	5.706E-06
0	2	1.125E-03
0	3	2.176E-05
0	4	1.763E-03
0	5	1.714E-05
1	2	3.580E-06
1	3	1.063E-03
1	4	2.528E-06
1	5	1.032E-04
2	3	1.365E-05
2	4	1.296E-03
2	5	1.075E-05
3	4	9.642E-06
3	5	8.344E-04
4	5	7.592E-06

\* All inner products with same index are 1.000 .

NOTE: Thirty LPF were used for generating the bare cavity modes. The grid had 523 points between  $x = -1$  and  $x = 1$  .

each case, the orthogonality was clearly evident. The cases where the integrand was the product of an even and an odd mode should have given exactly zero but a detailed study showed that the LPF were not precisely even or odd when they were numerically generated. The value of this calculation is two-fold. First, the demonstration confirms the analytic derivation of the orthogonality of the eigenfunctions of a complex-symmetric kernel. Second, the demonstration further supports the utility of the linear prolate functions as a basis set. It would be interesting to use the modes generated by the asymptotic approach to perform the same calculation.

#### H. Summary

This chapter has considered the analysis of the modes of a strip resonator that does not contain a saturable gain medium. We have discussed the basic geometry of the strip resonator as well as the underlying approximations. Also, we discussed the round trip integral equation that describes the modes. In particular, the fact that the kernel is complex-symmetric is important in that the modes have a certain orthogonality property but the modes have not been shown to be a complete set. Even this orthogonality property is different from that of the hermitian kernels. After discussing the general kernel expansion approach as well as highlighting several other approaches to solving the integral equation, we discussed the linear prolate functions as an optimal basis set in the sense that the resulting matrix

eigenvalue problem was of as small a dimension as possible. The LPF were used to obtain a matrix eigenvalue problem and this MEVP was solved numerically. In obtaining this solution, a code was developed that rapidly generated the LPF over the interval  $(-1,1)$ . Such a code may have many other uses. The validity of the numerical model was demonstrated in many ways. First, internal consistency was shown. Then agreement with other solution techniques was demonstrated for many cases of effective Fresnel number and magnification. In this process, we examined the interesting case of a mode crossing where the two lowest loss modes have the same loss. Here the LPF expansion model had no difficulty in predicting the eigenvalues or the eigenfunctions. The eigenvalues of the two lowest loss modes were nearly a complex conjugate pair. We also used the LPF expansion model to examine the validity of the asymptotic approach at low Fresnel numbers. This is the most useful application to date. We found that the asymptotic approach gave good results for the lower loss modes even at effective Fresnel numbers near unity. However, the higher loss eigenvalues appeared to be incorrect owing to a limiting approximation in the asymptotic approach. Finally, we used the LPF expansion to demonstrate the orthogonality of the bare cavity modes. This calculation serves as a final validation of the LPF expansion as well as being of general interest. The result will also prove useful in the study of loaded cavity modes, a study that begins in the next chapter.

### III. Modal Analysis of Loaded Resonators

#### A. Introduction

A realistic model of the laser resonator must properly account for the presence of a saturable gain medium. This analysis is made difficult because the gain depends on the field, making the equations nonlinear. This chapter begins with Maxwell's equations and ends with a round trip equation that describes the modal structure of the loaded strip resonator. In obtaining this final equation, all relevant assumptions and restrictions are discussed. The approach is rigorous and the intermediate results are applicable to more general resonators.

#### B. Derivation of Active Medium Propagator

Consider an isotropic, nonmagnetic medium that contains no currents or free charges. Further, assume the fields are time harmonic, with an  $\exp(i\omega t)$  dependence. Then Maxwell's equations in differential form and MKS units are

$$\nabla \times \bar{E}(\bar{r}, \omega) = -i\mu_0 \omega \bar{H}(\bar{r}, \omega) \quad (3.1)$$

$$\nabla \times \bar{H}(\bar{r}, \omega) = i\omega \bar{D}(\bar{r}, \omega) \quad (3.2)$$

$$\nabla \cdot \bar{D}(\bar{r}, \omega) = 0 \quad (3.3)$$

$$\nabla \cdot \bar{H}(\bar{r}, \omega) = 0 \quad (3.4)$$

In order to account for the interaction between the medium and the field, assume that

$$\bar{D}(\bar{r}, \omega) = \epsilon_0 [1 + \chi(\bar{r}, \omega)] \bar{E}(\bar{r}, \omega) \quad (3.5)$$

where the susceptibility is allowed to be complex:

$$\chi(\bar{r}, \omega) = \chi'(\bar{r}, \omega) + i\chi''(\bar{r}, \omega) \quad (3.6)$$

Suppressing the frequency dependence for the moment and considering Cartesian coordinates such as will be used in the strip resonator, the wave equation for the electric field is obtained by taking the curl of Eq(3.1) and using Eq(3.2) and Eq(3.5):

$$\nabla \times \nabla \times \bar{E} = \nabla(\nabla \cdot \bar{E}) - \nabla^2 \bar{E} = \mu_0 \omega^2 \epsilon_0 [1 + \chi] \bar{E} \quad (3.7)$$

Now

$$\nabla \cdot \bar{D} = \epsilon_0 [\nabla \cdot \bar{E} + \nabla \cdot \chi \bar{E}] \quad (3.8)$$

$$= \epsilon_0 [\nabla \cdot \bar{E} + \nabla \chi \cdot \bar{E} + \chi \nabla \cdot \bar{E}] \quad (3.8a)$$

and solving for the divergence of the electric field,

$$\nabla \cdot \bar{E}(\bar{r}) = \frac{-1}{1 + \chi(\bar{r})} \nabla \chi \cdot \bar{E}(\bar{r}) \quad (3.9)$$

Assuming the susceptibility varies slowly over one

wavelength, then  $\nabla \chi \cdot \bar{E} \approx 0$  and  $\nabla \cdot \bar{E} \approx 0$ . (Ref 37) Thus the wave equation becomes

$$\nabla^2 \bar{E} + \mu_0 \epsilon_0 \omega^2 [1 + \chi] \bar{E} = 0 \quad (3.10)$$

Defining

$$k^2 = \mu_0 \epsilon_0 \omega^2 = \frac{\omega^2}{c^2}, \quad (3.11)$$

then

$$\nabla^2 \bar{E} + k^2 \bar{E} = -k^2 \chi \bar{E} \quad (3.12)$$

The laser resonator acts to reinforce the field along the optical axis as discussed in Chapter 2. Thus we look for beam-like solutions to the wave equation. We write the field as

$$\bar{E}(\bar{r}) = \bar{\Psi}(\bar{r}) e^{-ikz} \quad (3.13)$$

and then find a differential equation for the complex amplitude function:

$$\nabla_{\perp}^2 \bar{\Psi} - 2ik \frac{\partial \bar{\Psi}}{\partial z} + \frac{\partial^2 \bar{\Psi}}{\partial z^2} = -k^2 \chi(\bar{r}) \bar{\Psi}(\bar{r}) \quad (3.14)$$

Here,  $\nabla_{\perp}$  refers to derivatives transverse to the optical axis (chosen as the  $z$  axis in the geometry set up in Chapter 2). Also, the term  $\frac{\partial^2 \bar{\Psi}}{\partial z^2}$  is neglected in the paraxial

approximation. This approximation is valid when the propagation distance is long compared to both the aperture size (height of the mirrors) and the wavelength. This implies that the variations in the field in the propagation direction occur over distances that are much greater than either the aperture size or the wavelength. For most resonators, the approximation is valid. Now this equation hold for each component of the field. We are mainly concerned with the components transverse to the optical axis and thus assume the field is polarized in one direction, defined as the x direction, i.e.,  $\vec{\Psi}(\vec{r}) = u(\vec{r}) \hat{i}$ . Then

$$\nabla_{\perp}^2 u(x,y,z) - 2ik \frac{\partial u(x,y,z)}{\partial z} = -k^2 \chi(x,y,z) u(x,y,z) \quad (3.15)$$

This is the paraxial wave equation that describes propagation through an active, inhomogeneous medium. If one neglects the transverse variations in the field by neglecting the transverse derivatives in Eq(3.15), one can define an intensity gain coefficient as related to the imaginary part of the susceptibility by

$$g_s(\vec{r}) = k \operatorname{Im} \chi(\vec{r}) \quad (3.16)$$

The intensity gain coefficient describes how the intensity (i.e. the square of the magnitude of the field) changes as the field propagates through the gain medium. The variations in the index of refraction as related to the real part of the susceptibility by

$$n(\vec{r}) = 1 + \frac{1}{2} \text{Re } \chi(\vec{r}) \quad (3.17)$$

The changes in the index of refraction cause phase shifts in the field that can be interpreted as optical path length differences (OPD).

Now the gain is nonlinearly related to the field since the medium equations are functions of the intensity, not the field. Properly, one should write  $g_s = g_s(\vec{r}, \omega, \vec{E})$  but this dependence on the electric field will be suppressed in the notation. Also note that the index of refraction is a function of both the frequency and the electric field. the phenomenon of anomalous dispersion arises if the frequency of the longitudinal resonator mode does not coincide with the line center of the laser transition. (Ref 6, page 156-8) In most of the analysis that follows, we will assume that the resonator modes oscillate at the center of the laser transition. This limitation is made to focus the attention on the saturable gain effects. The various nonlinear optics phenomena that also arise from expanding the susceptibility in a power series of the electric field lie outside the scope of this effort.

We now formally treat the right hand side of Eq(3.15) as a known function and use a Green's function to transform the differential equation into an integral equation. Appendix 3 contains the details of this transformation for the three dimensional case discussed here as well as the two

dimensional case to be treated later. The resultant equation is

$$u(x,y,z) = u_h(x,y,z) + u_i(x,y,z) \quad (3.18)$$

where

$$u_h(x,y,z) = \frac{ik}{2\pi} \iint_{-\infty}^{\infty} dx'dy' \frac{e^{-\frac{ik}{2z}[(x-x')^2+(y-y')^2]}}{z} u(x',y',0) \quad (3.19)$$

and

$$u_i(x,y,z) = \frac{k}{4\pi} \int_0^z dz' \iint_{-\infty}^{\infty} dx'dy' \frac{e^{-\frac{ik[(x-x')^2+(y-y')^2]}{2(z-z')}}}{(z-z')} k\chi(x',y',z') u(x',y',z'). \quad (3.20)$$

This equation can be used to propagate a scalar field through an active, inhomogeneous medium. This analysis to this point closely follows Milonni. (Ref 37) Note that the range of the transverse variables is the infinite interval. When these equations are applied to the resonator problem, we will find that this range is restricted by the mirror apertures.

The term  $u_h$  in Eq(3.18) represents the diffraction of the original field in the plane  $z = 0$ . This is the familiar Fresnel diffraction integral. However, the term  $u_i$  in Eq(3.18) represents the contribution to the final field due to the radiation stimulated as the original field propagates through the medium. Clearly, if the susceptibility is zero, then the equation reduces to the Fresnel propagator commonly used in resonator studies.

We now specialize the analysis for the strip resonator.

Here we assume  $\frac{\partial u}{\partial y} = 0$  and that  $\chi = \chi(x, z)$  only. (Although these assumptions are physically difficult to realize, they allow an understanding of how the physics works while keeping the analysis as simple as possible.) Then the wave equation can be written in a two-dimensional form:

$$\frac{\partial^2 u}{\partial x^2} - 2ik \frac{\partial u}{\partial z} + k^2 \chi(x, z) u(x, z) = 0 \quad (3.21)$$

Here, an appropriate Green's function is

$$G(x, z, x', z') = \sqrt{\frac{\lambda}{i}} \frac{e^{-\frac{i\pi(x-x')^2}{\lambda(z-z')}}}{\sqrt{z-z'}} \quad (3.22)$$

This Green's function and the propagator given below are derived in detail in Appendix 3. As before, an integral equation that describes the propagation of the field through an active, inhomogeneous medium is obtained. The same designations for the fields will be used since throughout the rest of the analysis, we will only be concerned with two dimensional fields. Letting the initial plane be at  $z = 0$ , the two dimensional propagator is

$$u(x, z) = u_h(x, z) + u_i(x, z) \quad (3.23)$$

where

$$u_h(x, z) = \sqrt{\frac{i}{\lambda z}} \int_{-\infty}^{\infty} dx' e^{-\frac{i\pi(x-x')^2}{\lambda z}} u(x', 0) \quad (3.24)$$

and

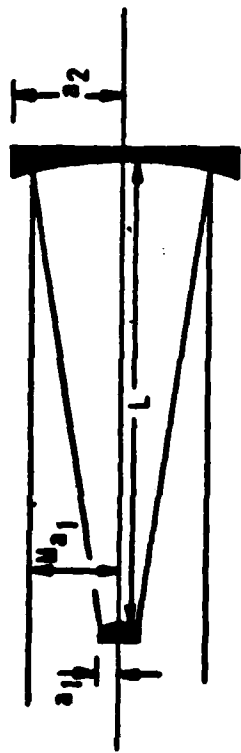
$$u_i(x, z) = \frac{1}{2} \sqrt{\frac{1}{i\lambda}} \int_0^z dz' \int_{-\infty}^{\infty} dx' \frac{e^{-\frac{i\pi(x-x')^2}{\lambda(z-z')}}}{\sqrt{z-z'}} k \chi(x', z') u(x', z'). \quad (3.25)$$

This concludes the derivation of a propagator appropriate to the strip resonator geometry.

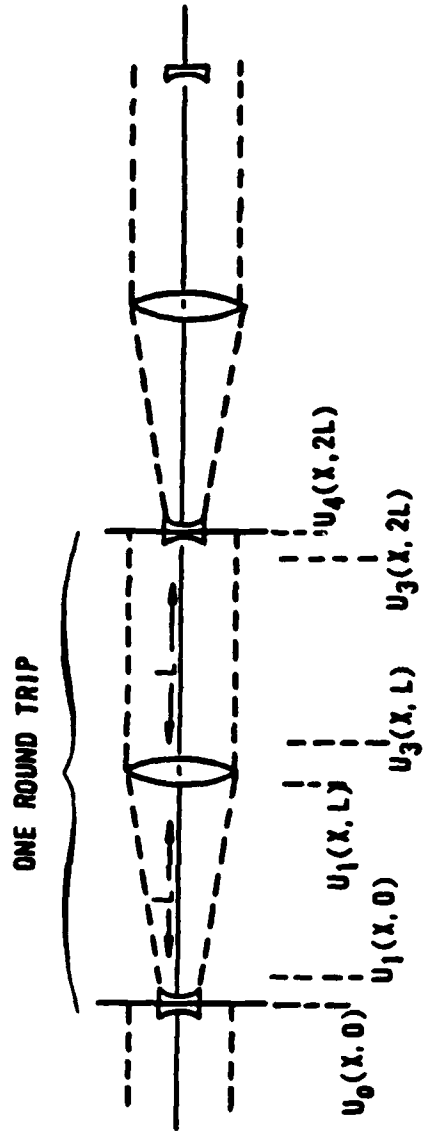
### C. Round Trip Integral Equation for Loaded Strip Resonator

We now use this propagator to derive a round trip integral equation for the modes of an aligned, strip resonator with mirrors of spherical curvature. In the paraxial approximation, the round trip is equivalent to propagating through the lens train shown in Figure 3.1. In this figure, the fields  $u_i$  are calculated in a manner analogous to the derivation of the round trip equation for the bare cavity. This lengthy but straightforward derivation is contained in Appendix 4. Also, we now restrict the susceptibility to be pure imaginary. Thus, neither index variations nor anomalous dispersion will be treated in the ensuing analysis. Although this limits the analysis to be applicable only to homogeneous media lasing at line center, the analysis still gives valuable insight into how gain is included in resonator mode calculations. Thus the susceptibility is replaced by the term in Eq(3.16). The final result can be expressed as the sum of three terms:

$$u_4(x, 2L) = I_0(x) + I_1(x) + I_2(x) \quad (3.26)$$



(a)



(b)

Figure 3.1 Single-ended Unstable Resonator (a) Resonator Geometry (b) Equivalent Lens Train.

where

$$I_0(x) = \frac{\sqrt{iF}}{a_1} \int_{-a_1}^{a_1} dx' e^{-\frac{i\pi F}{a_1} [g(x^2+x'^2) - 2xx']} u_0(x', 0) \quad (3.27)$$

and

$$I_1(x) = \frac{1}{2} \sqrt{\frac{i}{\lambda L}} \int_0^L dz' \int_{-\infty}^{\infty} dx' \frac{e^{\frac{i\pi}{\lambda} \left[ \frac{(x-x')^2}{L_e(z')} - \frac{g_1 x^2}{L} + \frac{x'^2}{L-z'} \right]}}{\sqrt{L_e(z')(L-z')}} g_s(x', z') u_1(x', z') \quad (3.28)$$

where the shorthand  $L_e(z')$  means

$$L_e(z') = \frac{2g_2 - 1}{L} - \frac{1}{L-z'} \quad (3.29)$$

and finally

$$I_2(x) = \frac{1}{2} \sqrt{\frac{i}{\lambda}} \int_L^{2L} dz' \int_{-\infty}^{\infty} dx' \frac{e^{-\frac{i\pi}{\lambda} \left[ \frac{(g_1-1)x^2}{L} + \frac{(x-x')^2}{L-z'} \right]}}{\sqrt{L-z'}} g_s(x', z') u_3(x', z') \quad (3.30)$$

Let us examine the round trip equation, Eq(3.26), to see what it means. We begin by discussing the terms  $I_1$  and  $I_2$ . We first examine the nonlinear coupling between the gain function and the field. Then we discuss the possible behavior of nonlinear equations of this type. Finally, we present two methods of solution.

Consider first the field terms in  $I_1$  and  $I_2$ . The gain function will be discussed in the next paragraph. Eq(3.28) accounts for the generation by stimulated emission and subsequent diffraction of fields in the first leg of the

round trip. Eq(3.30) accounts for the same phenomena in the second leg of the round trip. Note that the stimulated emission is due to the total field in the resonator, not just the original field at the feedback mirror. Now the field in Eq(3.28) is  $u_1(x,z)$ , not the original field,  $u_0(x,0)$ , that is present at the feedback mirror. This complicates the equation since one needs to solve for  $u_1$  throughout the resonator in order to find the final field  $u_4$ . Of course, the equation is just reflecting the physics of how the gain and the field interact throughout the resonator. The same complication arises in Eq(3.30) for evaluation of the field,  $u_3$ , although this field depends not only on the original field on the feedback mirror but also the fields stimulated in the first pass. In order to actually solve these equations either analytically or numerically, a scheme must be developed that accurately models the distributed interaction of the gain medium and the field. In the past this has given rise to the use of gain sheets and we will use a single gain sheet model in the next chapter.

As mentioned earlier, the gain function  $g(x,z)$  depends nonlinearly on the field  $u(x,z)$ . A frequently used model for homogeneously broadened gain is

$$g_s(x,z) = \frac{g_0}{1 + u(x,z)u^*(x,z)} \quad (3.31)$$

where  $g_0$  is the small signal intensity gain coefficient. (Ref 6) Thus the two terms  $I_1$  and  $I_2$  are nonlinear functions of the field since the gain is included in the

integrand.

In summary, Eq(3.26) can be classified as a nonlinear integral equation when we look for solutions where  $u_n = \nu u_0$ . Frequently nonlinear equations exhibit bifurcation of solutions. In other words, for the same parameter  $\nu$ , there may be several solutions. However, we may argue against bifurcation here on physical grounds. For a laser to operate in steady state (as is assumed in the derivation of the round trip integral equation for the resonator modes), gain must equal loss. This means acceptable solutions to the loaded cavity integral equation, Eq(3.26), must have the magnitude of the parameter  $\nu$  equal to unity. The phase of the parameter is not restricted. The gain and the field distributions within the resonator must be such that they are consistent. One actually is solving a set of coupled equations, Eq(3.26) and Eq(3.31). The coupling between these equations is the nonlinear aspect to the problem. Bifurcation would imply that different field distributions could arise from different initial gain distributions. Physically, this is reasonable. However, as changes to the gain medium occur over time scales that are long compared to the time required to establish the mode of the resonator, the mode that is established is a unique solution for that gain distribution and a new mode may result as the gain medium changes.

We now consider a perspective of Eq(3.26) that leads to two possible solution approaches. Consider the generic

integral equation

$$\alpha(x) = \int_{-a_1}^{a_1} dy K(x,y) \alpha(y) + \beta[\alpha(x)] . \quad (3.32)$$

This integral equation is clearly analogous to Eq(3.26) if the kernel is taken to be the bare cavity kernel. We discuss linear integral equations of this form in Appendix 1. They are called inhomogeneous Fredholm integral equations of the second kind. For all but some special cases, the linear equations have a unique solution which can be obtained by an iterative approach. (See Appendix 1 or Ref 54.) To find solutions to equations such as Eq(3.32), one can parallel the approach used in solving linear integral equations. One can formally assume that the functional  $\beta$  is known and then find a solution for that functional. Then, using this solution, a new functional is found and the cycle repeated until convergence is found. This approach is merely solving the integral equation with an iterative scheme. Essentially, one is solving the two coupled equations

$$\alpha = \alpha[\beta] \quad (3.33)$$

and

$$\beta = \beta[\alpha] \quad (3.34)$$

This iterative solution technique is one that will be used in the next chapter to solve the integral equation in the

approximation of a single gain sheet at the feedback mirror.

An alternative approach proves both interesting and informative, but has been much more difficult to implement. We consider expanding the "loaded cavity mode",  $\alpha(x)$ , in terms of the eigenfunctions of the kernel of Eq(3.32). In our case, these eigenfunctions are the bare cavity modes. Without considering the question of convergence for the moment, we use the expansion

$$\alpha(x) = \sum_{\lambda=0}^{\infty} b_{\lambda} u_{\lambda}(x) \quad (3.35)$$

where  $u_{\lambda}(x)$  are the bare cavity modes. Substituting the series into Eq(3.32) and using the orthogonality relation for the eigenfunctions of a complex-symmetric kernel, the coefficients are given by

$$b_{\lambda} = \frac{1}{a_{\lambda}(1 - \frac{\sigma_{\lambda}}{\nu})} \int_{-a_{\lambda}}^{a_{\lambda}} dx \beta[\cdot] u_{\lambda}(x) \quad (3.36)$$

where  $\sigma_{\lambda}$  is the bare cavity eigenvalue. Alternatively, one can solve for the coefficients in the more usual way:

$$b_{\lambda} = \frac{1}{a_{\lambda}} \int_{-a_{\lambda}}^{a_{\lambda}} \alpha(x) u_{\lambda}(x) dx \quad (3.37)$$

This technique follows the generalized Fourier series methods. One would hope that the expansion coefficients would be the same from either approach. Note that Eq(3.37) assumes some knowledge of the solution, obtainable from the

iterative approach described above. The calculation of the coefficients via Eq(3.36) does not assume such prior knowledge of the solution but does assume knowledge of the dependence of the solution on the functional. This suggests a different iterative scheme. Here one first guesses a solution such as the lowest loss bare cavity mode. Then the functional  $\beta$  is found, and the integral with the bare cavity modes is solved, giving the expansion coefficient. After a sufficient number of expansion coefficients have been found, a new guess at a solution can be made and the process repeated. The process assumes that the bare cavity modes are known. A procedure for finding these modes was developed in the previous chapter. Other techniques would also suffice. However, this procedure is more difficult since it does require an adequate number of bare cavity modes, with "adequate" not clearly defined. Indeed, as discussed in Chapter 2, the modes are not a complete set and thus the expansion in Eq(3.35) may not be valid.

One result that is desired from an analysis of the loaded cavity is how the bare cavity modes compete for the gain. Either the iterative solution with subsequent projection onto the bare cavity modes or the iterative scheme discussed above may give this information. Either approach suggest that there is only one field distribution for a given gain distribution. An interesting difference between the approaches is seen when the gain goes to zero, i.e., in the limit when the loaded cavity equation becomes the bare cavity equation. The iterative approach continues to be valid and

becomes the "power method" used by Fox and Li. However, in the "bare cavity mode expansion" method, the integrand in Eq(3.36) goes to zero. This seems to imply that the coefficients (and hence the loaded cavity mode) go to zero. However, as the gain is decreases below threshold, the parameter  $\gamma$  is no longer constrained to have unit magnitude and now tends toward the lowest loss eigenvalue. (Recall that when the gain is above threshold, the oscillation condition is such that the increase in the energy stored in the field is matched exactly by a decrease in the energy stored in the gain medium. Thus the loaded cavity eigenvalue always has unit magnitude for conditions above threshold.) Thus the denominator in Eq(3.36) also goes to zero. The limiting case would thus be the lowest loss bare cavity mode.

#### D. Summary

This chapter began with Maxwell's equations and ends with an equation that allowed a field to be propagated through an active, inhomogeneous medium. This propagator is applicable to problems where scalar, beam-like fields are appropriate. The results were specialized to two dimensions. A round trip equation was obtained for the strip resonator, namely Eq(3.26)-E(3.30). The nature of this equation was discussed in some detail, highlighting how the equations showed the nonlinear coupling between the gain and the field. Two solution techniques were discussed: an iterative scheme

analogous to the "power method" used for bare cavity modes and a bare cavity mode expansion. In the next chapter, we develop a single gain sheet model for the round trip strip resonator equation and apply these solution techniques to this model.

## IV. Modelling of Loaded Resonators

### A. Introduction

The goal of this chapter is to discuss how the loaded resonator can be modelled using the results of the previous chapter. We begin by reviewing the most relevant past work in the analysis of loaded resonators. Then a geometric approximation to the loaded cavity round trip equation is developed, by means of an approximation to Eq(3.26). The results agree with a comparable analysis done by Moore and McCarthy. (Ref.38) The majority of the chapter involves the diffractive model that was developed from the equations of Chapter 3. Here, we model the gain as a single gain sheet located at the feedback mirror in order to simplify the numerical model. A parallel derivation based on the more usual, heuristic inclusion of gain is also implemented. The results of these two models are discussed in detail. The chapter ends with a look at the limitations of the single gain sheet model and a summary.

### B. Review of Past Work in Loaded Resonator Modelling

In this section, we review the most relevant past work in the modelling of loaded laser resonators. The purpose of this review is to provide the background necessary to evaluate the models developed later in the chapter. The majority of the past work is based on Beer's Law. The papers that are reviewed includes the work of Rigrod (Ref 39,40), Fox and Li (Ref 41), Rensch and Chester (Ref 35), Rensch (Ref

42), Siegman and Sziklas (Ref 43,44), Moore and McCarthy (Ref 20,38) and Smith (Ref 36). The analyses span the range of geometric models of Rigrod through Smith's self-consistent model that is based on asymptotic approximations.

Before we begin the review, we need briefly to define what is meant by a gain sheet. As we found in Chapter 3, the proper analysis of the loaded cavity leads to integrals over  $z$ , the longitudinal dimension of the resonator axis, and over  $x$ , the transverse dimension. Thus the analysis allows for gain media with variations in both dimensions. The distributed gain complicates the numerical analysis since the gain depends on the fields that are propagating in both directions in the resonator and the fields depend on the gain. A frequently used approach is to lump the gain into a single transverse plane, and then propagate the fields between these planes using a free space propagator (e.g. Fresnel diffraction integral). This plane is called a gain sheet. Thus, the distributed gain media is treated as if it exists in discrete sheets. In order for this approach to be accurate, transverse field variations such as caused by diffraction, must be negligible (Ref 35). We will make use of this approximation in the numerical model to be developed in section D. In this section we will address the validity of the gain sheet models in more detail, examining how many gain sheets are needed to model accurately a given resonator.

The Rigrod analysis has become a classical work in this area because it provides an excellent first cut at how gain

affects the resonator analysis. Two key results are the establishment of the cavity threshold and the definition of extraction efficiency. The analysis ignores all transverse field variations but allows for longitudinal variations in the field. This approximation made the analysis one dimensional. It was used by Rigrod for flat-flat resonators and others have extended this model to unstable resonators and additional loss mechanisms such as unsaturable losses (Ref 45). (An unsaturable loss is any loss mechanism that is not a function of the field, for example, scattering. Absorption is an example of a saturable loss.)

The Rigrod model assumes the field is a uniform plane wave that propagates in accordance with geometric optics. The mirrors are simply modeled with a reflectivity and, when the gain is assumed to have no  $z$  dependence (as in a gain sheet), the gain is included with an exponential term:

$$I(x, z + \Delta z) = e^{g_s(x)\Delta z} I(x, z) \quad (4.1)$$

(Rigrod also analyzed distributed gain (Ref 40).) The gain is assumed to be homogeneously broadened, thus the gain function is

$$g_s(x) = \frac{g_0}{1 + I(x)/I_{sat}} \quad (4.2)$$

The parameters  $g_0$  and  $I_{sat}$  characterize the gain medium. The analysis is done by propagating a round trip in the cavity with these mirror and gain functions applied when

appropriate. Then one requires the field to reproduce in amplitude and phase in order to obtain the steady state results. By setting the length of the gain region to be equal to the length of the resonator, and letting the reflectivity of one mirror be unity and that of the other mirror be  $r$  (so that the outcoupling is by the transmission through this second mirror), the threshold gain is found to be

$$g_{th} = \ln\left(\frac{1}{r}\right) / 2L \quad (4.3)$$

(Note this is a power gain coefficient.) Following this analysis further, Rigrod allows a simple calculation of the extraction efficiency, defined as the ratio of the output power to the maximum power extractable from gain medium in the resonator. At steady state, gain equals loss and the operating gain for a homogeneously broadened medium is at the threshold level. Thus the extraction efficiency is just

$$\eta_{ext} = 1 - \frac{g_{th}}{g_0} \quad (4.4)$$

where  $g_0$  is the small signal gain.

All of these formulae change slightly for unstable resonators and for systems with more elements. However, the basic analysis put forth by Rigrod laid the foundation for the one dimensional analysis of laser resonators. His work also has been extended to include nonsaturable losses and Rigrod has examined optimum output coupling and compared his

analysis to the internal cavity power in inhomogeneously broadened helium-neon lasers. Good agreement was found between the theory and experiment. We will use the Rigrod results to assess the validity of the gain model that will be developed in this chapter.

The first attempts at including gain in a physical optics calculation were done by Statz and Tang (Ref 46) and Fox and Li (Ref 41). This work extended the calculation to two dimensions by including one transverse dimension. The work done by Statz and Tang was for a strip resonator with plane-parallel mirrors. Since the work done by Fox and Li is more extensive and since the approach used in both efforts is similar, we will review the Fox and Li paper. Their model was based on plane-plane and confocal resonators with circular mirrors containing a uniformly pumped saturable gain medium. The medium was assumed to be homogeneously broadened. They assumed the laser was operating at line-center so that anomalous dispersion would be ignored. They approach the problem by propagating the field between the mirrors using a Fresnel diffraction integral and applying gain at each end of the cavity using a multiplicative term which is the first two terms in a power series expansion of the exponential gain shown in Eq(4.1). We will see that the Fox-Li model is a special case of the analysis presented in Chapter 3. The method of successive approximations was used in the same manner as Fox and Li has used it in the analysis of bare cavity modes. The field gains energy from the gain

medium via stimulated emission and loses energy due to outcoupling. After many passes, a steady state solution was reached. Their conclusions were that "the distribution of field amplitude over the mirror, the diffraction loss, and the phase shift per transit are all essentially unchanged in the presence of saturation" (Ref 41, p. 782). We will see that the model they used is most appropriate for small gain and thus their conclusion is not surprising.

When Fox and Li examined the confocal case, they found that the intensity profile of the loaded cavity mode depended on the Fresnel number of the system. They also found that the solution was a superposition of the two lowest loss bare cavity modes. They conclude that the "presence of the saturable medium has imposed additional constraints which greatly limit the number of modes. While linear passive resonators may have an infinite number of quasi-modes, it appears that the nonlinear active resonator may have only one mode (or perhaps a few modes)...[The] field resembles the superposition of two modes of a linear passive resonator. However, the fact that they must be simultaneously present with the correct amplitudes suggests that it is more accurate to consider this combination as a single mode of the system" (Ref 41, p.783). This conclusion, that the loaded cavity mode is different from the bare cavity modes, is based on the numerical studies done by Fox and Li. It agrees with the conclusions made at the end of Chapter III that were based on a theoretical analysis.

While the Fox and Li analysis was done for the case of

circular mirrors, the analysis of Rensch and Chester was done for strip, confocal, unstable resonators (Ref 35). Thus their results are most applicable to this study. (This motivated the extensive use of their results in the bare cavity analysis of Chapter 2.) They studied the effects of uniform saturable gain (i.e. constant small signal gain and saturation intensity) and mirror misalignment. We will only discuss the work done on the loaded cavity. They used the same iterative procedure as Fox and Li, but included the gain by multiplying the field by an exponential factor as in Eq(4.1). As noted in Chapter 2, they let the back mirror be finite and approximated the distributed gain medium as a gain sheet at this plane. Their goal was not primarily to predict the mode shape or power extraction, but to find if a single mode would exist in the presence of a saturable gain medium. In all cases that they studied, the field distribution converged, and they concluded there was no mode competition. The change that was observed was a general broadening and flattening of the intensity distribution while the phase remained fairly unchanged. Since the effect of gain on the near field phase is negligible, little effect in the far field pattern was observed. They concluded that the single gain sheet approximation gave good results for magnifications of three or less. Even at values where the bare cavity modes showed an eigenvalue degeneracy, Rensch and Chester obtained a single stable mode. These results were obtained at values far above threshold. Their results are of value to this

research in three ways. First, they used a single gain sheet as we will do later in this chapter. Second, they observed that the gain only tended to fill in the intensity pattern, making it more like the geometric beam. This result does not agree with the results we will obtain later, primarily because Rensch and Chester include the gain as a multiplicative term while the analysis of Chapter III indicates that it should be included as an additive term. Third, they did not have any convergence problems as a result of including the gain medium. However, they studied cases where the gain was far above threshold. We will examine the same areas in the model developed in the next sections.

Rensch did subsequent work where he used an explicit finite difference algorithm to solve the wave equation in the presence of an active medium (Ref 42). This method allows the study of distributed effects arising from an active, flowing medium that may have index of refraction variations. The algorithm is supposed to be more efficient and more accurate at high Fresnel numbers. He also compared his results to experimental results for a gas dynamic carbon dioxide laser. His model still used a segmented gain medium that is equivalent to gain sheets. He let the index of refraction be complex to include the gain. Such a formulation leads to a multiplication of the field by the gain, unlike the addition of a gain term that we obtained in the analysis of Chapter 3. Rensch's model used up to thirty segments. The gain was calculated at each segment as the field arrived and then applied to the field. He found that

the field had converged after six or seven round trips, even for Fresnel numbers up to 78 (equivalent Fresnel number of 9.05). His calculated output power compared well with experimental results. His analysis is highly specific to the gas dynamic laser and thus no quantitative comparison between his work and our model will be made. However, his work is important in that it permitted realistic effects such as medium inhomogeneities and mirror distortions to be modelled.

Another analysis that examined a more realistic medium was the analysis done by Siegman and Sziklas (Ref 43,44). They modelled the gain medium with gain sheets placed throughout the medium. In the first reference, the propagation between gain sheets was accomplished by expanding the cavity field in hermite-gaussian functions. In the second article, a fast Fourier transform (FFT) was used to propagate the field between the gain sheets by using a plane wave expansion of the field. The approach was first to propagate a field through the entire resonator, applying a complex gain function which was an exponential function. However, in their model, the function allowed for index of refraction variations as well as a nonuniform, transversely flowing, gain medium. After making a round trip, the field was used to update the complex gain functions at each gainsheet. Their study was highly specialized to carbon dioxide gas dynamic lasers, but it is an excellent reference on the use of the FFT. They also introduced an expanding coordinate system that permits efficient application of the

FFT for more general geometries. The key point we note in this work is that the gain model is an exponential function that multiplies the field at several gain sheets.

The next analysis of loaded cavities that we discuss is the use of the asymptotic method discussed in Chapter 2 to model saturable gain. Moore and McCarthy laid the foundation with their analysis of unsaturable gain (i.e. the gain is independent of the intensity) in the laser cavity in the geometric optics limit (Ref 38) and in the case of very high Fresnel numbers (Ref 20). Smith extended their work to saturable gain (where the gain does depend on the intensity). (Ref 36) The theory of Moore and McCarthy is similar to that of Horwitz (Ref 19). Moore and McCarthy postulate that the output field is made up from source fields originating from successive images of the edges of the feedback mirror in the back mirror. The resultant field is expressed as the series sum of plane and cylindrical waves. In their geometric optics study of the resonator modes, they included the gain with a first order differential equation that ignored diffraction. This equation is equivalent to the loaded paraxial wave equation derived in Chapter 3 with the second order derivatives of the transverse coordinates set to zero. Although their method is complicated, they essentially use an exponential form that contains an integral over the gain in the exponent. This exponential function is included in the series sum of image sources. Smith extended the work to include an iterative scheme whereby the field is used to saturate the gain function, the new gain function used to

obtain a new field and the process repeated until convergence. The advantages of the asymptotic approach are the application to higher Fresnel numbers and the increased computational speed inherent in the asymptotic approach. In Smith's study, as in the previous studies, convergence was obtained rapidly. Smith uses the case of  $M = 2.5$  and  $F = 0.64$  studied by Rensch and Chester as a baseline for his approach. He comments that "saturable gain seems to produce an effect not unlike that of mirrors with rounded edges or tapered reflectivity, which reduce the influence of diffraction on mode properties" (Ref 36, p. 1619). Smith also goes on to examine the case of mode degeneracy and shows that the presence of gain splits the degeneracy. This result suggests that the possibility of multimode operation in actual lasers is lessened by the presence of a saturable medium.

This review of the key past work in the inclusion of a saturable gain medium in the analysis of cavity modes has highlighted the methods used by others to model this difficult problem. Most of the analyses used a multiplicative factor for the gain that usually was an exponential function similar to the function used by Rigrod. No one observed any evidence of multimode operation as evidenced by a failure to obtain convergence. Most of the results indicate that the presence of gain tended to smooth out the mode, making the intensity profile look more like the geometric mode while leaving the phase relatively

undisturbed. We will return to these points as we develop models for loaded cavities based on the theory of Chapter 3. First, we examine a geometric optics model in the next section. Then, in the sections that follow, we develop a numerical model based on physical optics.

### C. Geometric Optics Analysis of Loaded Strip Resonators

The analysis presented in this section was primarily developed by Erkkila (Ref 47). We begin with the final strip resonator round trip equation that included distributed gain, namely, Eq(3.26) and the detailed parts of that equation in Eqs(3.27) - (3.30). The right hand side of this equation has three parts. After specializing the equation to the case of a confocal resonator, we apply the method of stationary phase to each of the three parts. The confocal conditions are just

$$g_1 = \frac{M+1}{2} ; \quad g_2 = \frac{M+1}{2M} ; \quad g = \frac{M^2+1}{2M} . \quad (4.5)$$

We make this restriction for two reasons. Many other studies have been done using confocal resonators since these resonators have collimated outputs. Also, the analysis is somewhat simplified.

The method of stationary phase is an approximation that can be applied to physical optics formulae (such as Fresnel propagators) to obtain geometric optics results in the limit as the wavelength goes to zero. (This technique was used by Moore and McCarthy (Ref 20), Horwitz (Ref 19) and Smith (Ref 36).) Born and Wolf have a general discussion of this

technique (Ref 48, p 752). We present the relevant result:

$$\int_a^b dx e^{-itp(x)} q(x) \simeq e^{-\frac{i\pi}{4}} e^{-itp(x')} q(x') \sqrt{\frac{2\pi}{t p''(x')}} \quad (4.6)$$

where  $p(x)$  and  $q(x)$  are slowly varying functions of  $x$ ,  $t$  is a very large parameter, and the stationary point,  $x'$ , is the value of  $x$  at which the first derivative of  $p(x)$  is equal to zero. This formula neglects terms of order  $1/t$  and higher. When this formula is applied, one must insure that  $q(x)$  is a slowly varying function.

In the case of Eq(3.26), the field is specified at the plane of the feedback mirror and thus it has a rapidly varying term due to the lens factor. One can obtain a slowly varying term by the transformation,

$$u^c(x) = u(x) e^{\frac{i\pi}{\lambda L} (g_1 - 1)x^2} \quad (4.7)$$

By finding the stationary phase points for each term separately and applying the formula of Eq(4.6), one finds the geometric optics approximation to Eq(3.26). The details of this derivation are contained in Appendix 8. The results are presented here:

$$u_4^c(x, zL) = I_1 + I_2 + I_3 \quad (4.8)$$

where the first term of Eq(3.26) became

$$I_1 = \frac{1}{\sqrt{M}} u_0^c\left(\frac{x}{M}, 0\right) \quad (4.9)$$

and the second term of Eq(3.26) became

$$I_2 = \frac{1}{2} \int_0^L dz g_s(x_s, z) u_1^c(x_s, z) \sqrt{\frac{Mz+L-z}{ML}} \quad (4.10)$$

where

$$x_s = \frac{Mz+L-z}{ML} x \quad , \quad (4.11)$$

and the third term of Eq(3.26) became

$$I_3 = \frac{1}{2} \int_L^{2L} dz g_s(x, z) u_3(x, z) . \quad (4.12)$$

(The "c" superscript denotes a collimated field.)

Some comments can be made about this result. First, we see that in the absence of gain, the field after a round trip is expanded and diminished in amplitude by the square root of the magnification. (For three dimensional resonators, the factor would be  $1/M^2$  .) The second two terms act to make up for the decrease in amplitude by an increase from stimulated emission. The second term shows the weighting in the integrand that accounts for the expanding leg of the confocal resonator. The third term does not have this term, since that leg is collimated.

We now examine this equation under the special case of a single gain sheet at the feedback mirror and set  $x = 0$  to look only at the value on-axis. This special case will serve as a limiting value for the diffractive model that will be

developed in the next sections. This special case also serves as a case that can be checked against the work of other authors.

The single gain sheet approximation is made by setting  $z = 0$  in Eq(4.9) - (4.12), replacing  $\int dz$  by  $L$  (we assume that the gain completely fills the resonator). The on-axis case is obtained by setting  $x = 0$ . Thus Eq(4.8) with the detailed terms substituted in becomes

$$u_4^c(0, zL) = \frac{1}{\sqrt{M}} u_0^c(0, 0) + \frac{L}{2} g_s(0, 0) u_1^c(0, 0) \sqrt{\frac{1}{M}} + \frac{L}{2} g_s(0, 0) u_3(0, 0) . \quad (4.13)$$

(At steady state, the field reproduces itself without any amplitude loss so  $u_4^c(0, 0) = u_0^c(0, 0)$ .) Also, for  $x = 0$ ,

$$u_0^c(0, 0) = u_1^c(0, 0) = u_3(0, 0) . \quad (4.14)$$

Thus the gain function can be found to be

$$g_s(0, 0) = \frac{2}{L} \left[ \frac{\sqrt{M} - 1}{\sqrt{M} + 1} \right] . \quad (4.15)$$

We assume here as we do throughout this work that the gain is represented by a homogeneously broadened model:

$$g_s(0, 0) = \frac{g_0}{1 + 2 |u_0^c(0, 0)|^2} . \quad (4.16)$$

(All fields are normalized by  $\sqrt{I_{sat}}$  .) Then we can find the on-axis intensity,

$$|u_0^c(0,0)|^2 \equiv I_{oa} = \frac{g_0 L}{4} \left[ \frac{\sqrt{M} + 1}{\sqrt{M} - 1} \right] - \frac{1}{2} , \quad (4.17)$$

and by multiplying by  $2a_1$  , we find the power on the feedback mirror:

$$P_{oa} = 2a_1 I_{oa} = \frac{a_1 g_0 L}{2} \left[ \frac{\sqrt{M} + 1}{\sqrt{M} - 1} \right] - a_1 . \quad (4.18)$$

The power on the mirror will be a parameter that the diffractive model calculates, and Eq(4.18) will serve as a limiting value for this code since as the Fresnel number increases, the power on the mirror should approach this value. Also, these results are in excellent agreement with Moore and McCarthy's results in the case of distributed gain and they are in excellent agreement with results obtained by Rinaldi for the single gainsheet model. (Ref 49) Thus the rigorous derivation of the loaded cavity solution in Chapter 3 is supported by past work in the area of loaded resonator calculations by this asymptotic analysis.

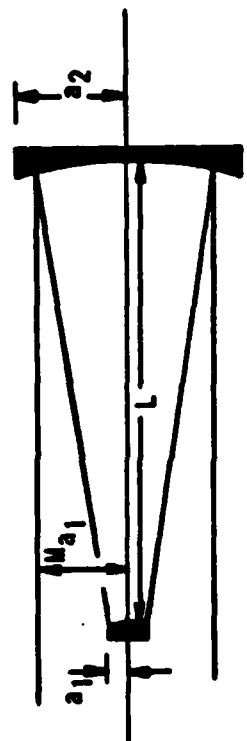
This special case concludes the discussion of the geometric optics approximation to the loaded cavity round trip integral equation. In the next section we develop the equations for a diffractive model of a strip resonator with a single gain sheet at the feedback mirror.

#### D. Single Gain Sheet Diffractive Model

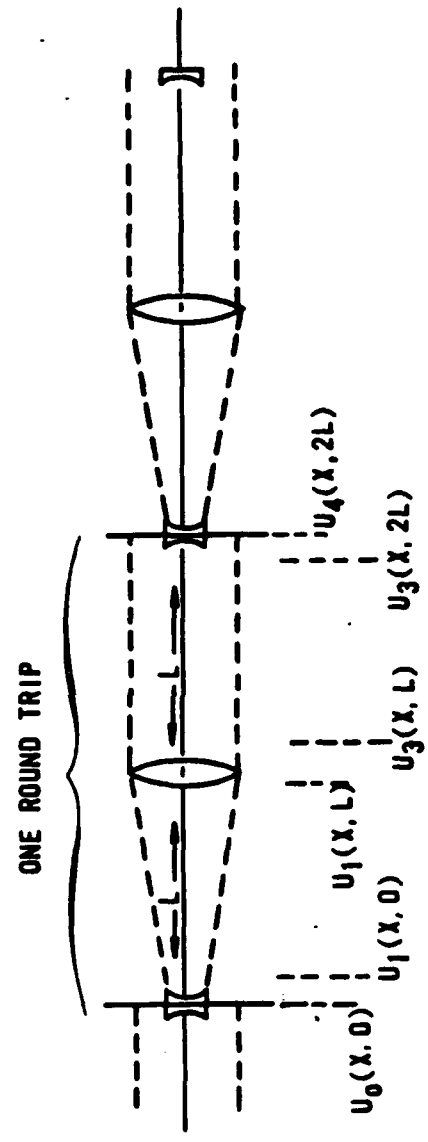
In this section, we derive the analytic model of a strip resonator with a single gain sheet at the feedback mirror based on the analysis of Chapter 3. The single gain sheet approximation is chosen because it is the simplest model to build numerically, thus making it a logical starting point.

We begin by rederiving the loaded cavity round trip equation. The intent of the rederivation is to eliminate the effects of diffraction in the gain term of the two term propagator, while keeping the diffractive effects in the Fresnel propagation term. This is the next step beyond the geometric optics model discussed in the previous section. In a more sophisticated model, diffraction would be left in all the terms and the round trip equation, Eq(3.26), would be used. However, we want to introduce complications in an orderly manner, so the effects of these complications can be observed. Furthermore, the full diffraction model is computationally very difficult.

We also restrict the model to the case of a positive branch, confocal, unstable resonator (PBCUR). As mentioned in the preceding section, this case is of general interest because of the collimated output beam, and it further simplifies the model. A round trip in the PBCUR consists of an expanding leg and a collimated leg. (See Figure 4.1.) The method of stationary phase, introduced in the last section, will be applied to each leg. In the leg where the field is expanding, the curvature of the field is modified



(a)



(b)

Figure 4.1 Round Trip in Positive Branch Confocal Unstable Resonator (a) Resonator Layout (b) Equivalent Lens Train.

in order that the function,  $q(x)$ , is slowly varying, as required by the method of stationary phase. Physically, the use of the method of stationary phase means that the radiation that is stimulated on the particular leg of the round trip is propagated geometrically through that leg.

The derivation begins with the two-term propagator for the strip resonator, Eq(3.23) - Eq(3.25). The method of stationary phase will be applied only to the term containing gain. Appendix 5 gives the details of this approximation for both the collimated and expanding legs of a PBCUR. The resulting two term propagators are given below. First, we present the collimated leg propagator.

$$u(x, z) = \sqrt{\frac{i}{\lambda z}} \int_{-\infty}^{\infty} dx' e^{-\frac{i\pi}{\lambda z} (x-x')^2} u(x', 0) + \frac{1}{2} \int_0^z dz' g_s(x, z') u(x, z') \quad (4.19)$$

The expanding leg propagator is more complicated:

$$u(x, z) = \sqrt{\frac{i}{\lambda z}} \int_{-\infty}^{\infty} dx' e^{-\frac{i\pi}{\lambda z} (x-x')^2} u(x', 0) + \frac{1}{2} \int_0^z dz' \frac{e^{-\frac{i\pi x^2}{\lambda(f+z')} \left[ \frac{(f+z')(z-z')}{(f+z)^2} \right]}}{\sqrt{\frac{f+z}{f+z'}}} u\left(\frac{x(f+z')}{f+z}, z'\right) g_s\left(\frac{x(f+z')}{f+z}, z'\right). \quad (4.20)$$

We now use these propagators with the mirror factor given earlier,

$$A_i(x) = \begin{cases} e^{-\frac{i\pi}{\lambda l} (g_i - 1) x^2} & , |x| \leq a_i \\ 0 & , |x| > a_i \end{cases} \quad (4.21)$$

to obtain a loaded cavity round trip integral equation similar to Eq(3.26). The derivation parallels Appendix 4 and will not be presented here. The resultant equation is

$$U_4(x, 2L) = I_1(x) + I_2(x) + I_3(x), \quad |x| \leq a, \quad (4.22)$$

where the first term is

$$I_1(x) = \sqrt{\frac{i}{2g_1 \lambda L}} \int_{-a_1}^{a_1} dx' e^{-\frac{i\pi}{2g_1 \lambda L} [g_1(x^2 + x'^2) - 2xx']} u_0(x', 0), \quad (4.23)$$

the second term is

$$I_2(x) = \frac{1}{2} \sqrt{\frac{i}{\lambda L}} \int_0^L dz' \int_{-\infty}^{\infty} dx' \frac{e^{-\frac{i\pi}{\lambda L} [g_1 x^2 - 2xx' + (2g_2 - 1)x'^2]}}{\sqrt{\frac{f+L}{f+z'}}} \cdot e^{-\frac{i\pi(L-z')x'^2}{\lambda(L+f)}} u_1(x' \frac{f+z'}{f+L}, z') g_5(x' \frac{f+z'}{f+L}, z'), \quad (4.24)$$

and the third term is

$$I_3(x) = \frac{1}{2} e^{-\frac{i\pi(g_1 - 1)x^2}{\lambda L}} \int_L^{2L} dz' g_5(x, z') u_3(x, z'). \quad (4.25)$$

Now the first term is just the bare cavity integral equation if gain were not present. The second term is the diffraction through the second (collimated) leg of the stimulated emission generated on the first (expanding) leg. The third term is just the geometric optics propagation of the stimulated emission generated on the second leg. The final

field is again written for a plane halfway through the feedback mirror in order to preserve symmetry in the first term and to make this analysis parallel the bare cavity analysis of Chapter 2.

The integral equation, Eq(4.22), still contains distributed gain (i.e. gain that is distributed throughout the cavity). One difficulty with distributed gain in a resonator is that the gain depends on the two-way fields. The usual approximation is to segment the gain into multiple segments and lump the gain in each segment into a single plane, propagating between segments as if the field were in free space. (This approach was used in several of the papers reviewed in section B.) We want to pause for a moment in our derivation to examine the criteria for the gainsheet approximation and how many gainsheets are required to adequately model a given resonator. The discussion that follows is a summary of a paper by P.W. Milonni. (Ref 37) (We note here that Milonni studied the accuracy of a propagation, not a round trip in a resonator.)

Milonni begins by deriving the loaded cavity paraxial wave equation as we did in Chapter III. He then uses the Green's function method to obtain a propagator that has two terms. The first is the usual Fresnel diffraction integral. The second contains the contribution due to the stimulated fields. Milonni then expands the gain term in a Taylor series about the observation point. He finds two conditions that, when satisfied, allow for accurate modeling using gain sheets. These two conditions are

$$|\nabla_T^2(\chi E)| \ll \frac{2k}{z} |\chi E| \quad (4.26)$$

and

$$\int_0^z dz' \chi(x,y,z') E(x,y,z') \approx z \chi(x,y,0) E(x,y,0) \quad (4.27)$$

The first of the conditions, Eq(4.26), essentially states that the transverse variations of the field must change little over the propagation distance. This can be expressed as a Fresnel number argument for the strip case:

$$F \gg \frac{1}{4\pi} \approx 0.0796 \quad (4.28)$$

This expression gives conditions so that the effects of diffraction are negligible over the gain segment. The second condition, Eq(4.27), restricts the amount of variation in the susceptibility (or the gain). That is, the gain must be fairly uniform across the gain segment that the gain sheet is modelling. The number of gain sheets required to model accurately a given propagation through an active medium is set by these two restrictions.

The results obtained by Milonni parallel the results obtained by others. Fox and Li used gain sheets if (1) the gain per pass was small ( $g_0 L \ll 1$ ) and (2) the transverse field distribution does not change substantially along the axial direction (Ref 41). Siegman and Sziklas state that the

gain sheet model is valid if "neither the accumulated differential phase shift nor the fractional gain in a single segment" is large (Ref 43,44). Rensch states the same restriction that Siegman and Sziklas used and added that the segment size  $z$  (where the number of segments is approximated by  $L/z$ ) should be less than the transverse field variations (Ref 42). Clearly, these authors are all stating the same general rules for the use of gain sheets.

With this brief discussion of the gain sheet approximation, we would like to next turn to the numerical model that was developed to implement Eq (4.22). However, before we discuss this model, we want to derive a parallel model based on a more conventional inclusion of gain. This model, termed the "multiplicative model" for convenience, assumes a single gainsheet at the feedback mirror and implements this gain as a multiplicative factor:

$$u_{\text{after}}(x) = e^{\frac{g_s(x)}{2} L} u_{\text{before}}(x) \quad (4.29)$$

This gain term is essentially a Beer's Law gain model. Using the same lens factors and the Fresnel propagator as used in Appendix 4, one can readily find a round trip equation for the loaded cavity mode. The resulting integral equation has a radically different form from Eq(4.22):

$$u_u(x, 2L) = \sqrt{\frac{i}{2g_s \lambda L}} \int_{-a_1}^{a_1} dx' e^{\frac{[g_s(x) + g_s(x')]}{2} L} e^{-\frac{i\pi}{2\lambda g_s L} [g(x^2 + x'^2) - 2xx']} u_o(x') \quad (4.30)$$

Here, the equation is a homogeneous integral equation,

although the kernel is nonlinearly related to the field through the gain term. Note also that the gain term depends on both coordinates,  $x$  and  $x'$ . We show this equation and later implement a numerical model of it to compare with the model of Eq(4.22). We now turn our attention to the development of the numerical models.

#### E. Numerical Implementation of Loaded Cavity Models

In this section, we describe how the analytic model developed earlier in this chapter is implemented in a computer model. In the next section, we will discuss the results obtained with the model. The numerical model solves the loaded cavity round trip equation using the iterative technique. The equation that will be solved is Eq(4.22) with the detailed parts in Eqs(4.23)-(4.25). In Eq(4.22), we replace  $u_4$  with  $\nu u_0$ , in order to form the mode equation. A similar model is developed for Eq(4.30) in order to observe the differences between the two approaches.

As mentioned earlier, only a single gainsheet will be used in the numerical model. We choose to place this gainsheet at the feedback mirror. This is accomplished by replacing  $\int_0^L dz$  by  $L$ , setting  $z$  to zero in Eq(4.24) and  $z$  to  $2L$  in Eq(4.25). However, Eq(4.24) and Eq(4.25) contain the fields  $u_1$  and  $u_3$ . These fields can be related to the field  $u_0$  at the feedback mirror plane by the following relations:

$$u_1(x) = \begin{cases} \exp\left[-\frac{i\pi}{\lambda L}(g_1-1)x^2\right] u_0(x) & , |x| \leq a_1 \\ 0 & , |x| > a_1 \end{cases} \quad (4.31)$$

$$u_2(x) = \exp\left[\frac{i\pi}{\lambda L}(g_1-1)x^2\right] u_0(x) \quad \forall x \quad (4.32)$$

Now the gain function is modelled with a simple homogeneously broadened gain model:

$$g_s(x) = \frac{g_0}{1 + |u_1(x)|^2 + |u_2(x)|^2} \quad (4.33)$$

When Eq(4.31) and Eq(4.32) are used, this gain model will be saturated by two fields for values of  $x$  on the mirror, and only by one field off the mirror.

Using the relations in Eqs(4.31)-(4.33), a numerical model was constructed to solve the integral equation using an iterative technique. First, a trial solution for  $u_0$  was constructed. Then the right-hand side of Eq(4.22) was solved, generating a new trial solution for  $u_0$ . By comparing the last trial solution to the current one, the loaded cavity eigenvalue,  $\nu$ , can be estimated. This process is repeated until the eigenvalue estimate does not change significantly (less than one percent) between iterations. (A similar model was developed by Fox and Li (Ref 15) and a bare cavity numerical model was developed in Chapter 2 to serve as a baseline for the kernel expansion.) In the bare cavity case, only the lowest loss mode was found. In the loaded cavity case, the form of the equations suggest that there may only be one solution, although a proof of this is not offered due to the nonlinear form of the second and third term on the

right-hand side of Eq(4.22).)

Several comments can be made about the loaded cavity eigenvalue. First, when the gain is set above the cavity threshold, we expect to find steady state operation, i.e. the equations should show that the gain in the field due to stimulated emission equals the loss in the field due to outcoupling. Then the magnitude of the eigenvalue should be unity. Second, the phase of the eigenvalue will still indicate a frequency offset just as the phase of the bare cavity eigenvalues did. Thus if the model is working correctly, we should find this behavior predicted by the code.

The functions were evaluated on a uniform grid. An odd number of points was used in order to use Simpson's rule integration. Due to the integral over  $x$  in Eq(4.24), the grid needs to extend at least out to the geometric shadow boundary defined by  $x = Ma_1$ . Taking the grid over a smaller region gives incorrect answers for the mode on the mirror.

The output of the model includes the loaded cavity eigenvalue discussed above, intensity and phase plots of the mode, and three power calculations. The first is an estimate of the power based on a Rigrod calculation. The equation used is Eq(4.18), repeated here:

$$P_{0a} = \frac{a_1 g_0 L}{2} \left[ \frac{\sqrt{M} + 1}{\sqrt{M} - 1} \right] - a_1 \quad (4.34)$$

Also, the power on the mirror and the total power across the outcoupling plane (as limited by the extent of the transverse grid,  $x_{max}$ ) are calculated, and the values listed. These values are used to calculate an outcoupling fraction, defined by

$$\delta_{est} = 1 - \frac{\int_{-a_1}^{a_1} |u(x)|^2 dx}{\int_{-x_{MAX}}^{x_{MAX}} |u(x)|^2 dx} \quad (4.35)$$

This value is also listed. These outputs allow one to study the eigenvalue behavior, the changes in intensity and phase and the power on the mirror as the gain is increased. Also the outcoupling should increase as the gain is increased, but some saturation effects should also be apparent, as illustrated by the fractional outcoupling.

The model was written using FORTRAN IV. It was first implemented on the Aeronautical Systems Division (ASD) Control Data Corporation Cyber series computer, and then transferred to the Air Force Weapons Laboratory (AFWL) CRAY-1 supercomputer. The results that are shown in this chapter were obtained with the CRAY.

The initial baseline for the code was to compare it against a bare cavity calculation obtained from any of the methods discussed in Chapter 2. The code predicted identical eigenvalues, intensity and phase plots for all cases examined. The verification of the loaded cavity calculations is more difficult since no past work included a saturable medium in the same manner. This is one reason that the multiplicative model of the loaded cavity was derived at the

end of the last section. Eq(4.30) was also solved in an iterative manner that paralleled the procedure used to solve Eq(4.22). The same gain model was used to allow direct comparison of the results. The outputs that will be compared include the saturation characteristics, the eigenvalue behavior, the intensity and phase of the mode, and the behavior of the power on the mirror. The iterative model based on the analysis of Chapter 3 was also checked for internal consistency, i.e., did it predict behavior that agreed with qualitatively observed laser behavior? Also, a wide range of cases were studied in an attempt to see if the bifurcation of solutions could be observed. (No such behavior was observed. Near the mode crossing points predicted by the bare cavity theory, both models showed difficulty in converging as indicated by the number of iterations needed to obtain a converged solution, but the multiplicative model behaved much worse than the model developed here and actually did not converge even after many iterations for some cases.)

#### F. Results of the Numerical Model of the Loaded Cavity

In this section, we examine the major results obtained from the numerical model of the strip resonator. Recall that the numerical model uses the analysis of Chapter III with the method of stationary phase applied to the integral that contains the gain. Then the gain is further approximated by a single gain sheet at the feedback mirror. This numerical

model will be used in this section to analyze the modes of the loaded cavity. Since the gain is being included in an additive manner rather than a multiplicative fashion, there are limited published results against which the model can be compared.

The results that will be discussed include (1) restrictions on transverse grid size, (2) convergence test of the model by varying the number of points in the grid, (3) convergence test by examining the number of iterations needed for a converged mode, (4) examination of the power on the feedback mirror, amplitude of the loaded cavity eigenvalue and phase of the loaded cavity eigenvalue as a function of the small signal gain, (5) examination of intensity/phase as a function of small signal gain for the additive and multiplicative models, (6) examination of a mode crossing where the amplitude of two lowest loss bare cavity eigenvalues are equal, (7) examination of the phase of the loaded cavity eigenvalue and the power on the mirror as a function of the equivalent Fresnel number, and (8) a preliminary examination of how the loaded cavity mode maps onto the bare cavity modes. These results comprise a broad range of phenomena that will illustrate the similarities and differences between the additive model developed in Chapter III and the multiplicative model frequently encountered in the literature.

#### 1. Transverse Grid Extent

The approach to solving the loaded cavity integral

equation, Eqs (4.22)-(4.25), will be an iterative technique as described above. Of concern here is the extent of the transverse grid necessary to yield an accurate answer. The  $x$  integral in Eq(4.24) is the most restrictive term in the grid determination. This integral is over the back mirror and the grid must extend over at least the width of this mirror. Picking the upper limit on the grid to be greater than or equal to  $M_a$  gave intensity and phase plots that were in good agreement while picking the upper limit to be less than  $M_a$  gave mode plots that varied radically as the upper limit changed. The conclusion is to always set the grid limits to be at least as large as the back mirror size. Here the back mirror size is set by the geometric beam size.

## 2. Convergence as a Function of Number of Points

We now vary the number of points and look for changes in the loaded cavity mode solution. The purpose of this test is to verify the numerical stability of the results. Table IV-4 summarizes the effect of varying the number of points by examining the effect on the loaded cavity eigenvalue. The gain is set to be initially three times the geometric threshold value. Note that the amplitude of the eigenvalue is unity even for a small number of points ( $N=25$ ). However, the phase of the eigenvalue changes as the number of points changes until at least 99 points have been used. Plots of the intensity and phase of the converged solution for the loaded cavity mode show similar results. As long as at least

TABLE IV-1.

Convergence History As Number of Points is Varied  
 $M = 10$      $F_{eff} = 0.225$      $g_0 = 3.0$      $g_{th}$      $x_{max} = 3.0 a_1$

N	eigenvalue magnitude	eigenvalue phase	power on mirror
25	0.9999	0.257	0.014225
49	1.0003	0.024	0.01345
75	1.0001	0.037	0.0117
99	1.0001	0.043	0.01166
125	1.0001	0.044	0.011645
149	1.0001	0.045	0.011638
175	1.0001	0.046	0.01165
199	1.0001	0.046	0.01165

NOTE: 1. Data shown is for the fifteenth iteration.  
 2. Power on mirror is in normalized units.

99 points are used for this particular case, a converged solution is obtained that accurately represents the loaded cavity mode as modeled by this approach.

This study was not intended to set definitive requirements on the number of points required for a particular case (as specified by the magnification and equivalent Fresnel number of the resonator). Rather, each case should be considered separately by varying the number of points until the converged solution no longer varies. (Sziklas and Siegman developed a criterion for the number of points required to resolve the mode in their FFT model (Ref 44:1878). However, their work involved guardbands for the FFT. If we set a guardband of about 0.5 and allow only 0.001 of the energy to be aliased from higher spatial frequencies into lower ones, then their criterion (Eq(19) of Ref 44) gives a required number of points similar to that obtained here.) This study did show that the same loaded cavity mode was obtained as the number of points was increased beyond some minimum. This study is necessary as an internal verification of the numerical model.

### 3. Convergence as Function of Number of Iterations

We now examine another internal check on the numerical model. The loaded cavity mode is obtained after a number of iterations and we examine here the number of iterations required to produce a converged solution. The final solution did not depend on the initial field.

Figures 4.2 and 4.3 show the magnitude and phase,

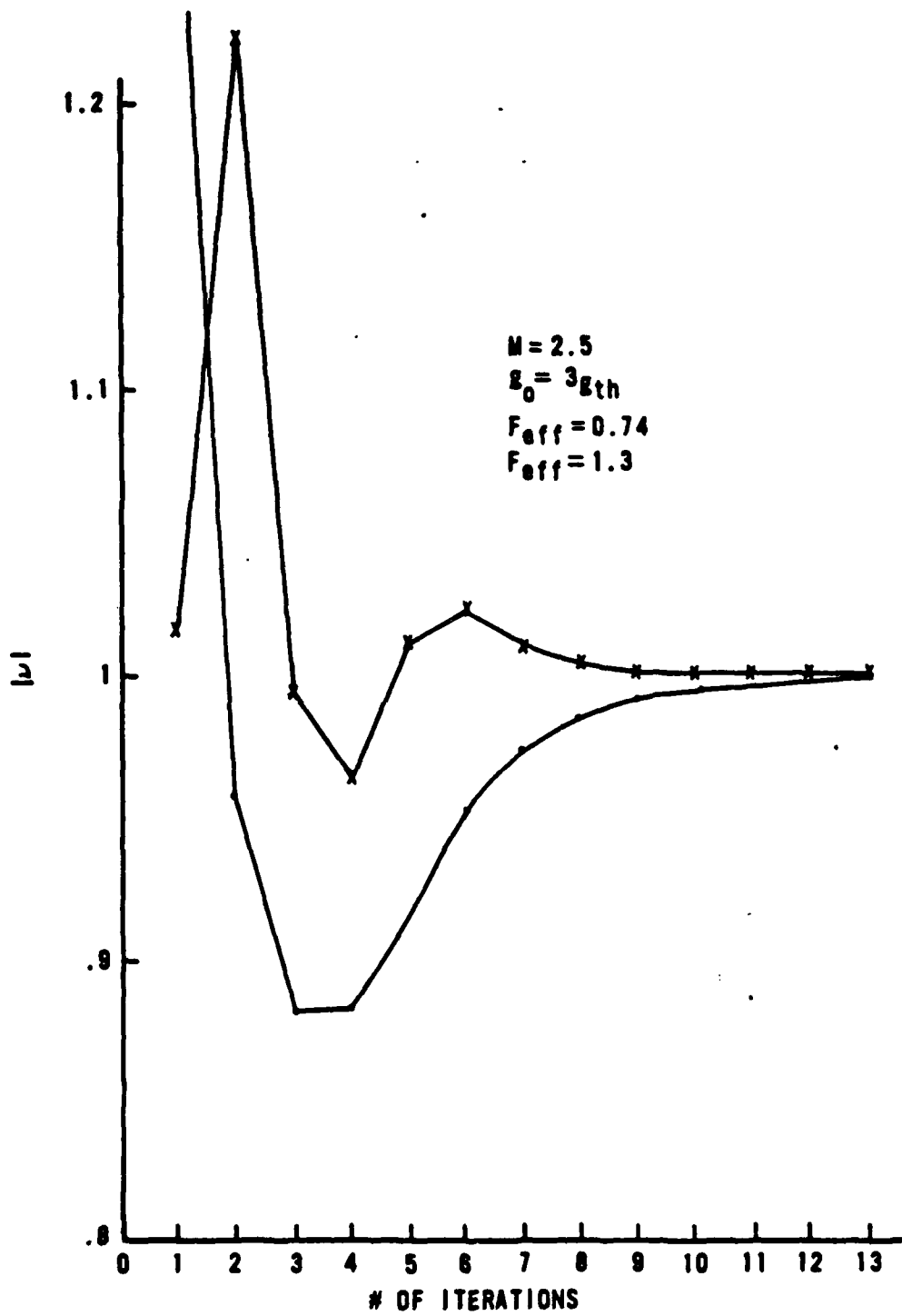


Figure 4.2 Convergence History - Magnitude of Eigenvalue.

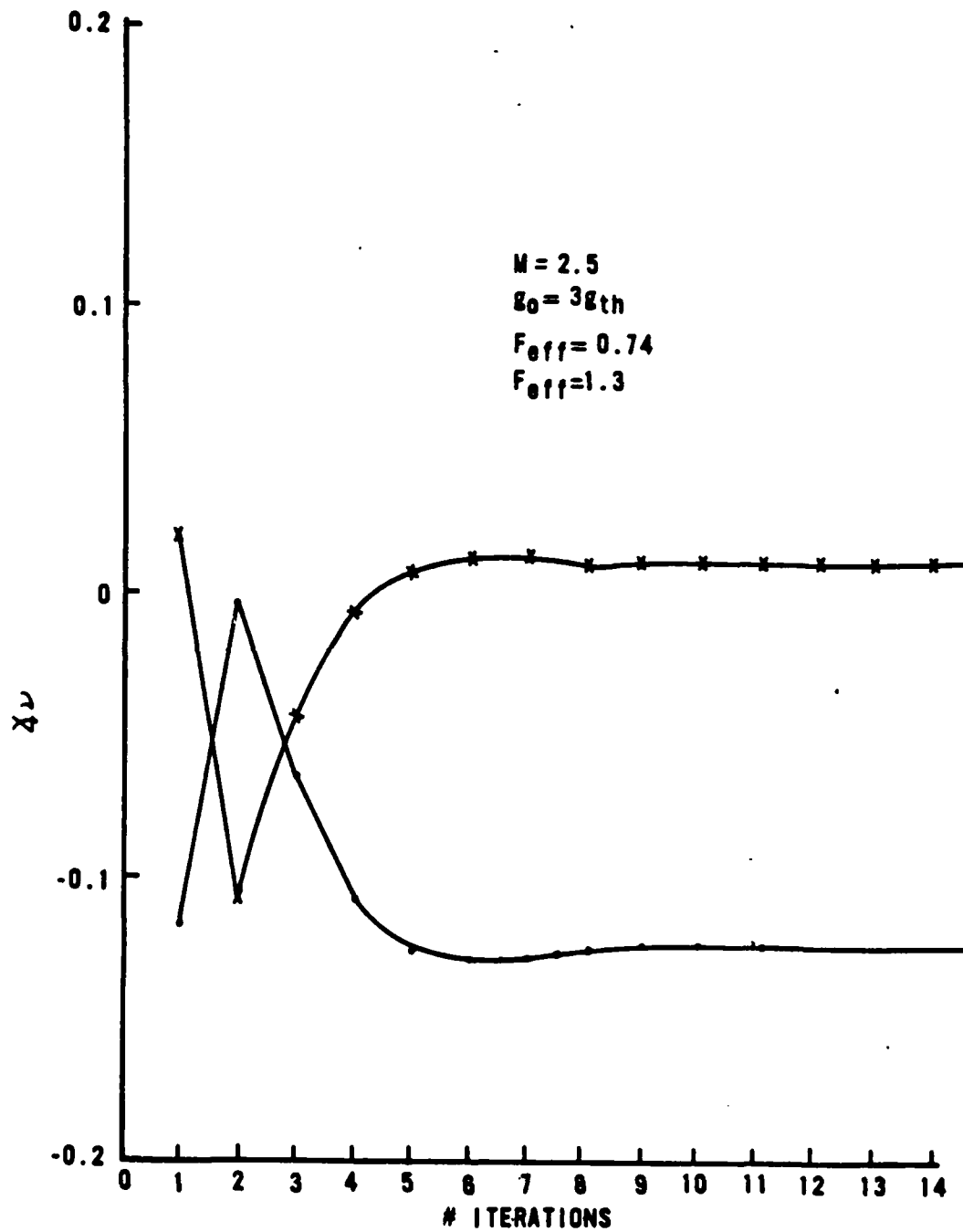


Figure 4.3 Convergence History - Phase of Eigenvalue.

respectively, of the loaded cavity eigenvalue. This eigenvalue is the parameter that is used in the model to assess convergence. The figures show two cases of equivalent Fresnel number, 0.74 and 1.3, for the same magnification and small signal gain. The first case is near a mode crossing where the two lowest loss bare cavity eigenvalues have nearly the same eigenvalue. This case usually exhibits difficulty in convergence when the method of successive approximation is used (Ref 15). (We will examine a mode crossing in more detail in Section 6.) The second case is a case where the two lowest loss bare cavity eigenvalues are widely separated. The figures show that convergence was obtained rapidly in both cases. For the particular cases studied, convergence was obtained in about ten iterations. Similar results were obtained for all the other cases studied with this model.

This study showed that the numerical model was stable and that convergence was obtained for a reasonable number of iterations. This study also showed that the loaded cavity eigenvalue was a useful parameter for assessing convergence. The number of iterations required for convergence increases as the equivalent Fresnel number. In the cases that were studied, the convergence was checked manually. When the eigenvalue did not change by more than about one percent for several iterations, convergence was said to have been obtained. When this criterion was satisfied, the intensity and phase did not vary with more iterations.

#### 4. Variations in Loaded Cavity Mode Parameters as Function of Small Signal Gain

In this section, we apply the model to study the trends in the loaded cavity mode as the small signal gain is varied. The parameters that are studied are the amplitude and phase of the loaded cavity eigenvalue and the power on the feedback mirror.

The case presented here is the same one that will be presented for the majority of this chapter:  $M = 2.5$  and  $F_{eff} = 1.2$ . Other cases were studied and this case was chosen as representative. The equivalent Fresnel number is low enough that convergence is rapidly obtained. Therefore many computer runs can be made to explore the parameter space.

We examine first the amplitude of the loaded cavity eigenvalue as a function of small signal gain. Figure 4.3 shows the behavior. In this figure, the results from both the additive model (denoted by the "x's") and the multiplicative model (denoted by the dots) are displayed. The two models give very similar results for this parameter. Two principal conclusions are apparent from these plots. First, the threshold predicted by the two models is below the geometric threshold. (The abscissa is scaled by the geometric threshold.) This behavior is physically meaningful because diffraction tends to peak the intensity towards the center of the resonator for equivalent Fresnel numbers near  $n + 0.375$  ( $n$  any integer), thus allowing the gain to be more rapidly saturated in the central "core" region of the resonator. Second, both models predict that the loaded

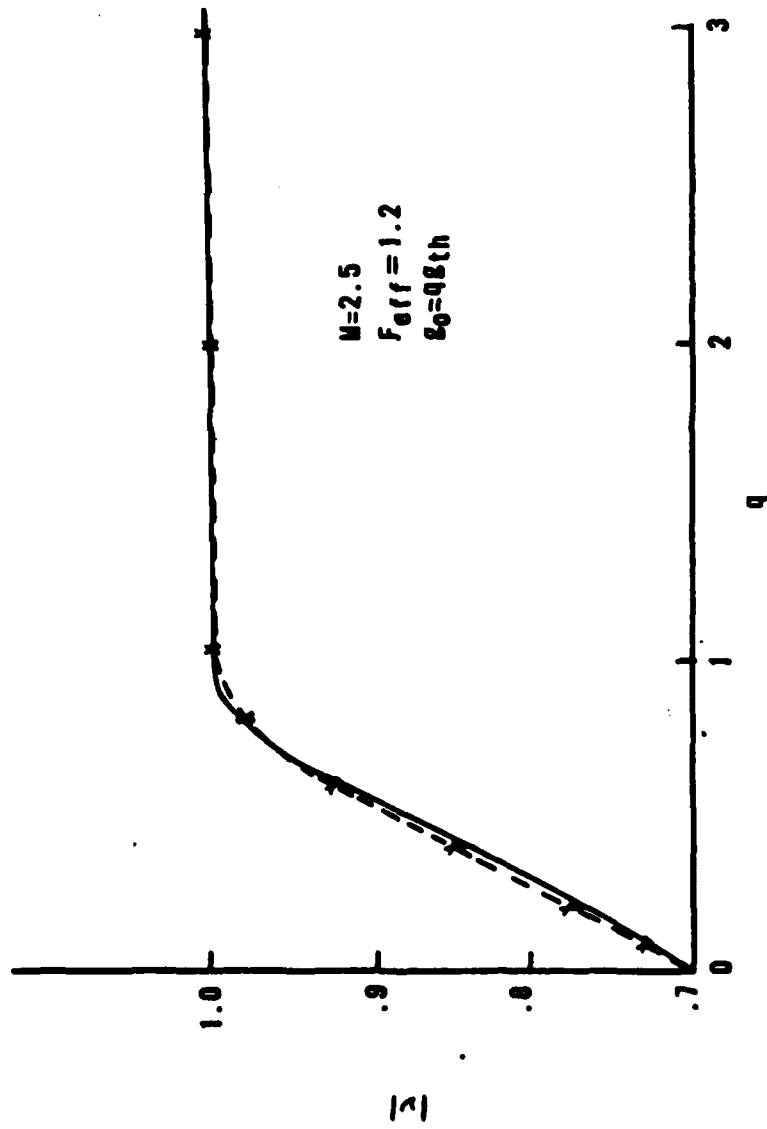


Figure 4.4 Amplitude of Eigenvalue as Function of Small Signal Gain.

cavity eigenvalue has a magnitude of unity for small signal gains above threshold. The numerical models did not contain any algorithm that forced this result. Rather, the gain from the stimulated radiation acted to balance the losses due to diffraction. The behavior of the numerical models thus shows the "gain equal loss" behavior expected from laser theory for the above threshold case. A final conclusion is that the magnitude of the loaded cavity eigenvalue is not a good discriminator between the two models.

A better discriminator is the phase of the loaded cavity eigenvalue. Figure 4.5 shows this parameter as a function of the small signal gain, again scaled by the threshold gain value. The top plot shows the results of the multiplicative model while the bottom plot shows the behavior for the additive model. For gains below threshold, the phase doesn't depart significantly from the phase of the bare cavity eigenvalue for the multiplicative model but it does change for the additive model. This is more significant when we recall that the phase of the eigenvalue is associated with the frequency of the mode that exists in the resonator (Ref 6:179). Thus the additive model predicts the frequency of the loaded cavity mode shifts as the small signal gain is increased toward threshold. This result is more physically realistic than the lack of a frequency shift predicted by the multiplicative model as the presence of the gain medium begins to affect the mode. Both models predict that the frequency shifts as the gain is increased above threshold.

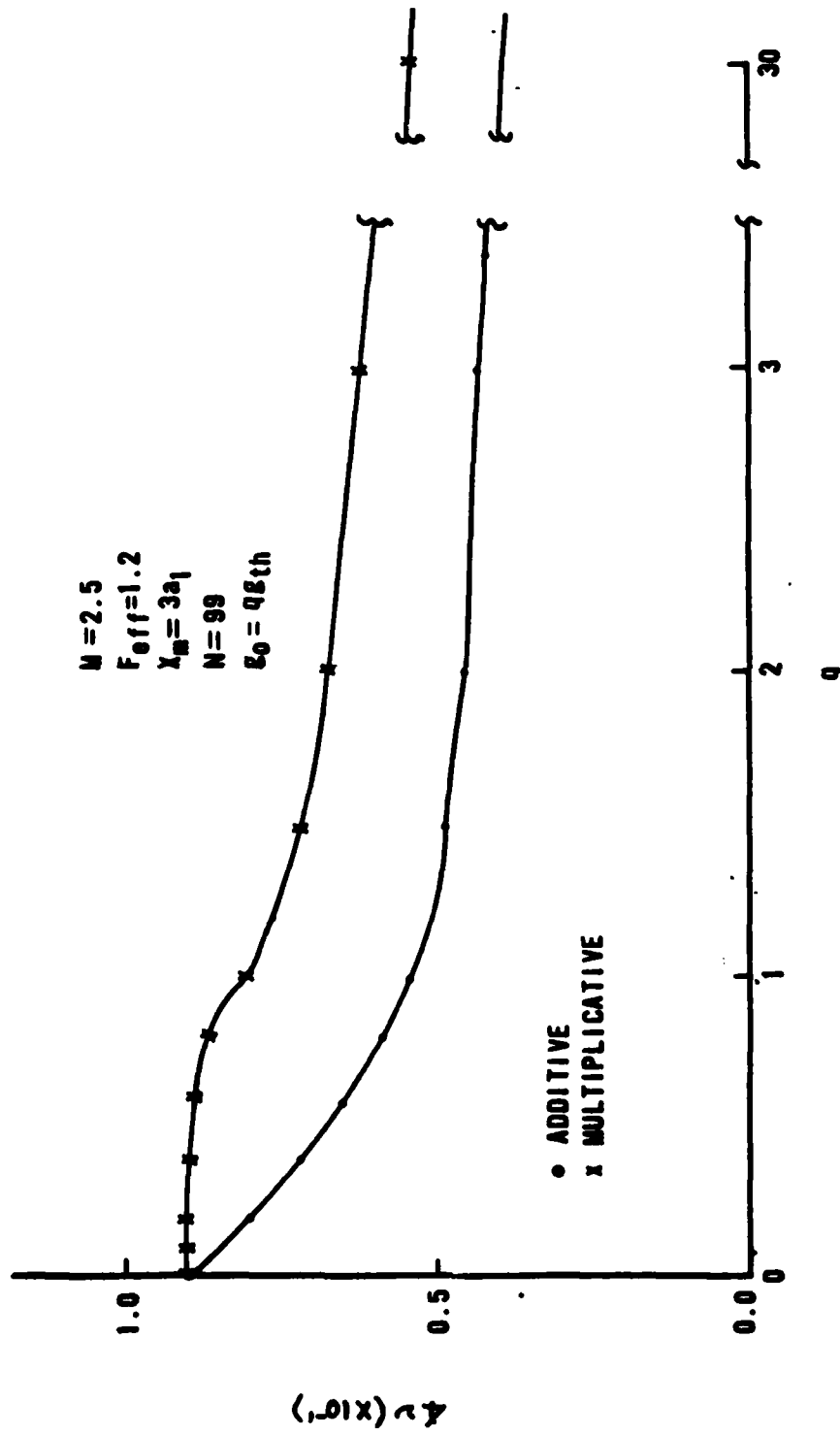


Figure 4.5 Phase of Loaded Cavity Eigenvalue as Function of Gain.

The amount of frequency shift eventually becomes constant for gains far above threshold. Different oscillation frequencies are predicted by the two models. The direction of the frequency shifts varied for the different Fresnel numbers studied. In a subsequent section we will examine the variation of the eigenvalue phase as a function of the equivalent Fresnel number. Here we only note that the two models yield different behavior for the frequency of the loaded cavity mode but both show the frequency shift becomes fixed for gains far above threshold.

The last result that is discussed in this section is the variation of the power on the feedback mirror as a function of the small signal gain. Figure 4.6 shows this variation as predicted by both models. Also shown on this plot is the geometrical optics prediction derived earlier in the chapter. The line labeled  $P_{oa}$  is obtained from Eq(4.18). The first point to be made about these plots is that there is essentially no power on the feedback mirror until the gain is increased above threshold. Both models predict about the same threshold. Note that Eq(4.18) also gives a threshold that is slightly below the geometric threshold developed by Rigrod:

$$g_{th} = \frac{\ln(M)}{2L} \quad (4.36)$$

The results of the multiplicative model deviates farther from the geometrical optics prediction than those of the additive model in this case and all the other cases studied. While

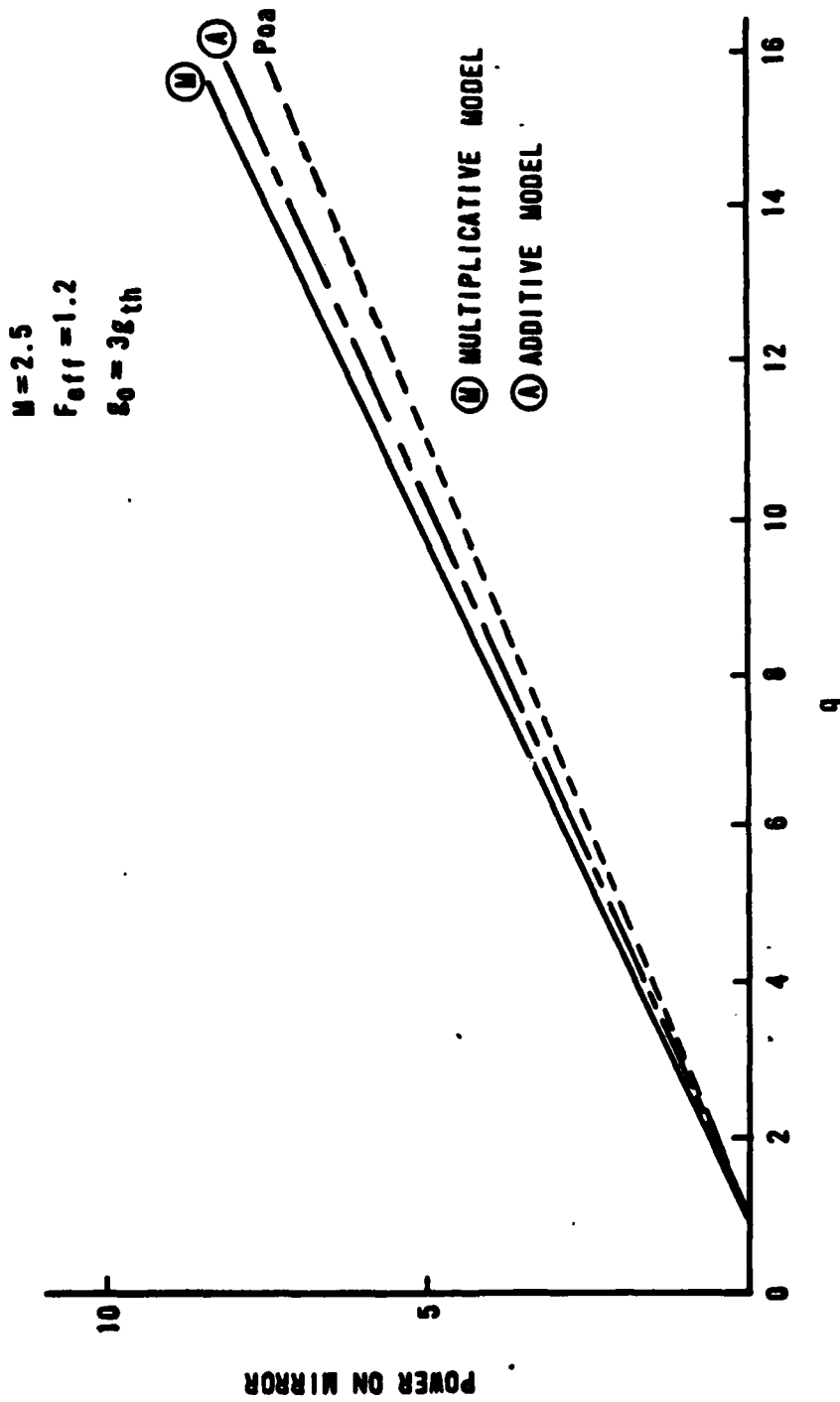


Figure 4.6 Power on Mirror as Function of Small Signal Gain.

this doesn't prove that the additive model is more correct than the other model, it does suggest that the additive model is in closer agreement with the geometrical optics prediction than the multiplicative model. A final statement about Figure 4.6 is that the power on the feedback mirror increases linearly with increasing gain. Figure 4.7 shows the outcoupled fraction of the power as a function of small signal gain. (See Eq(4.35)) Again, a threshold behavior is exhibited by both models. In this case, the only reference that can be used is the geometric outcoupling fraction shown by the horizontal dashed line. (Whether the curves predicted by the diffractive models will lie above or below the geometric outcoupling fraction depends on the Fresnel number. The behavior will be discussed in Section 7.) Here, the outcoupling shows saturation as the gain is increased. This saturation occurs as the gain in the region off the feedback mirror is saturated. The gain on the feedback mirror saturates faster than the gain off the mirror since the gain on the mirror is saturated by two way flux. The results in Figure 4.7 agree well with the basic understanding of laser physics, i.e. both models predict the correct trends.

##### 5. Intensity/Phase Plots for Small Signal Gain Variations

In this section we will examine the variations in the intensity and phase of the loaded cavity mode as the small signal gain is increased from zero to far above threshold. Both the additive and multiplicative models are used to

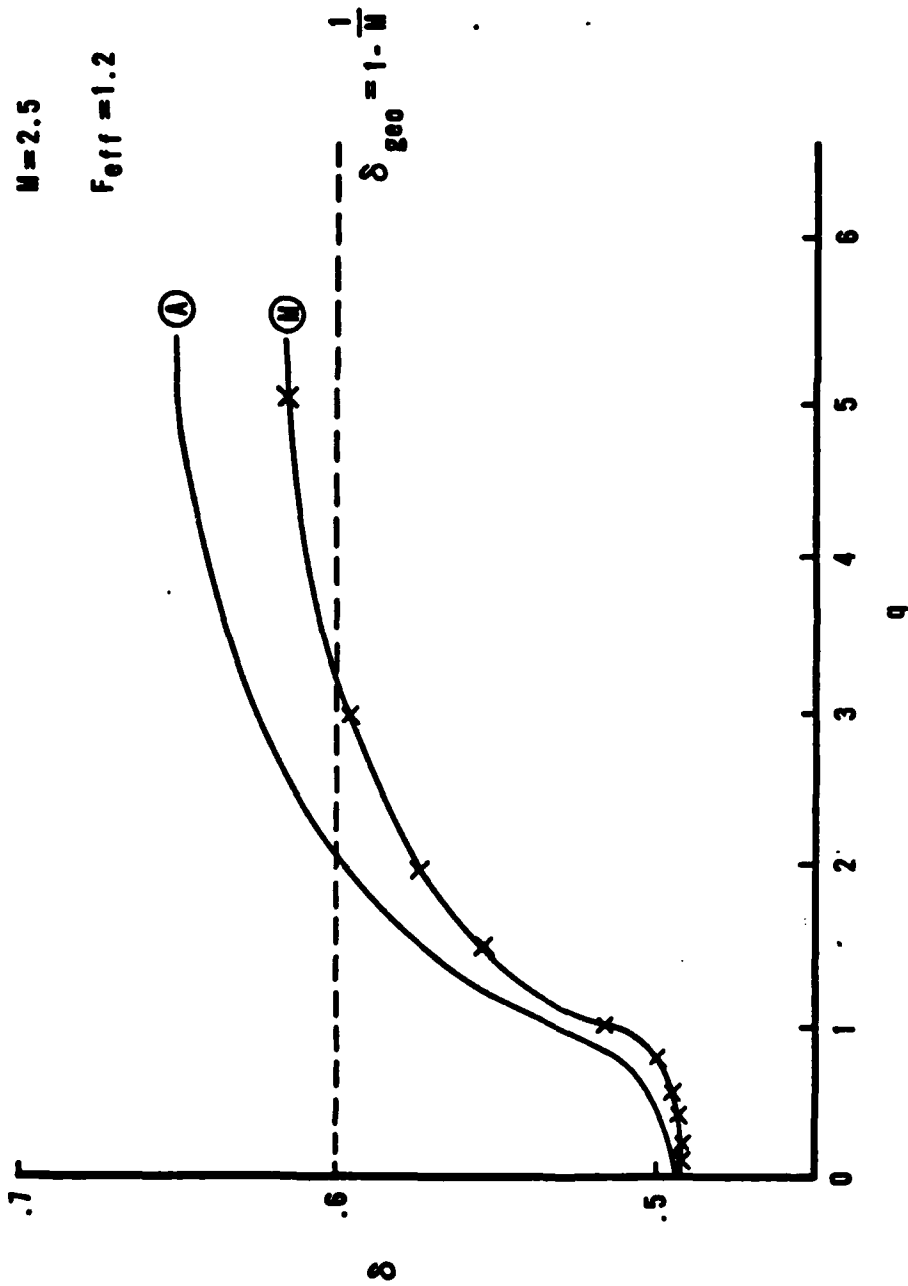


Figure 4.7 Outcoupling as a Function of Small Signal Gain.

generate these plots so that a further comparison can be made between the two models. Again, the case that is presented is the case of a positive branch confocal resonator with a magnification of 2.5 and equivalent Fresnel number of 1.2 . All of the plots represent numerical calculations that converged in the sense that the loaded cavity eigenvalues did not vary for several iterations by more than one percent. An adequate number of points was taken on a grid that extended at least from  $-Ma_1$  to  $Ma_1$  , based on the discussions of convergence given above.

Figures 4.8 to 4.13 show the intensity of the loaded cavity mode in the plane just before the feedback mirror. The gain varied from zero (Figure 4.8) to five times the geometric threshold (Figure 4.13). The intensity is normalized such that the peak value is set to unity. The abscissa is scaled by the halfwidth of the feedback mirror so that  $-1$  and  $+1$  represent the edges of the mirror. In these figures, the plots labeled with A represent the results of the additive model and the plots labeled with M represent the results of the multiplicative model. We will now discuss each intensity profile separately.

Figure 4.8 is the intensity of the lowest loss bare cavity mode. This plot agrees well with the results of Chapter II where the matrix approach was used to obtain the bare cavity modes. This profile is shown as the baseline against which the other intensity profiles can be compared.

Figure 4.9 is the intensity profile for the case where the small signal gain is 0.4 times the geometric threshold.

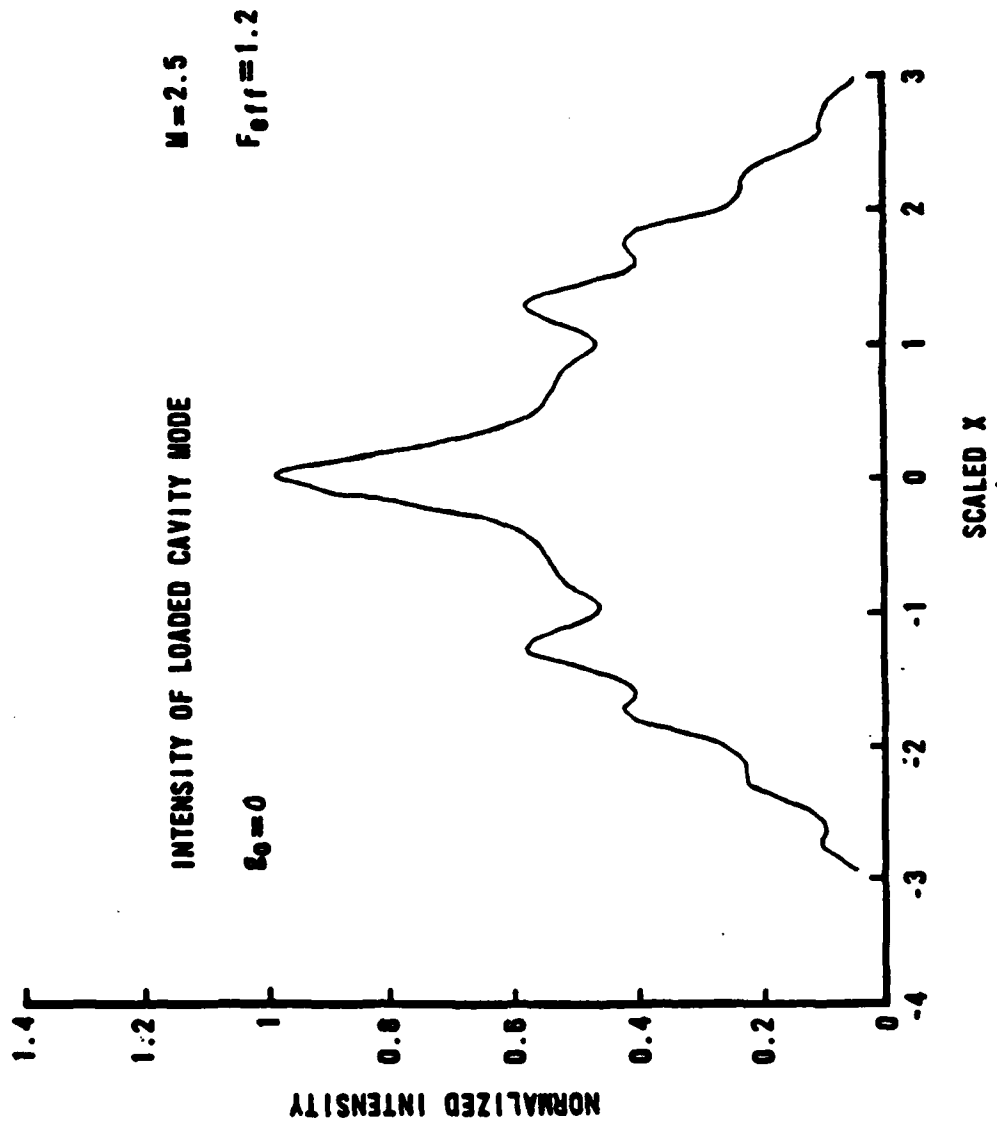


Figure 4.8 Intensity of Loaded Cavity Mode:  $\epsilon_0 = 0.0$  .

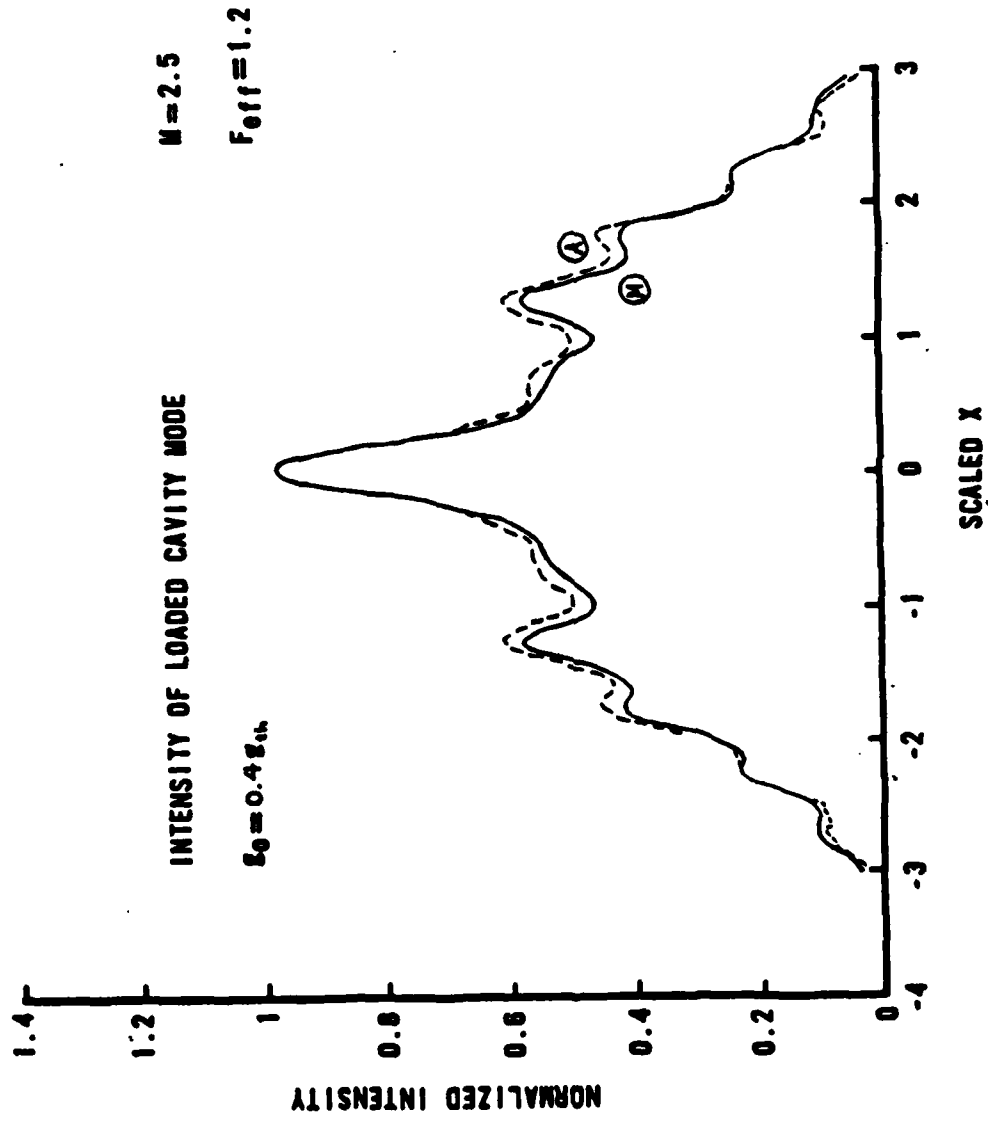


Figure 4.9 Intensity of Loaded Cavity Mode:  $\delta_0 = 0.48^{th}$  .

Here the results of the two models are already showing slight differences, although the plots are in good agreement. The additive model shows the mode filling in faster on the mirror as well as increasing more rapidly off the mirror. The general profile has not changed significantly from the bare cavity mode. The peaks and valleys have not shifted in location, and the profile is still dominated by a central peak.

The next figure, Figure 4.10, has the small signal gain set at 0.8 times the geometric threshold. Again the additive model shows significantly more filling in of the mode on the feedback mirror. What had been a mild shoulder at the edge of the mirror has become another peak. This is the only significant change in the general profile. In fact, when the results of the multiplicative model for this gain level are overlaid on the bare cavity mode, only a slight increase in the intensity is noticed. Recall that the phase of the eigenvalue, Figure 4.5, and the outcoupling, Figure 4.7, did not change significantly from the bare cavity value for the multiplicative model. This correlates well with the intensity profile.

Figure 4.11 is the intensity of the loaded cavity mode when the small signal gain is equal to the geometric threshold. The trends discussed above continue, with the new peak at the edges of the feedback mirror becoming more pronounced for the additive model. The intensity predicted by the multiplicative model differs from the bare cavity plot

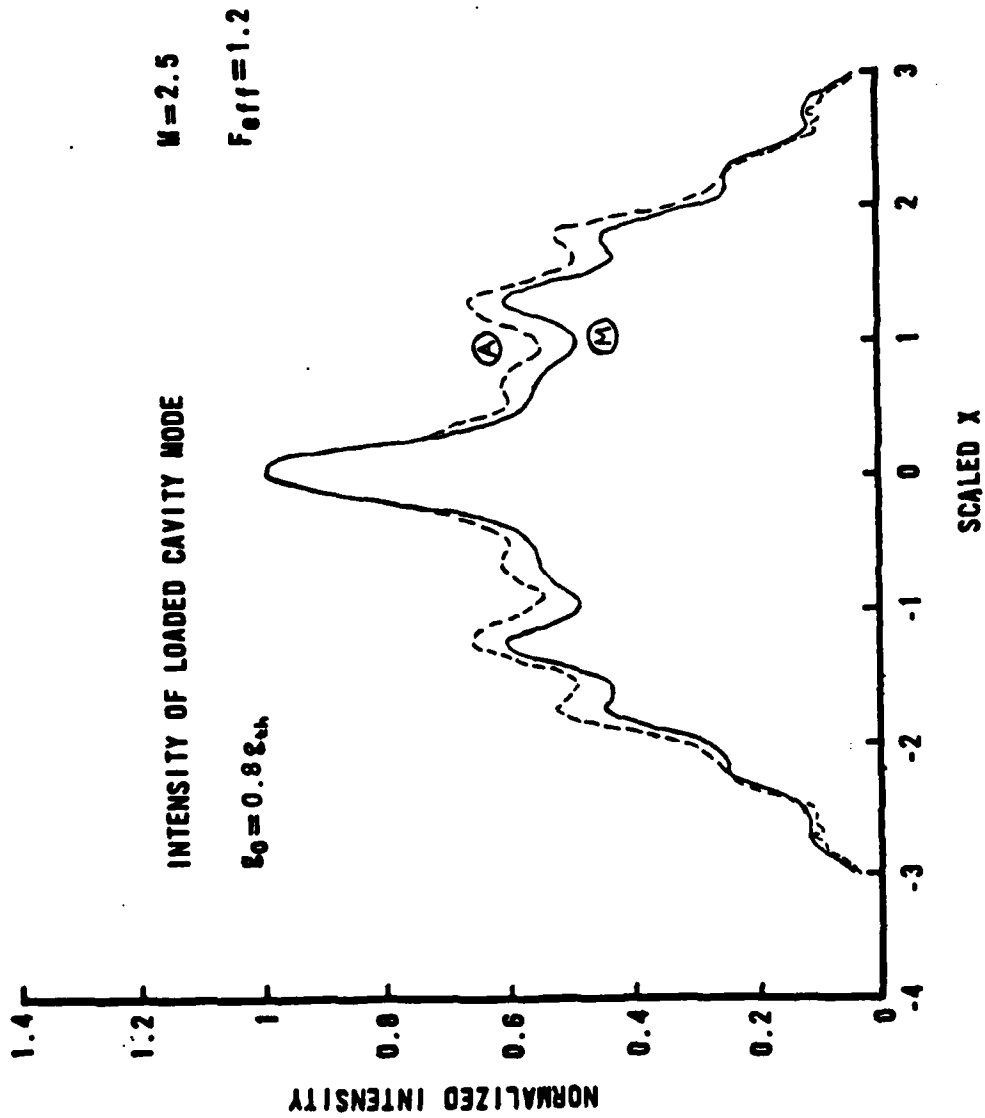


Figure 4.10 Intensity of Loaded Cavity Mode:  $\epsilon_0 = 0.8 \epsilon_{sh}$  .

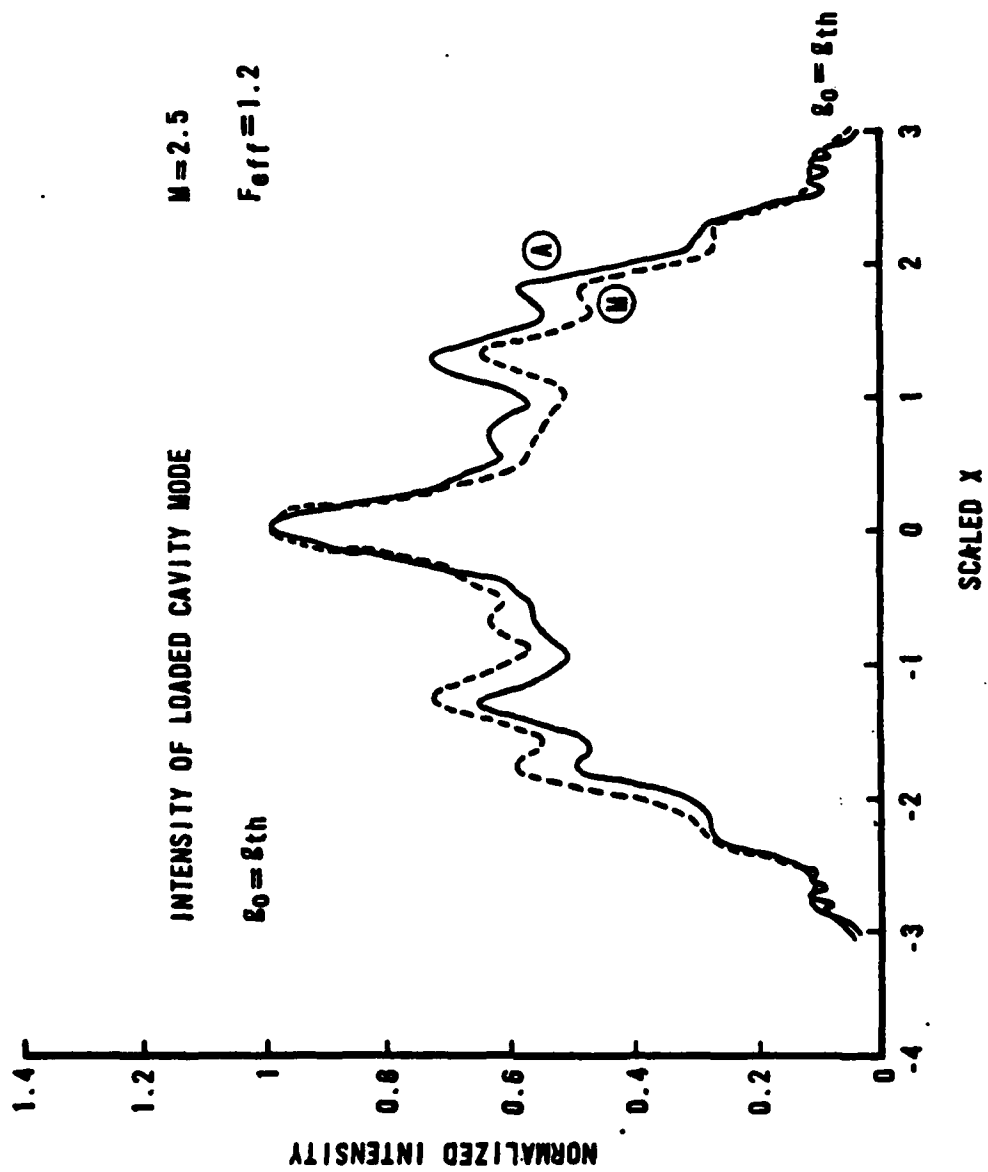


Figure 4.11 Intensity of Loaded Cavity Mode:  $g_0 = 8th$  .

only in that the intensity is increased across the mode. Neither the location of the peaks and valleys nor the relative heights of the peaks have changed.

When the small signal gain is set to twice the geometric threshold, a sharp jump at the edge of the feedback mirror is apparent in both plots. (See Figure 4.12) This is due to the gain model, which sharply changes the saturation of the gain from two way flux to one way flux. The intensity profile predicted by the additive model shows the intensity on the feedback mirror has continued to fill in. One expects the mode to fill in on the feedback mirror since the gain is less strongly saturated where the intensity is lower and thus the field should increase more rapidly here. This behavior is shown in the region off the mirror, where the gain is only saturated by one way flux. The intensity on the feedback mirror that is predicted by the multiplicative model still resembles the bare cavity mode. Some filling in of the intensity is apparent when this plot is compared to the bare cavity mode.

The last intensity profile, Figure 4.13, shows the results when the small signal gain is five times the geometric threshold. (This case is more representative of an actual laser system. Only by having the small signal gain significantly higher than the geometric threshold of the resonator can significant amounts of power be extracted from the medium.) Here the additive model shows the central peak to be lower than peaks located off the mirror while the multiplicative model still shows the central peak to

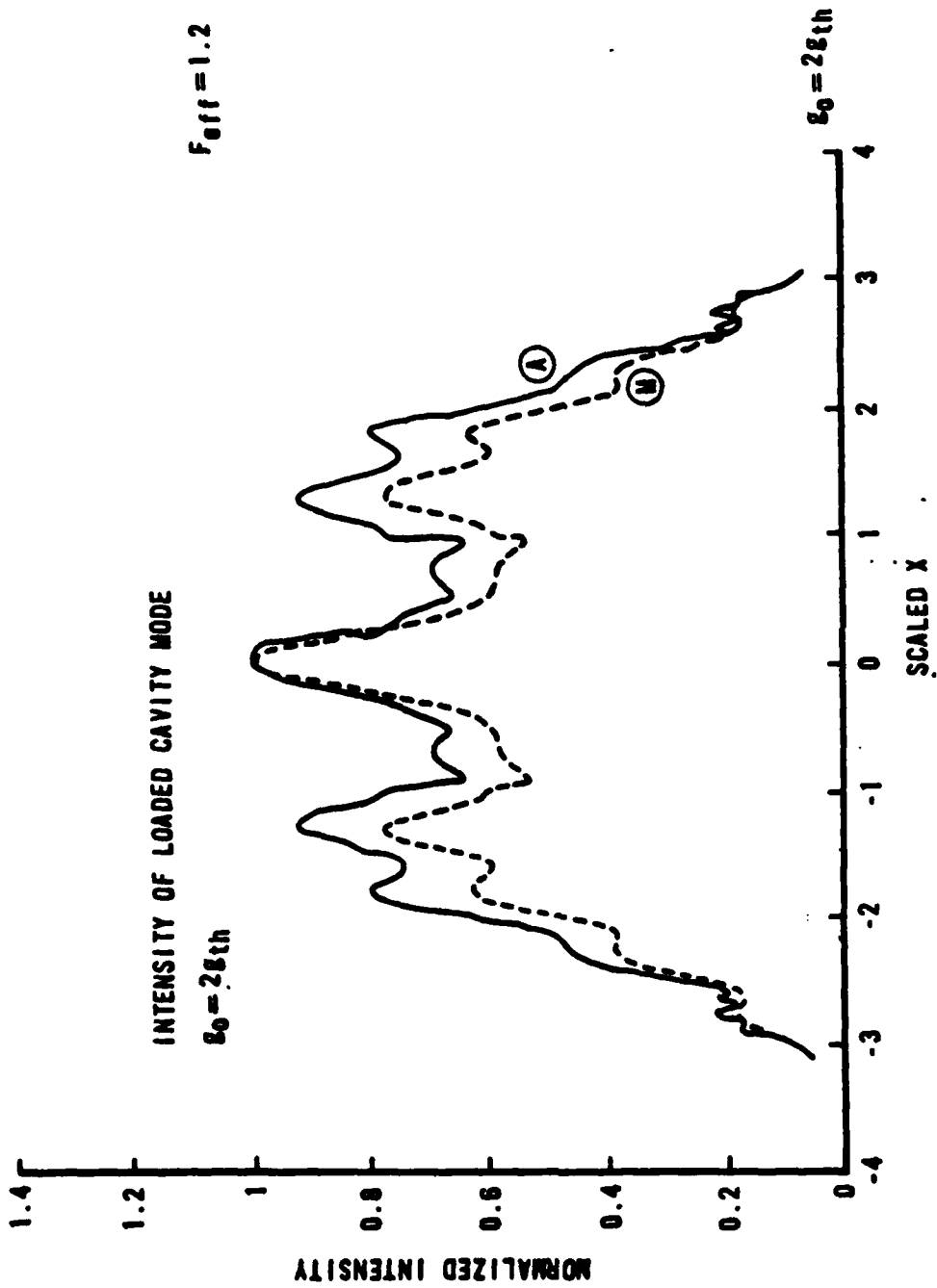


Figure 4.12 Intensity of Loaded Cavity Mode:  $g_0 = 2.0 g_{th}$  .

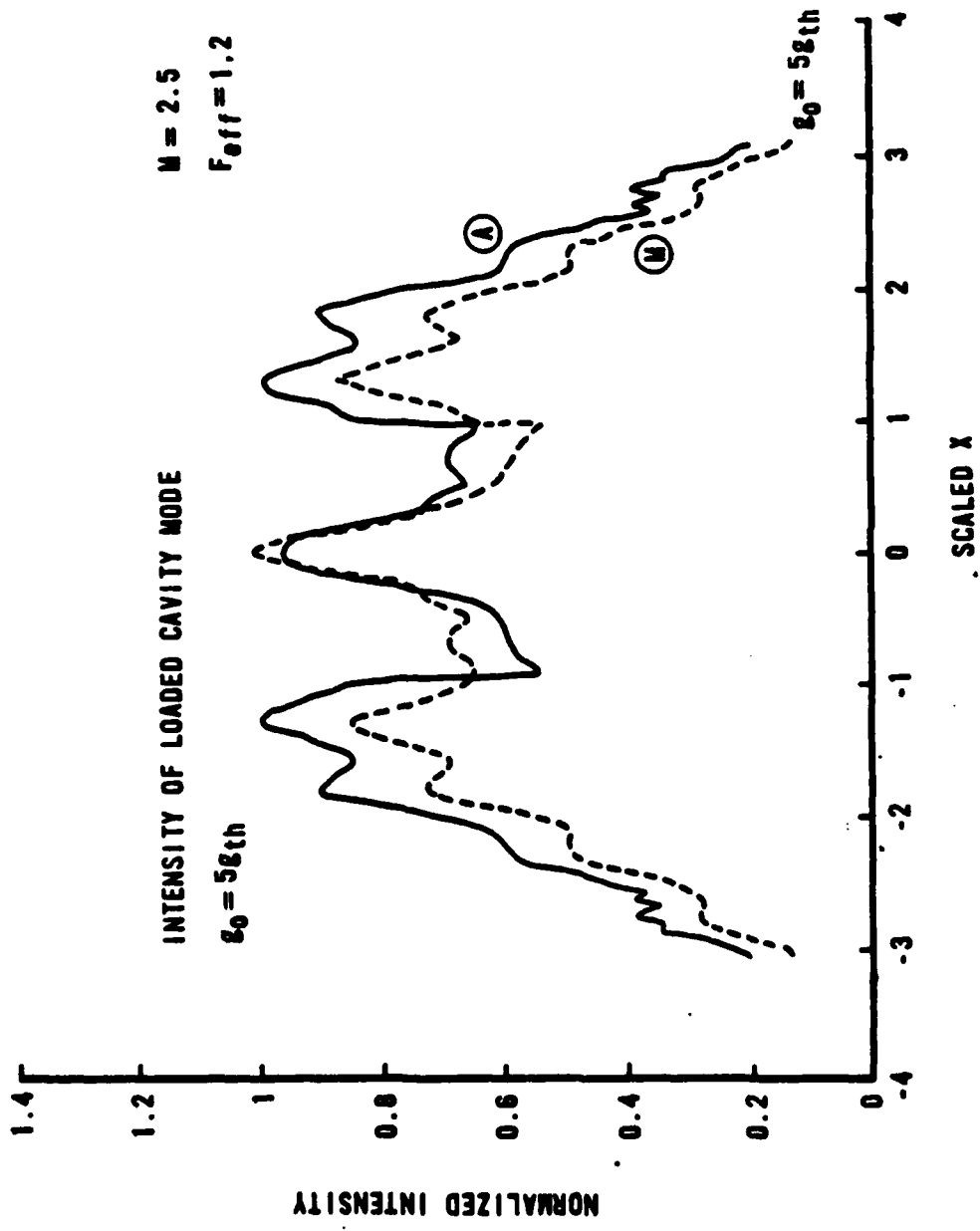


Figure 4.13 Intensity of Loaded Cavity Mode:  $g_0 = 5.0 g_{th}$

dominate. The new peaks near the edges of the feedback mirror that were predicted by the additive model were never predicted by the multiplicative model. These peaks are a result of the more complicated additive term that includes the diffraction of the radiation stimulated on the first pass as this radiation propagates out of the resonator. If more gain sheets had been used or if the full diffraction terms given in Chapter III were used, these peaks may have been different. But the significant point is that the profile differs from the bare cavity mode. The multiplicative model does not show these changes. As the gain is increased further in both models, the mode on the mirror does not change much since the gain is now nearly saturated. For very high gains, even the gain off the mirror exhibits saturation in that the intensity profile does not increase significantly as the gain is increased.

The phase of the loaded cavity mode does not change appreciably as the gain is increased from zero. Figure 4.14 shows the phase predicted by both models for small signal gain set at five times the threshold value. The bare cavity phase is also shown for reference purposes. Since the phase does not change significantly, we expect the far field beam quality will be unchanged from the beam quality of the lowest loss bare cavity mode. This is important since the lowest loss bare cavity mode calculations can be used for beam quality calculations. This conclusion is limited to the simplified model of simple saturable gain. More realistic

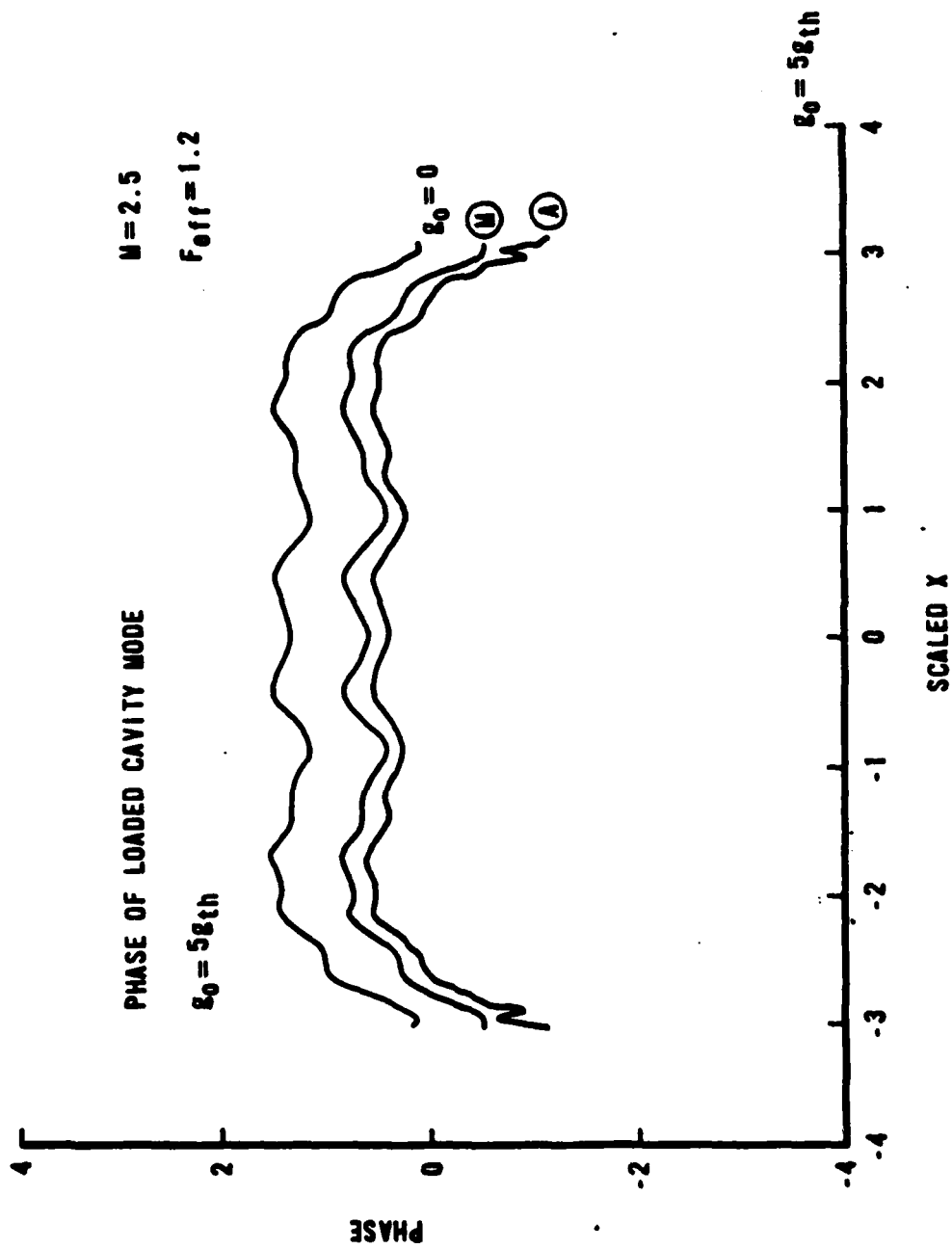


Figure 4.14 Phase of Loaded Cavity Mode:  $g_0 = 5.0 g_{th}$  .

kinetics might introduce asymmetries and phase shifts that would change the beam quality of the loaded cavity mode as compared to the bare cavity mode.

The final figure of this section, Figure 4.15, shows the gain profile from the additive model for the case where the small signal gain is set at five times the geometric threshold. The first observation is that the actual threshold is lower than the geometrically estimated value. Even using the geometrical optics analysis of Section C, the threshold is given by

$$g'_m = \frac{2}{L} \left( \frac{\sqrt{M} - 1}{\sqrt{M} + 1} \right) . \quad (4.37)$$

For this case ( $M=2.5$ ), Eq(4.37) gives a threshold of 0.306 instead of the geometric threshold of 0.312 predicted by Eq(4.36). Examining Figure 4.15, we find that the diffractive model still gives a lower threshold of about 0.22. This lower threshold was also shown in earlier plots of the amplitude and phase of the loaded cavity eigenvalue. Figure 4.15 also shows the distinct jumps at the edges of the mirror that are an artifact of the single gain sheet model used in the models. This gain profile is typical of the profiles obtained with either model for various gains. Because of the single gain sheet model, the gain profile tends to look like an inverted plot of the intensity profile. This appearance can be understood by realizing that the gain begins at the small signal gain level and then the intensity decreases this gain by an amount that is proportional to the

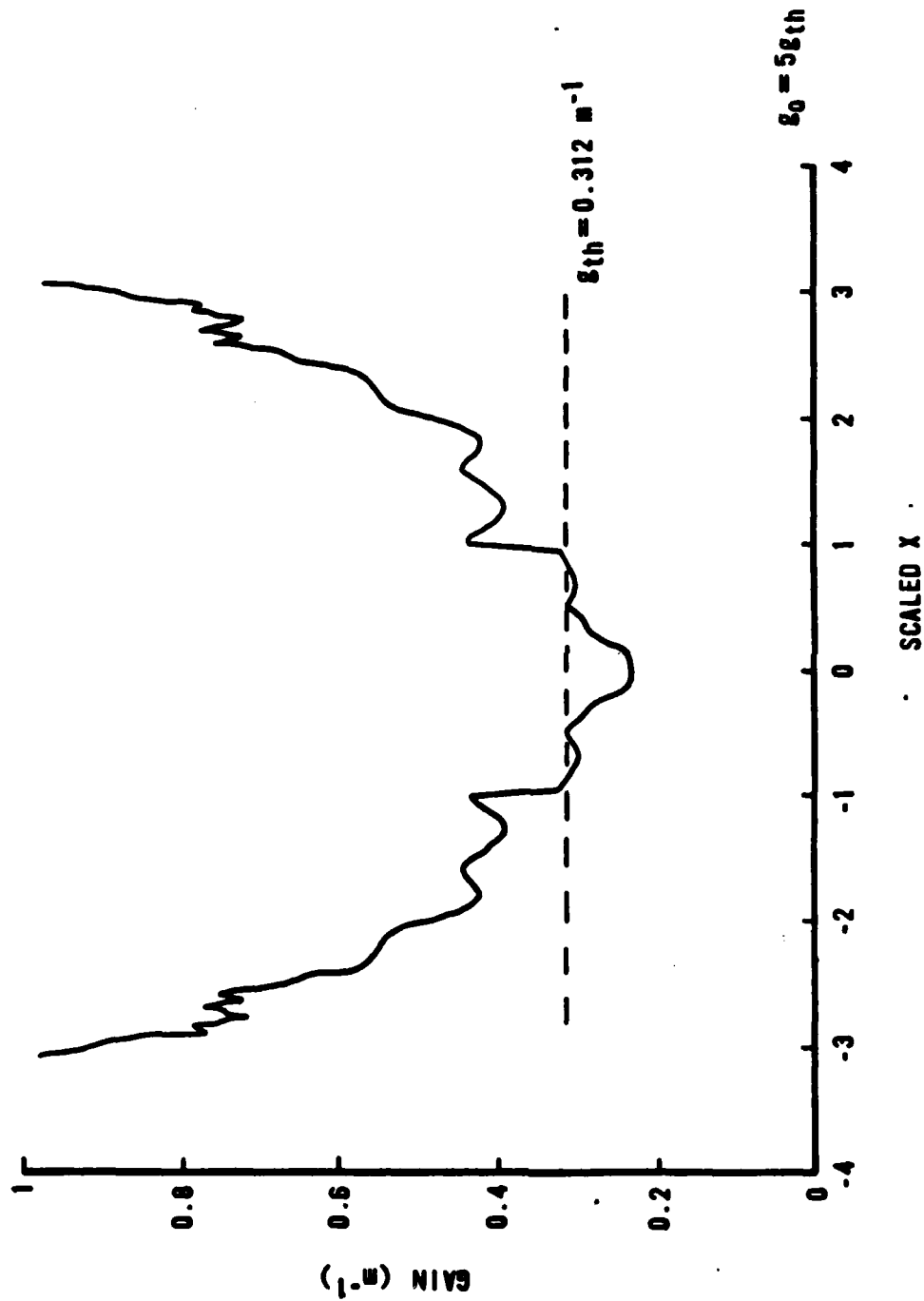


Figure 4.15 Gain Profile.

intensity. Thus where there is higher intensity, there will be lower gain. (Note also that the function  $1/(1+x)$  can be approximated to first order by  $1-x$ . This can be applied to the simple saturable gain model, Eq(4.2).)

This discussion of the intensity and phase profiles of the loaded cavity mode as the small signal gain is increased has four main points that are briefly restated here. First, the multiplicative model tends to underestimate the power output of the resonator as compared to the additive model. This may be due to the behavior of the exponential function for the field off the feedback mirror. Second, the additive model shows that the profile may change from the bare cavity mode due to the diffraction of the stimulated radiation and its coherent addition with the stimulating field in the resonator. This combination might introduce new structure in the mode. Third, the phase of the loaded cavity mode does not significantly differ from the bare cavity mode, indicating that the beam quality from the two modes should be about the same. Finally, the threshold predicted by the diffractive models is less than the threshold predicted by the one dimensional models. This is probably due to the peaking of the intensity near the axis. There are some Fresnel numbers where a minimum occurs on axis and these cases might show different threshold behavior. We now consider a case of a different Fresnel number, namely the case of a mode crossing.

## 6. Loaded Cavity Mode Near a Mode Crossing

A mode crossing occurs for a magnification of 3 and equivalent Fresnel number of 1.8742. This case was studied in Chapter II in depth and the matrix technique showed the two lowest loss even modes had the same loss as measured by the magnitude of the eigenvalue. The iterative approach could not be applied to the bare cavity mode crossing case since convergence is extremely slow. In this section, this case is examined with the loaded cavity models to see if convergence can be obtained and what the mode characteristics would be.

Figures 4.16 and 4.17 show the convergence history as measured by the magnitude of the loaded cavity eigenvalue. The first figure is for the case where the small signal gain is equal to the geometric threshold. The multiplicative model did not converge in the twenty iterations shown while the additive model showed good convergence in about fourteen iterations. However, the magnitude of the loaded cavity eigenvalue was less than one, showing that threshold had not been reached. The important point is that the additive model did converge and the multiplicative model did not. This supports the supposition at the end of Chapter III that the additive model may have a unique solution since it is an inhomogenous integral equation while the multiplicative model may not have a unique solution since it is a homogeneous integral equation. In fact, a linear homogeneous Fredholm integral equation of the second kind usually has a spectrum of eigenfunctions as was seen in the bare cavity analysis of

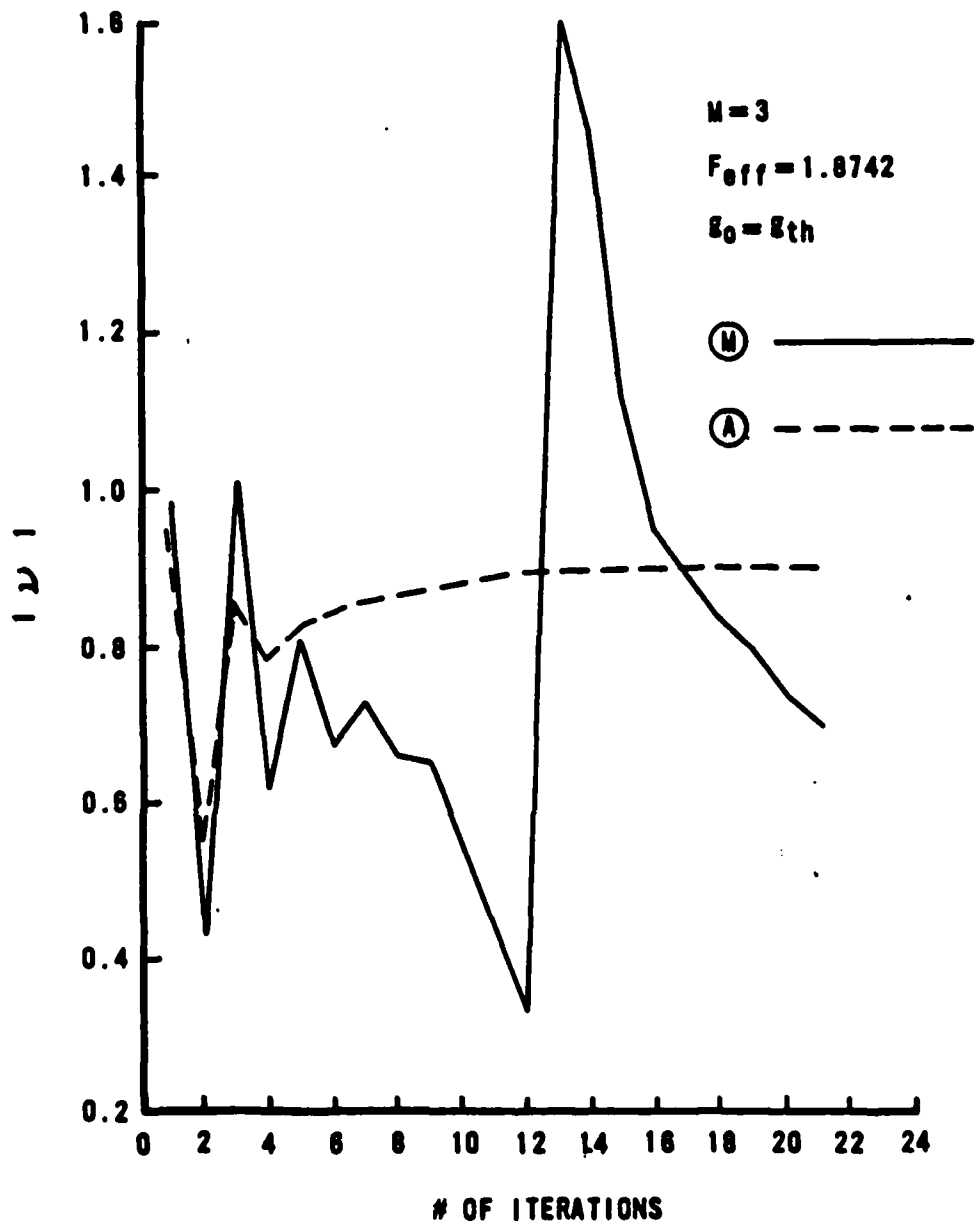


Figure 4.16 Convergence History:  $S_0 = 8th$ .

## Chapter II.

In Figure 4.17, the gain has been increased to three times the threshold value. Here, both models did converge to an answer where the loaded cavity eigenvalue had a magnitude of one. However, the additive model gave more rapid convergence, converging in about ten iterations versus thirteen for the other model. Also, the magnitude of the variations was more pronounced for the multiplicative model. The fact that this latter model did converge for this case indicates that the gain now dominates the kernel of the integral equation and the degeneracy observed for the bare cavity mode is no longer apparent for this case. At some point where the gain is far above threshold, the gain becomes the dominant term in both models and the bare cavity terms are the perturbations.

We next examine the power on the mirror as the small signal gain is increased from zero to above threshold. Figure 4.18 shows the behavior. As discussed earlier, the additive model gives results that agree more closely with the geometrical optics prediction given by Eq(4.18) and plotted as the uppermost line. Note also that because of convergence problems, the multiplicative model was only used to calculations well above threshold. The resonator designer intentionally tries to avoid mode crossings in the design of high energy laser resonator in order to obtain good "mode control" and so the utility of either model at a mode crossing is of more academic than practical interest. The

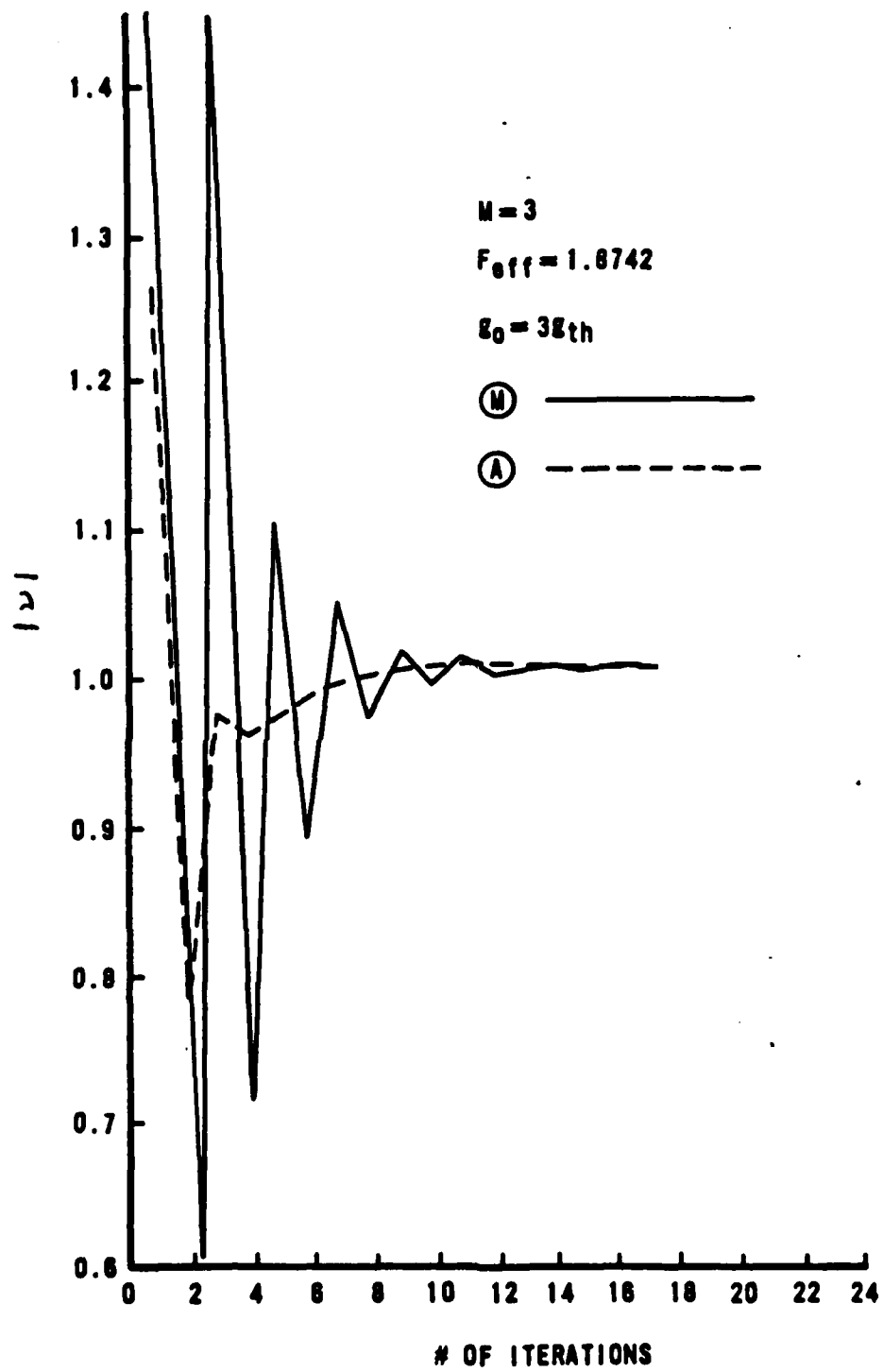


Figure 4.17 Convergence History:  $g_0 = 3.0 g_{th}$ .

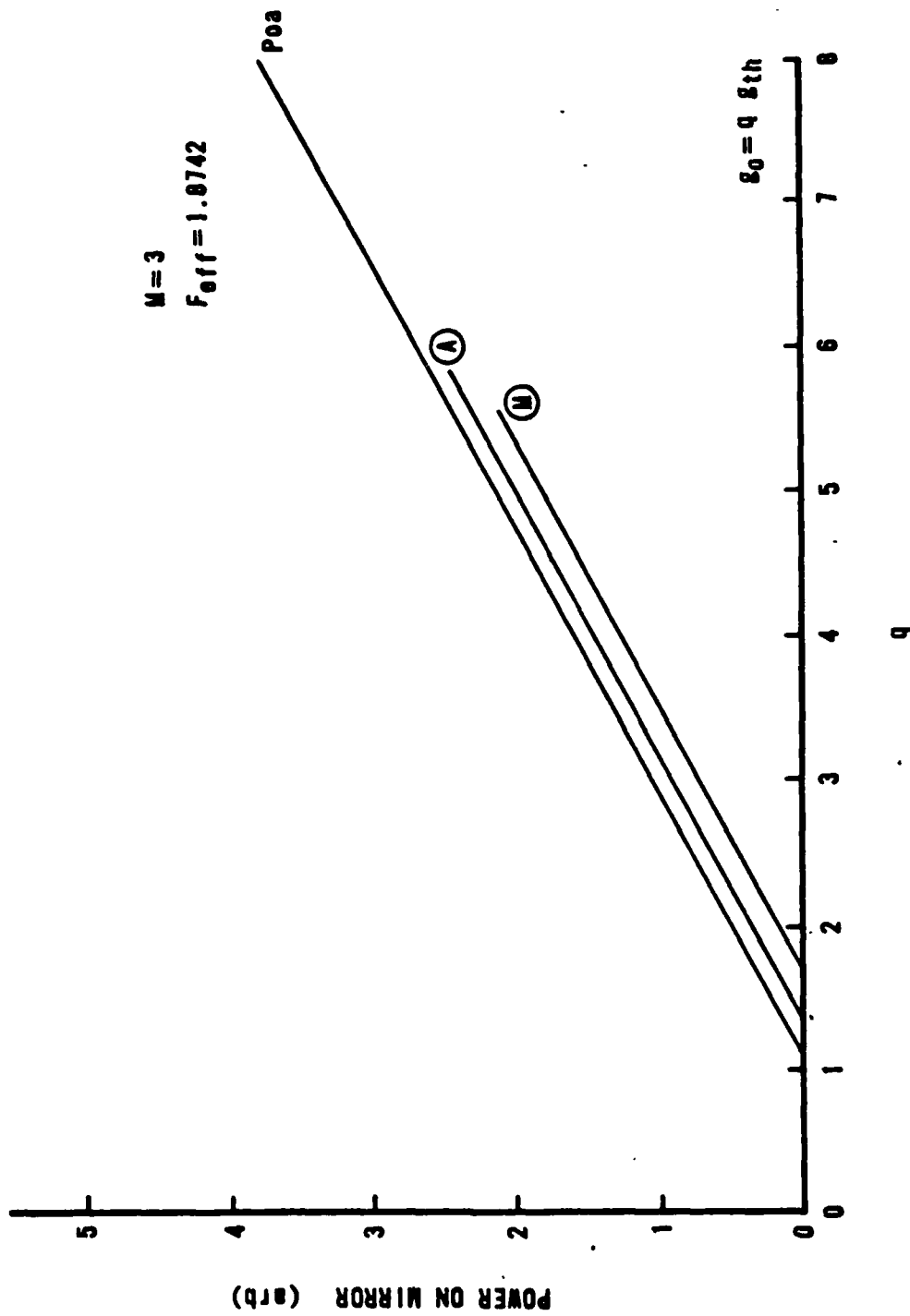


Figure 4.18 Power on mirror at Mode Crossing.

results indicate that the additive model is a more stable model of the loaded cavity.

#### 7. Trends in Loaded Cavity Eigenvalues and Power on Mirror With Variations in Fresnel Number

In this section we return to examining the phase of the loaded cavity eigenvalue and the power on the feedback mirror as the equivalent Fresnel number is varied. In the bare cavity case, we observed a periodic fluctuation in the magnitude of the eigenvalue with variations in the equivalent Fresnel number. (See Figure 2.9) The fluctuations had maxima at equivalent Fresnel numbers of about  $n+0.375$  and minima (mode crossings) at equivalent Fresnel numbers of about  $n+0.875$  where  $n$  is any positive integer. In the loaded cavity case, the magnitude of the eigenvalue is fixed at unity for gains at or above threshold. However, we will observe a similar fluctuation in other parameters.

The first parameter we examine is the power on the feedback mirror after convergence is obtained. Figure 4.19 shows the results obtained with the additive model. Here the small signal gain is set at three times the geometric threshold value. The oscillations are evident and the location of the maxima and minima are about the same as those observed in the bare cavity case. However, the amplitude of the oscillations appears to damp out with increasing Fresnel number. In fact, the results appear to be damping out to a value that is in good agreement with the geometrical optics

$M = 2.5$   
 $E_0 = 38\text{th}$

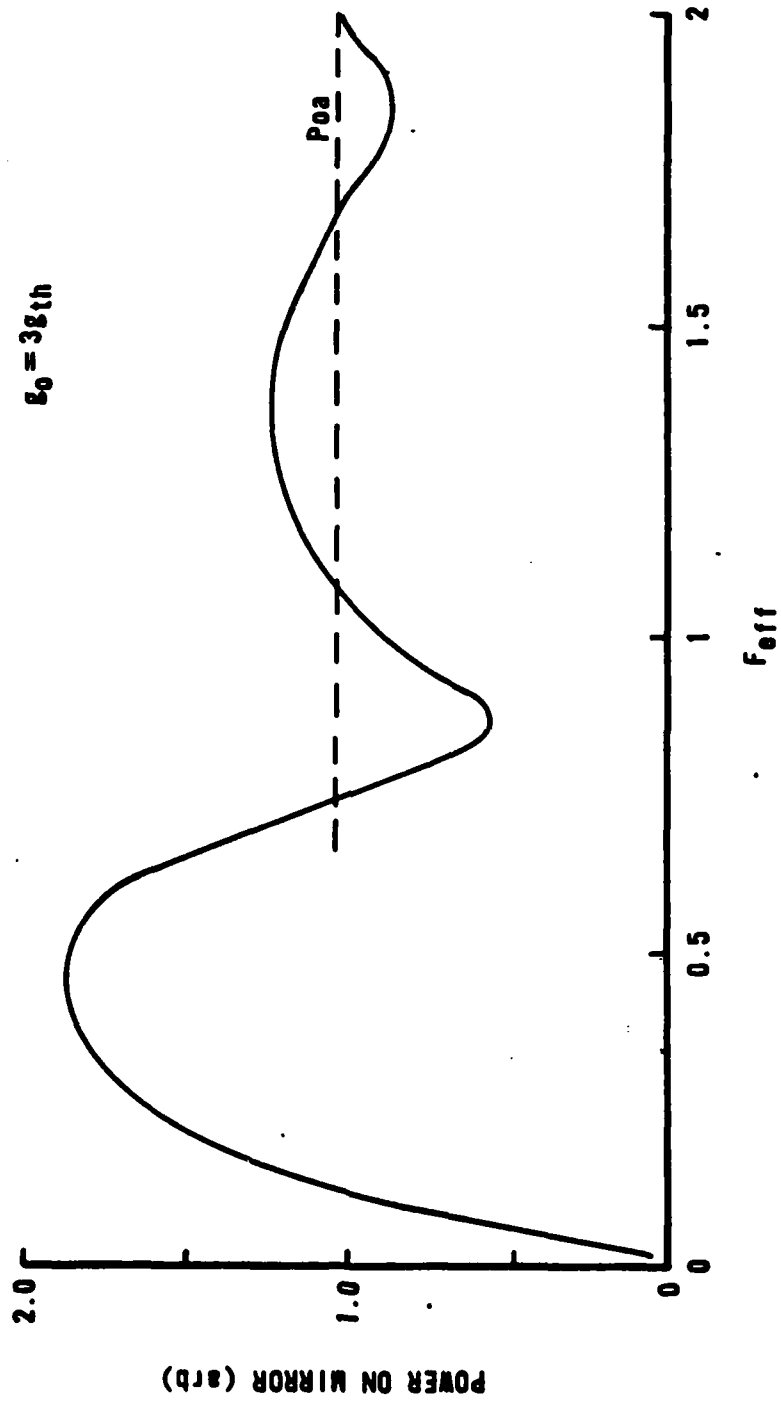


Figure 4.19 Power on Mirror versus Equivalent Fresnel Number.

prediction given by Eq(4.18). A limited number of calculations were made at higher equivalent Fresnel numbers and the agreement with the geometrical optics prediction was even better. As a function of Fresnel number, the diffractive model rapidly approaches the geometrical optics limit. One other series of calculations was made with the small signal gain set at the threshold gain and similar behavior was observed. The expense involved with such calculations has prohibited a more in-depth study. The main observation is that the location of the maxima/minima are the same as those observed for the bare cavity case. The power on the mirror is similar to the magnitude of the eigenvalue as a measurement of the amount of feedback in the resonator. In fact, some large resonator codes such as the System Optical Quality (SOQ) code used at the Air Force Weapons Laboratory use power calculations for convergence criteria instead of field points, as in this model.

The second parameter we examine is the phase of the loaded cavity eigenvalue. Figure 4.20 shows the results obtained from the same series of calculations that produced the power on the mirror results discussed above. Again the oscillatory behavior is evident but here the locations of the maxima and minima do not correspond to the previous results. The maxima occur at about integer equivalent Fresnel numbers and the minima occur at equivalent Fresnel numbers of about  $n+.7$ , where  $n$  represents a positive integer. However, a close examination of the results shows that near the values  $n+.375$  and  $n+.875$  the phase of the eigenvalue passes

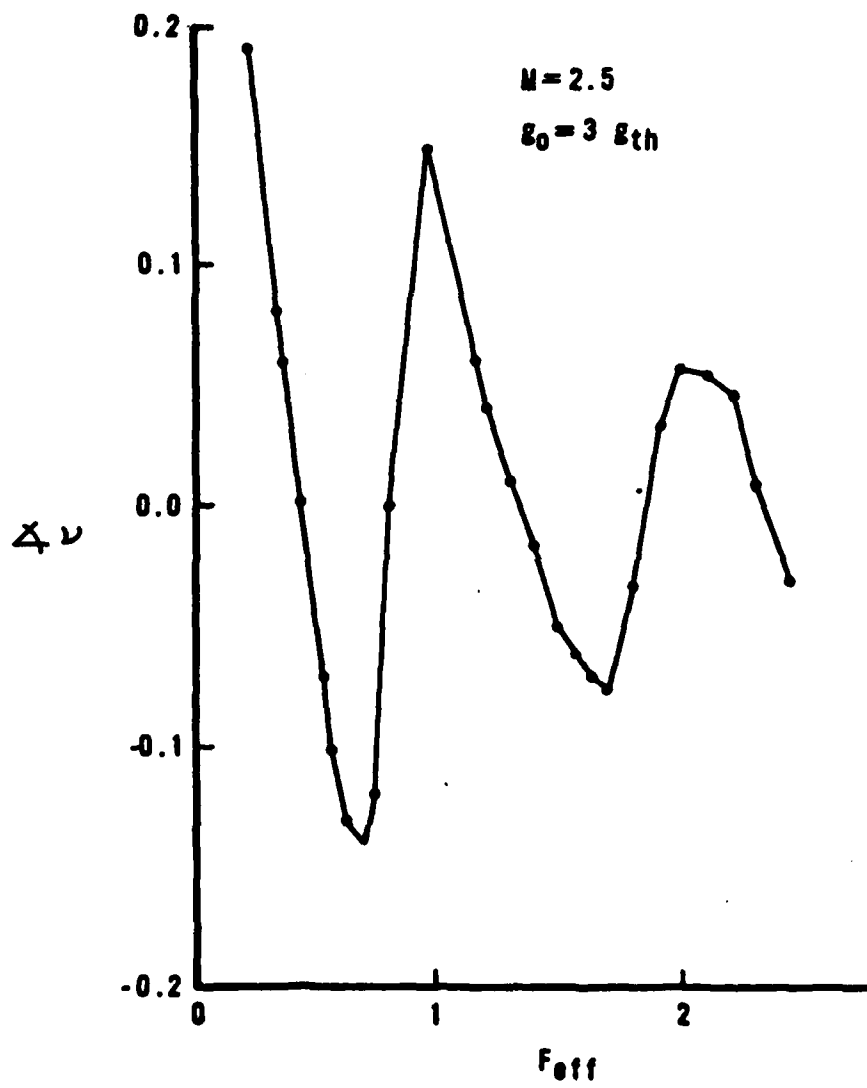


Figure 4.20 Eigenvalue Phase Variations with Fresnel Number.

through zero. In these cases the eigenvalue is purely a real number. One other observation is that the oscillations damp out with increasing Fresnel number over the limited range studied here. The limiting value would appear to be zero for the phase. This is in good agreement with the geometrical optics predictions, since there is zero phase in the geometrical optics model. Thus the frequency shift would be zero, but this shift is applied to the infinite frequency (or zero wavelength) case. As was stated earlier, the primary conclusion to be drawn from these results is that the oscillatory behavior observed in the bare cavity eigenvalue as a function of Fresnel number can also be seen in the loaded cavity. The practical application of this result is that the conventional resonator design criteria of choosing the physical parameters to avoid a mode crossing is still a good design criteria for the loaded cavity. Maximizing the power on the feedback mirror would give the best gain saturation in the "core" of the resonator and thus the most efficient energy extraction from the gain medium.

#### 8. Mapping the Loaded Cavity Mode onto the Bare Cavity Modes

At the end of Chapter III, the expansion of the loaded cavity modes in terms of the bare cavity modes was discussed. The intent of this expansion is to observe how well the bare cavity modes model the loaded cavity as well as to find out how the bare cavity modes combine to make the loaded cavity mode. In this section, some preliminary results are

presented showing how the loaded cavity mode calculated with the additive model can be projected onto the bare cavity modes. The results are very interesting, but the limitations on the resolution of the higher order bare cavity modes as well as some numerical code difficulties restrict the amount of data to be presented and limit the conclusions that can be drawn from the results.

The methodology of obtaining the expansion coefficients is described here. The additive model is used to obtain the loaded cavity mode through the iterative method. Then this mode is projected onto the bare cavity modes (BCM) as described at the end of Chapter III. The bare cavity modes are obtained with the kernel expansion method described in Chapter II using the linear prolate functions as a basis set. Any method of generating the bare cavity modes would be useable for this expansion. The results are expansion coefficients that can be used to reconstruct an estimate of the loaded cavity mode using the bare cavity modes. The numerical model for this projection was complicated by the fact that (1) the bare cavity modes exist only on the feedback mirror while the additive model must use a grid that extends out to the shadow boundary, and (2) the bare cavity modes were calculated on a nonuniform grid due to the requirements for generating the linear prolate functions and the additive model uses a uniform grid. The first difficulty was resolved by integrating only over the feedback mirror as the integral in Eq(3.37) required. The second difficulty was more challenging. The BCM were interpolated onto the uniform

grid of the additive model and a numerical quadrature routine (trapezoidal rule) was employed in the integration. The bare cavity modes were normalized by the orthogonality relationship after they were interpolated. Then these functions were used as a basis set and the expansion coefficients were calculated.

The first case that is examined here is the case that was discussed extensively in Chapter II. The magnification is 2.5 and the equivalent Fresnel number is 0.6. Table IV-2 shows the expansion coefficients for the BCM that were used in the approximation of the loaded cavity mode. Note that the lowest loss mode has the largest coefficient by a factor of 30. Also, the odd parity BCM have very small coefficients. However, the higher order even modes do not show a large difference in their coefficients. No clear cut-off that would indicate how many BCM are required is evident, although the lowest loss BCM is always the most significant function in the expansion. When these coefficients are used in a finite series to see how closely this series reproduces the loaded cavity mode (LCM), we find that the approximate LCM varies greatly. Figure 4.21 shows the reconstructions. The LCM is plotted against the normalized intensity scale on the ordinate. The approximate LCM intensities were intentionally shifted down to allow them to be displayed on the same plot. Thus one should mainly consider the shape of the approximate LCM and how they compare to the LCM produced by the additive model. The curve marked "1 BCM" uses only the lowest loss BCM; the curve marked "2 BCM" uses the two

TABLE IV-2.

Bare Cavity Mode Expansion Coefficients  
 $M = 2.5$        $F_{\text{eff}} = 0.600$        $g_0 = 3.0 g_{\text{th}}$

BCM	coefficient magnitude	coefficient phase
$u_0(x)$	0.904	-0.614
$u_2(x)$	2.88E-02	0.556
$u_4(x)$	5.15E-02	4.13E-02
$u_6(x)$	3.39E-02	1.05
$u_1(x)$	2.52E-06	1.90
$u_3(x)$	7.79E-06	-0.602

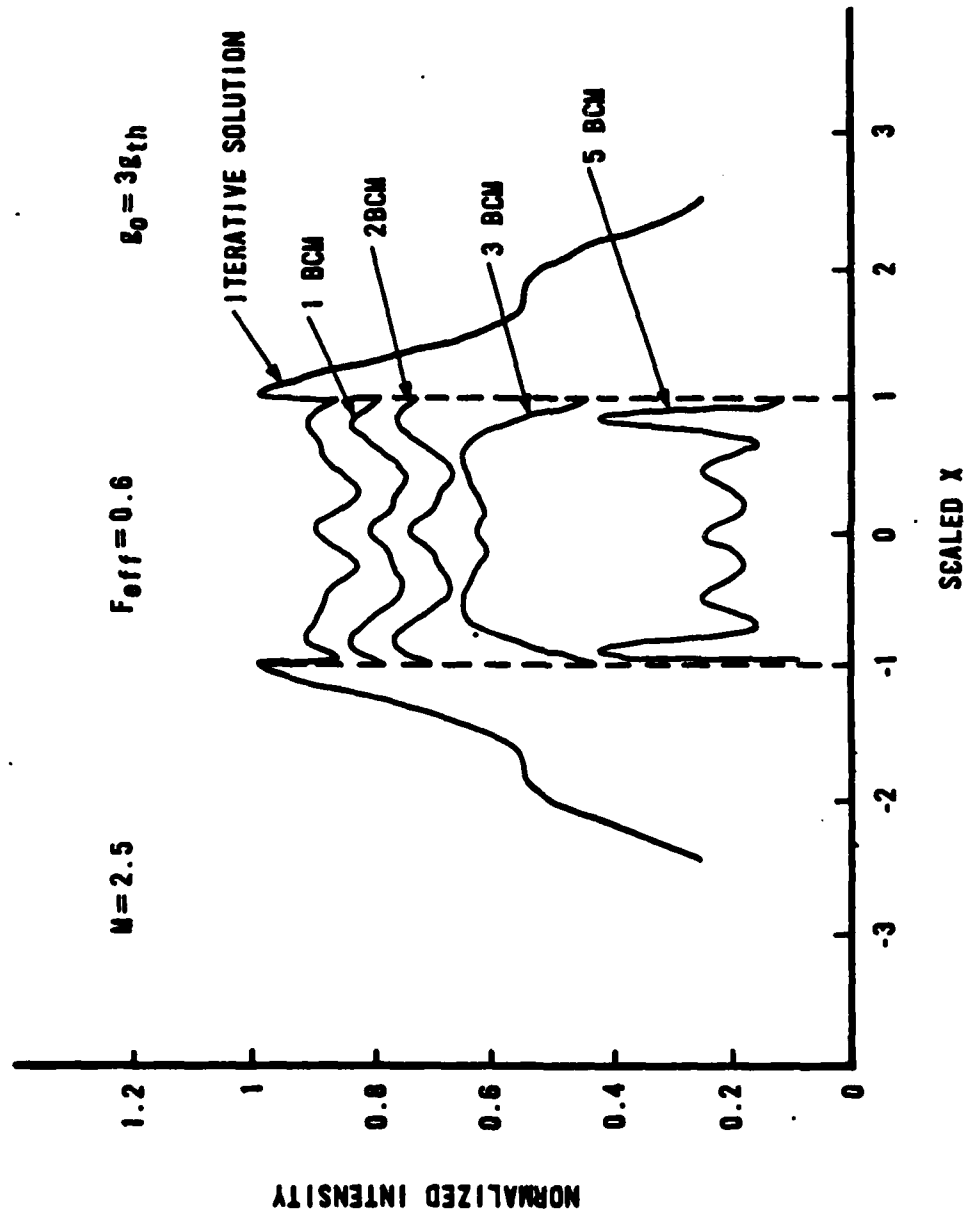


Figure 4.21 Loaded Cavity Mode Expansion.

lowest loss even parity modes; the curve marked "3 BCM" uses the three lowest loss even parity BCM; the curve marked "5 BCM" uses the four lowest loss even parity BCM and the lowest loss odd parity BCM. In the last case, the inclusion of the odd parity mode made no difference from a plot that only used the four lowest loss even modes. The best approximation appears to be either of the first two plots marked "1 BCM" and "2 BCM". The other plots differ significantly from the iterative solution. It is most likely that a combination of inaccuracies in the generation of the original and interpolated BCM produce the deviations. However, one cannot predict from the expansion coefficients the behavior that is observed in Figure 4.21. Rather than pursue this case in more depth, let us consider another case to see if the same behavior is observed.

This case is the case that has been considered at length in the preceding sections. The magnification is 2.5 and the equivalent Fresnel number is 1.2. Table IV-3 shows the expansion coefficients for this case. Again, the lowest loss BCM dominates the next mode by a large amount (a factor of 11). Again, no clear cut-off is evident in the even parity modes. The odd parity modes have much smaller expansion coefficients as before. Figure 4.22 shows LCM calculated by the additive model as well as three approximate LCM that are labeled in the same manner as those shown in Figure 4.21. Here the best match is the last approximate LCM, using the location of the small peaks as the deciding factor. However,

TABLE IV-3.

Bare Cavity Mode Expansion Coefficients  
 $M = 2.5$        $F_{\text{eff}} = 1.200$        $g_0 = 3.0 g_{\text{th}}$

BCM	coefficient magnitude	coefficient phase
$u_0(x)$	0.846	0.301
$u_2(x)$	7.50E-02	1.601
$u_4(x)$	3.16E-02	1.458
$u_6(x)$	5.07E-02	2.845
$u_1(x)$	3.57E-06	-2.294
$u_3(x)$	2.15E-05	-2.513

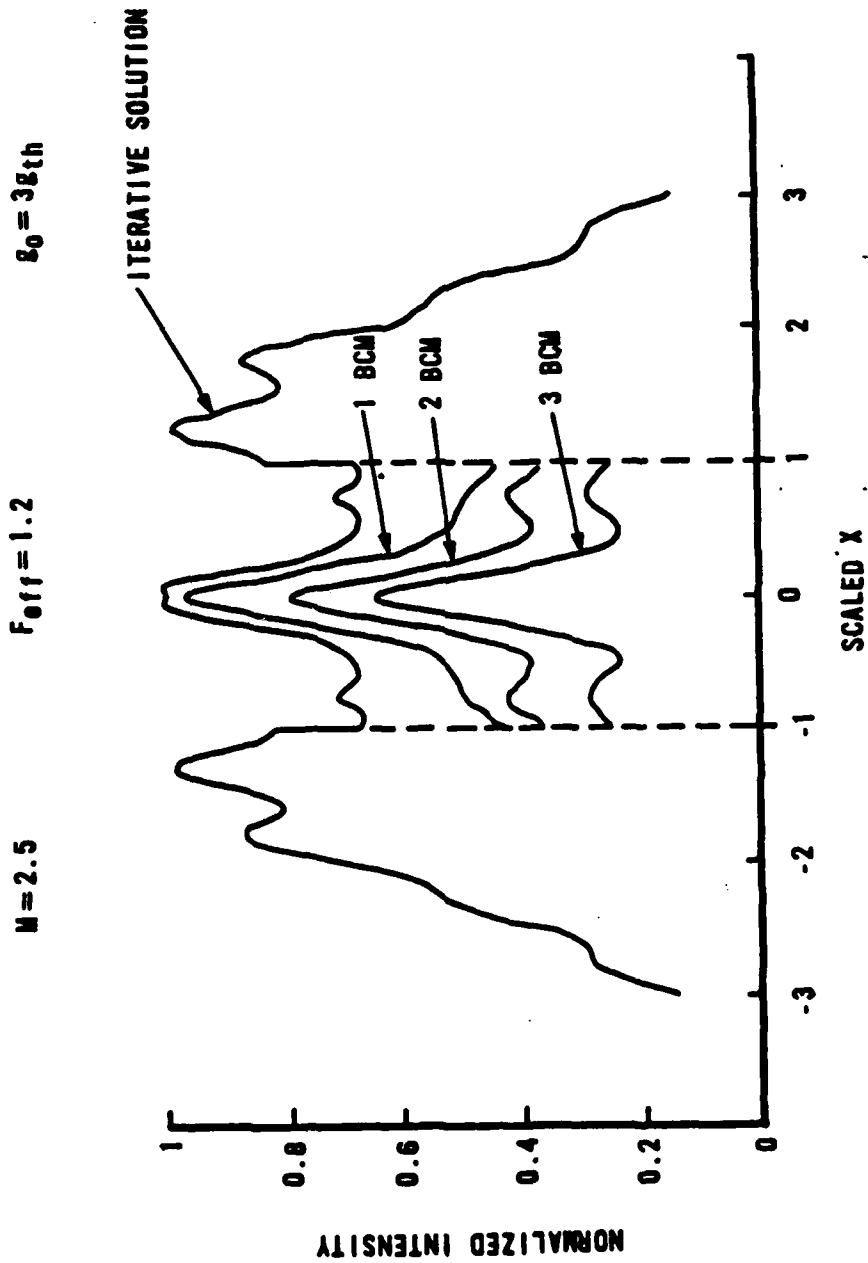


Figure 4.22 Loaded Cavity Mode Expansion.

when the fourth lowest loss even parity BCM is included the intensity of the approximate LCM differs radically from the iterative solution. It seems that the inaccuracies in the higher order modes is the most likely source of the difficulty, although the results studied to date represent only a preliminary study of the expansion of the loaded cavity mode in a series of the bare cavity modes. Several other cases were studied and similar behavior was found.

Recall that the bare cavity modes are not power orthogonal and so when the series approximation to the LCM is used to obtain an intensity, the cross terms do not vanish but remain as products of the BCM. This can be made more clear by considering the intensity of the approximate LCM when the three lowest loss BCM are used:

$$\begin{aligned}
 |\alpha_c(x)|^2 &= |b_0 u_0(x) + b_2 u_2(x) + b_4 u_4(x)|^2 \\
 &= |b_0|^2 |u_0(x)|^2 + |b_2|^2 |u_2(x)|^2 + |b_4|^2 |u_4(x)|^2 + \quad (4.38) \\
 &+ \{ [b_0 b_2^* u_0(x) u_2^*(x) + b_0 b_4^* u_0(x) u_4^*(x) + \\
 &+ b_2 b_4^* u_2(x) u_4^*(x)] + \text{complex conjugate of } [\cdot] \}
 \end{aligned}$$

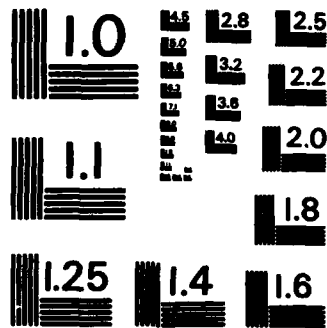
The cross terms may interact in an unpredictable manner. It is through these terms that the higher order modes can interact to give the correct LCM. Further study is required to fully explore this bare cavity mode expansion. It is left as a recommendation for future work.

## G. Summary

In this chapter, we have developed a numerical model that implemented the analysis of the loaded cavity that had been developed in Chapter III. The model had two major restrictions in it. First, the method of stationary phase was applied to the the term in the propagator that contained the gain. This meant that the stimulated radiation was propagated in a geometric manner, neglecting diffraction. Second, the gain was approximated by a single gain sheet located at the feedback mirror. These approximations are justified. The use of the method of stationary phase is justified by the application of the method of stationary phase to the entire integral equation that was discussed in Section C of this chapter. The results of that section were in excellent agreement with previous results published by Moore and McCarthy. The second approximation is justified by the analysis done by Milonni that showed that the single gain sheet is a good approximation even for low Fresnel number propagations. The gain model was a simple saturable gain model that used homogeneously broadened gain.

This model was then implemented as was another model that included the gain as a multiplicative factor in the integral equation. A wide variety of phenomena was examined with both codes. Convergence studies were done to validate the internal consistency of the models. Then the behavior of parameters such as the magnitude and phase of the eigenvalue was studied. The magnitude of the eigenvalue was unity when the small signal gain was above threshold. The phase changed





MICROCOPY RESOLUTION TEST CHART  
NATIONAL BUREAU OF STANDARDS-1963-A

as the gain was increased showing that the oscillation frequency of the loaded cavity mode would be different from the lowest loss bare cavity mode. The power on the feedback mirror was also studied and the results showed that the additive model was in better agreement with geometrical optics predictions than was the multiplicative model. Both models predicted a threshold small signal gain that was lower than the geometrical optics threshold gain. Plots of the intensity of the loaded cavity mode as the gain was increased showed significant differences between the two models. The additive model gave results that had slightly different maxima and minima from both the lowest loss bare cavity mode and the multiplicative model. The phases of the modes from the two models and the lowest loss bare cavity mode were in excellent agreement for all the values of small signal gain that were studied. Thus, for this simplified gain model, the beam quality of the loaded cavity mode should be about the same as that of the lowest loss bare cavity mode. Another study was done of the phase of the eigenvalue and the power on the mirror as a function of the equivalent Fresnel number. An oscillation in these parameters was found to agree well with the oscillatory behavior reported in the literature for the magnitude of the bare cavity eigenvalues. One peculiarity was that the phase of the loaded cavity eigenvalues was zero when an extrema was observed in the power on the feedback mirror. The case of a mode crossing was examined and the additive model was found to give much better

convergence than the multiplicative model. Finally, a preliminary study was made of projecting the loaded cavity mode onto the bare cavity modes of the resonator. The bare cavity modes were generated with the methodology developed in Chapter II. Although a fairly good approximation to the loaded cavity mode could be found, no clear criteria were found to indicate which higher loss bare cavity modes were required in the expansion in order to accurately model the loaded cavity mode.

The general conclusion of this chapter is that the numerical model gave results that agreed well with previous models of the laser. The loaded cavity eigenvalue showed that gain equal loss by converging to a value that had a magnitude of one. The model exhibited a threshold behavior, below which the magnitude of the loaded cavity eigenvalue was less than one and the power on the feedback mirror was negligible. This threshold was in fairly good agreement with the one dimensional predictions. The model predicted the variations of the power on the feedback mirror and the phase of the eigenvalue with the Fresnel number that were well correlated with the variations in outcoupling with Fresnel number discussed in Chapter II. The expansion of the loaded cavity mode in terms of the bare cavity modes was a new application of these modes.

## V. Conclusions and Recommendations

### A. Introduction

In this chapter, we summarize the work that has been detailed in Chapters II, III and IV. We will review each chapter separately, highlighting key conclusions and commenting on recommendations for future work in the topic covered by each chapter. This summary is not intended to be a detailed review of the work, but rather is aimed at showing the most significant results obtained in this research effort.

The goal of this work was to increase the understanding of laser resonators by developing a consistent formulation of the modes of empty and loaded resonators. The majority of the study dealt with the modes of bare and loaded strip resonators. The strip resonator was further restricted to be a single-ended, unstable resonator. The approach broke naturally into three parts. Chapter II presented an analysis of the bare strip resonator modes. This provided the fundamental description of the natural properties of the resonator; in addition, it developed the use of a new basis set, the linear prolate functions, in the calculation of the bare cavity modes. Chapter III developed the theory of the modes of resonators that contain a saturable gain medium. The analysis began with Maxwell's equations and ended with an integral equation for the modes of a loaded resonator. This analysis led into Chapter IV, in which the numerical implementation of a simplified model of the loaded strip

resonator based on the theoretical analysis was accomplished. Here, in Chapter V, we review each of the earlier chapters, beginning with the bare cavity analysis.

#### B. Bare Cavity Mode Analysis and Modelling

The analysis of the resonator that does not contain a gain medium lays the foundation for the analysis of resonators that do contain a gain medium. Thus, we began with an analysis of the bare strip resonator. Although the basic properties of such resonators are well known, the results presented in Chapter II introduce three important issues: the use of the linear prolate functions as a basis set for the bare cavity modes (BCM), the study of the validity of the asymptotic approach at low Fresnel numbers, and the demonstration of the orthogonality of the BCM.

The analysis of the BCM was done using the kernel expansion technique. This approach transforms the homogeneous Fredholm integral equation of the second kind (FIE(II)) that describes a round trip in the bare cavity into a matrix eigenvalue problem that is readily solved on a computer provided a "good" basis set is chosen. The analysis is complicated by the fact that the kernel of the FIE(II) is complex symmetric. Thus the eigenvalues and eigenfunctions are complex, and the eigenfunctions obey an orthogonality relation that is different from the more frequently encountered relationship for the eigenfunctions of hermitian kernels. Streifer had shown that the use of the linear prolate functions (LPF)

would be an optimum basis set in the sense that they would provide the best N-term series representation of the BCM (Ref 25). However, the basis set had not previously been used in a numerical model of the resonator. (The linear prolate functions have been approximated as the hermite gaussian functions, and in this form, they have been used in numerical models of the resonator modes.) This implementation was the first significant result. Two conclusions can be made about this implementation. First, a nonuniform grid was required to allow an accurate calculation of the linear prolate functions with the finite difference algorithm. Second, the matrix that was used in the matrix eigenvalue problem needed to retain the complex symmetric nature of the kernel in order to obtain the best N-term series representation that Streifer discussed. The proper choice of coefficients in the series guaranteed this property for the matrix.

The asymptotic approach to finding the bare cavity modes has been quite useful for large Fresnel numbers. However, even at these Fresnel numbers, the behavior of the higher loss modes seemed unphysical in that the magnitudes of the eigenvalues tended to a nonzero limit. By using the linear prolate function (LPF) expansion technique, we explored both the behavior of the higher order modes as well as the validity of the asymptotic method at low Fresnel numbers. The first conclusion is that the higher order modes given by the asymptotic method do not agree with those generated by the LPF expansion. The use of the asymptotic approach to obtain the high loss modes of the bare resonator is not

recommended. For example, one might need these higher order modes as an expansion set for the loaded cavity modes. The second conclusion is that the asymptotic method gives good lower loss bare cavity modes for equivalent Fresnel numbers down as low as one. This technique is very fast and thus knowing it is accurate at low Fresnel numbers would allow it to be used for the calculation of the lower loss modes. These modes are frequently used to characterize the resonator for mirror loadings, misalignment sensitivities and beam quality calculations. Thus the LPF expansion technique has been useful in learning more about the validity of the asymptotic method.

The third significant result from the bare cavity analysis is the numerical demonstration of the orthogonality of the BCM. The analytic demonstration was shown in Appendix 1, and the numerical demonstration proved useful for two reasons. First, it can be used as a check on numerical calculations of the bare cavity modes. Also, it is useful when the bare cavity modes are used as an expansion set, as discussed in Chapter III.

Some further work can be recommended based on the analysis and modelling of the bare cavity modes. First, a numerical implementation of the matrix eigenvalue problem for BCM of the stable resonator (derived in Appendix 6) would be of interest to study the modes of these resonators. Stable resonators might be used in free electron lasers (FEL) since FEL have a gain volume that has a small transverse extent.

Stable resonators have a narrow mode volume that can closely match the FEL gain volume. The implementation of the matrix eigenvalue problem for the resonator with cylindrical symmetry (derived in Appendix 7) is also of interest as an alternative method of finding the bare cavity modes of these resonators. This effort would require the development of a numerical model for the circular prolate functions.

The analysis and modelling of the empty strip resonator provided the foundation needed for the analysis of the loaded cavity modes. The results also provided some new results that should be useful in future resonator research.

### C. Loaded Cavity Analysis

The analysis of the modes of resonators that contain a saturable gain medium began with Maxwell's equations. The effect of a gain medium was included through a susceptibility term. The principal result of this analysis was the derivation of an integral propagator for an optical field in a gain medium. The result was used to obtain a round trip integral equation for the loaded cavity modes. The integral equation showed that the gain medium is included in terms that are added to the bare cavity integral equation. Previous studies usually included the gain as a multiplicative term. This additive model of the loaded cavity modes is a significant, new result, for two reasons. First, the loaded cavity integral equation is similar in form to an inhomogeneous Fredholm integral equation of the second kind. These equations are characterized by a unique

solution, if they have a solution at all. However, due to the nonlinear dependence of the gain on the field, this property cannot be ascribed to the loaded cavity equation in a rigorous manner. The uniqueness of the loaded cavity mode is suggested by this result and by past analyses that showed no evidence of multimode behavior. Thus, this derivation gives increased insight into the loaded cavity mode. The second useful result is that the additive model suggests two new solution techniques. The first method is the usual iterative approach that has been used in the past. The second method uses the bare cavity modes as a basis set to obtain the loaded cavity mode. The orthogonality of the BCM is used in this method, thus connecting the analysis of Chapter II. Thus, the primary result of this analysis is that a fairly rigorous derivation of the loaded cavity shows the gain should be included in terms that are added to the bare cavity mode integral equation.

Some additional work is recommended for further analysis of the loaded cavity modes. The analysis included a complex susceptibility but the final results were restricted to the case where the real part of the susceptibility was set to zero. This restricted the results to the case where the longitudinal mode of the resonator coincided with the center of the lasing transition. The result could be extended to examine cases where there was a frequency difference between the cavity mode and the center of the lasing transition. Also, further mathematical study of the properties of

nonlinear integral equations could provide a proof that, if there are any solutions to the loaded cavity integral equation, then they are unique.

Although this analysis was a general treatment of the loaded cavity, the numerical implementation of the results was much more restricted. Chapter IV discussed this modelling.

#### D. Loaded Cavity Modelling

The numerical models developed in Chapter IV were restricted to a single gain sheet located at the feedback mirror. A review of the past work showed that such a model was a fairly good approximation for low Fresnel numbers. But most of the previous work included the gain as a multiplicative term. Both an additive model based on the analysis of Chapter III and a multiplicative model based on Beer's Law were developed for the strip resonator. The models used a simple saturable gain model for a homogeneously broadened medium. Both models used an iterative technique to find the loaded cavity mode. Also, a geometrical optics approximation was made to the additive model developed in Chapter III that gave good agreement with past work. This agreement gives support to the validity of the analysis of the loaded cavity as well as provides useful limiting values for the diffractive models. A number of parameters were studied with the diffractive models as the small signal gain and the equivalent Fresnel number were varied. Also a preliminary study was made of mapping the loaded cavity mode

onto the bare cavity modes. The study of these parameter variations gave six important results.

The first conclusion is that the phase of the loaded cavity eigenvalue was not equal to that of the lowest loss mode of the bare cavity, indicating that the loaded cavity mode will have a different oscillation frequency. Second, the threshold of the oscillation (where gain equals loss) was slightly lower than that predicted by geometrical optics or an even more simplistic argument. (This threshold behavior was only examined for a limited number of cases and the trend with variations in Fresnel number has not been studied.) Third, the additive model predicted higher outcoupling than the multiplicative model, indicating that this latter model would underestimate the output power of a loaded resonator. Fourth, the power on the mirror showed fluctuations with equivalent Fresnel number that were in good agreement with the fluctuations in the lowest loss bare cavity mode eigenvalue as far as the location of the maxima and minima. Studying the phase of the loaded cavity eigenvalue showed that the phase was zero at both the maxima and minima. This behavior is a new result. Fifth, the phase profile of the loaded cavity modes did not vary significantly from the lowest loss bare cavity mode when either model was used. This indicates that the beam quality of the loaded cavity mode would be about the same as the beam quality of the lowest loss BCM, at least within the simple saturable gain model that was used. Sixth, the intensity profiles of

the loaded cavity eigenfunctions differed significantly between the two models. The additive model showed more filling in of the "peaks and valleys" of the intensity profile as the small signal gain was increased than did the multiplicative model. Also, the location and number of peaks and valleys remained unaltered with the multiplicative model but the additive model showed noticeable changes to the intensity profile as the small signal gain increased. These results show that even a simplified model such as the additive model described here provides useful, physically meaningful information. However, a more definitive description of the differences between the additive and multiplicative models would require analysis involving more gain sheets or a distributed gain model.

The preliminary study of the mapping of the loaded cavity mode (LCM) onto the bare cavity modes (BCM) showed that the LCM was a combination of the first few lower loss even parity BCM. The symmetry of the gain model did not allow the odd parity BCM to contribute. The main difficulty was that no clear cut-off was evident to show how many BCM were needed to give a good approximation to the LCM.

A number of recommendations can be made for future modelling of the loaded cavity. First, the problem of how to include a distributed gain in a code without using gainsheets needs to be further addressed. The variations with  $z$  could give significantly different results from the gain sheet models. Such a model would most likely consume large amounts of computer time since a closely spaced three dimensional

grid would be required but it would be useful in verifying how many gain sheets are required to give accurate results. A second recommendation would be to include the behavior off the line center by allowing the susceptibility to be complex. This extension would allow index of refraction variations to be studied even though it would still be a single frequency model. Third, a more realistic gain model could be included even into the loaded strip resonator model. A model that included a flowing medium or simplified rate equations for the medium could be substituted for the simple saturable gain model that was used here. Finally, a full three dimensional model could be developed based on the integral equation derived in Chapter III. Such a model would permit the modelling of physically realizable laser resonators. A final recommendation is to continue the study of expanding the loaded cavity mode in terms of the bare cavity modes. This exploits the known characteristics of the bare cavity modes in the design of laser resonators. However, more cases need to be studied and different numerical models that avoid some of the interpolation errors need to be developed.

The principal result is that the additive model that was derived in Chapter III can be implemented in a simple single gain sheet model that provides results that make physical sense. One new result is that the phase of the loaded cavity eigenvalue exhibited zero crossings when the power on the feedback mirror had a maximum or a minimum.

## E. Summary

The research described here covers a wide range of topics. The common thread is the study of the modes of a strip resonator. First, we considered the bare cavity modes which are the natural modes of the strip resonator. Then we included the effect of a gain medium on the modes of a general three dimensional resonator, specializing to the strip resonator at the end of Chapter III. The effort concluded with the numerical modelling of the strip resonator with a single gain sheet approximation for the gain medium. Significant results that were learned include (1) the first implementation of the linear prolate functions as a basis set, (2) the derivation of the loaded cavity round trip integral equation where the gain was included as an additive term to the bare cavity round trip equation and (3) the numerical model of the loaded cavity round trip equation which showed, among other results, that the phase of the loaded cavity eigenvalue was zero when the power on the feedback mirror was at an extremum.

In this study, we developed a formulation of the modes of optical resonators that consistently included both the empty and loaded resonator. The development of Chapter III laid the foundation while Chapter II examined the empty resonator case and Chapter IV modeled the loaded resonator. The structure of the round trip integral equation that was developed in Chapter III is what gives the increased understanding of the resonator modes. We again make the analogy to an inhomogeneous Fredholm integral equation of the

second kind (which was discussed in Appendix 1). The kernel of the equation gives insight into the natural or normal mode structure of the resonator, which are the bare cavity modes. Any changes to the resonator itself, such as changes in mirror reflectivity profiles, mirror curvatures or aberrations, and aperture sizes, would alter the kernel of the round trip integral equation. However, the impact of an active medium does not modify the kernel but rather appears as an inhomogeneous term. In linear integral equations, this would mean that a unique solution would exist (subject to the conditions discussed in Appendix 1). Even in the case where the inhomogeneous term depends on the solution, as it does for the case of saturable gain, a solution is obtained that is consistent with the gain function. If the gain function changes, then the loaded cavity mode would change. Thus, this formulation gives new understanding of the modes of loaded optical resonators. Further insight will be gained as the theory of nonlinear integral equations of the type derived in Chapter III is developed.

### Bibliography

1. Siegman, A.E., "Unstable Optical Resonators", Applied Optics, 13:2, 353 (1974).
2. Kogelnik, H. and Li, T., "Laser Beams and Resonators", Applied Optics, 5:10, 1550 (1966).
3. Anan'ev, Y.A., "Unstable Resonators and Their Application", Soviet J. of Quant. Elect., 1, 565 (1972).
4. Ronchi, L., "Optical Resonators", Laser Handbook, Vol 1, 151 (Amsterdam: North-Holland Pub. Co, 1972).
5. Siegman, A.E., Introduction to Lasers and Masers, (New York: McGraw-Hill Book Co, 1971).
6. Yariv, A., Quantum Electronics, (New York: Wiley and Sons, 1967).
7. Rogers, M.E. and Erkkila, J.H., "Resonator Modes Analysis Using Linear Prolate Functions", Applied Optics, 22:13, 1992 (1983).
8. Rogers, M.E. and Erkkila, J.H., "Analysis of Strip Resonator Modes Using Linear Prolate Functions", Laser Digest, AFWL-TR-83-49, p. 38, October, 1983.
9. Vainstein, L.A., "Open Resonators for Lasers", Soviet JETP, 17:3, 709 (1963).
10. Cochran, J.A. and Hinds, E.W., "Eigenvalues Associated with the Complex-Symmetric Kernels of Laser Theory", SIAM J. Appl Math, 26:4, 776 (1974).
11. Oughstun, K., "On the Completeness of the Stationary Transverse Modes in an Optical Cavity", Optics Comm., 42:1, 72 (1982).
12. Cochran, J.A., "Existence of Eigenvalues for the Integral Equations of Laser Theory", Bell Sys Tech J., 44, 77 (1965).
13. Morgan, S.P., "On the Integral Equations of Laser Theory", IEEE Trans Microwave Theory and Tech., MTT-11, 191 (1963).
14. Newman, D.J. and Morgan, S.P., "Existence of Eigenvalues of a Class of Integral Equations Arising in Laser Theory", Bell Sys Tech J., 43, 113 (1964).
15. Fox, A.G. and Li, T., "Resonant Modes in a Maser Interferometer", Bell Sys Tech J., 40, 453 (1961).

16. Bergstein, L., "Modes of Stable and Unstable Optical Resonators", Applied Optics, 7:3, 495 (1968).
17. Siegman, A.E. and Miller, H.Y., "Unstable Optical Resonator Loss Calculations Using the Prony Method", Applied Optics, 9:12, 2729 (1970).
18. Henderson, E.J. and Latham, W.P., "Matrix Eigenvalue Analysis for a Bare Strip Resonator", Laser Digest, AFWL-TR-80-4, May 1980, p. 21.
19. Horwitz, P., "Asymptotic Theory of Unstable Resonator Modes", J Opt Soc Am, 63:12, 1528 (1973).
20. Moore, G.T. and McCarthy, R.J., "Theory of Modes in a Loaded Strip Confocal Unstable Resonator", J Opt Soc Am, 67:2, 228 (1977).
21. Butts, R.R. and Avizonis, P.V., "Asymptotic Analysis of Unstable Laser Resonators with Circular Mirrors", J Opt Soc Am, 68:8, 1072 (1978).
22. Sanderson, R.L. and Streifer, W., "Comparison of Laser Mode Calculations", Applied Optics, 8:1, 131 (1969).
23. She, C.Y. and Heffner, H., "Analysis of Spherical Sector Resonators for the Production of a Focused Laser Beam", Applied Optics, 3:6, 703 (1964).
24. Rowley, J.E., "Computer Analysis of Modes in an Unstable Strip Resonator", Masters thesis, Air Force Institute of Technology, 1980.
25. Streifer, W., "Optical Resonator Modes - Rectangular Reflectors of Spherical Curvature", J Opt Soc Am, 55:7, 868 (1965).
26. Flammer, C., Spheroidal Wave Functions, (Stanford: Stanford University Press, 1957).
27. Frieden, R., "Evaluation, Design and Extrapolation Methods for Optical Signals, Based on Use of Prolate Functions", Progress in Optics, IX, chapt 8 (Amsterdam: North-Holland Pub Co., 1971).
28. Slepian, D. and Pollak, H.O., "Prolate Spheroidal Wave Functions, Fourier Analysis and Uncertainty - I", Bell Sys Tech J, 43, 43 (1961).
29. Slepian, D., "Some Asymptotic Expansions for Prolate Spheroidal Wave Functions", J Math and Phys, 44, 99 (1965).
30. Rhodes, D.R., J Research of Natl Bureau Stds, 74B, 187 (1970).

31. Stratton, Spheroidal Functions, Proc Natl Acad Sci, 21, 51 (1935).
32. Slepian, D. and Sonnenblick, E., "Eigenvalues Associated with Prolate Spheroidal Wave Functions of Zero Order", Bell Sys Tech J, 44:8, 1745 (1965).
33. Van Buren, A.L., King, B.J., Baier, R.V. and Hanish, S., "Tables of Angular Spheroidal Wave Functions, Vol 1, Prolate,  $m = 0$ ", Navl Research Lab Report, 1975.
34. Van Buren, A.L., "FORTRAN Code for Linear Prolate Functions", Naval Research Lab Report 7994, (1976).
35. Rensch, D.B. and Chester, A.N., "Iterative Diffraction Calculations of Transverse Mode Distributions in Confocal Unstable Laser Resonators", Applied Optics, 12:5, 997 (1973).
36. Smith, M.J., "Mode Properties of a Strip Confocal Unstable Resonator with Saturable Gain", Applied Optics, 20:9, 1611 (1981).
37. Milonni, P.W., "Criteria for the Thin Sheet Gain Approximation", Applied Optics, 16:11, 2794 (1977).
38. Moore, G.T. and McCarthy, R.J., "Lasers with Unstable Resonators in the Geometrical Optics Limit", J Opt Soc Am, 67:2, 221 (1977).
39. Rigrod, W.W., "Gain Saturation and Output Power of Optical Masers", J Appl Phys, 34, 2602 (1963).
40. Rigrod, W.W., "Saturation Effects in High Gain Lasers", J Appl Phys, 36, 2487 (1965).
41. Fox, A.G. and Li, T., "Effect of Gain Saturation on the Oscillating Modes of Optical Masers", IEEE J Quant Elect, QE-2, 774 (1966).
42. Rensch, D.B., "Three Dimensional Unstable Resonator Calculations with Laser Medium", Applied Optics, 13:11, 2546 (1974).
43. Siegman, A.E. and Sziklas, E.A., "Mode Calculations in Unstable Resonators with Flowing Saturable Gain. I. Hermite Gaussian Expansion", Applied Optics, 13:12, 2775 (1974).
44. Sziklas, E.A. and Siegman, A.E., "Mode Calculations in Unstable Resonators with Flowing Saturable Gain. II. Fast Fourier Transform Method", Applied Optics, 14:8, 1874 (1975).

45. Chernin, D.P., "Optical Extraction Efficiency in Lasers with High Fresnel Number Confocal Unstable Resonators", Applied Optics, 18:21, 3562 (1979).
46. Statz, H. and Tang, C.L., "Problem of Mode Deformation in Optical Masers", J Appl Phys, 36:6, 1816 (1965).
47. Erkkila, J.H., private communication, April - May, 1984.
48. Born, M. and Wolf, E., Principles of Optics, (Oxford: Pergamon Press, 1975).
49. Rinaldi, S.M., unpublished work in strip resonator Rigrod analysis for Air Force Institute of Technology PhD coursework, 1983.
50. Goodman, J., Introduction to Fourier Optics, (San Francisco: McGraw-Hill Book Co, 1968), p. 77-83.
51. Stark, H., and Tuteur, F.B., Modern Electrical Communications, (New Jersey: Prentice-Hall, 1979), p 55.
52. Boyd, G.D., and Gordon, J.P., "Confocal Multimode Resonator for Millimeter Through Optical Wavelength Masers", Bell System Tech J, 40, 489 (1961).
53. Latham, W.P., and Dente, G.C., "Matrix Methods for Bare Resonator Eigenvalue Analysis", Applied Optics, 19:10, 1618 (1980).
54. Cochran, J.A., Analysis of Linear Integral Equations, McGraw-Hill, New York, 1972.
55. Siegman, A.E., "Orthogonality Properties of Optical Resonator Eigenmodes", Optical Communications, 31:3, 369 (1979).

## Appendix 1. Orthogonality of the Eigenfunctions of Complex Symmetric Kernels

We begin this appendix with a brief discussion of a part of integral equation theory. This review is intended to provide some needed background for the discussions in chapters 2 and 3. The general form of the inhomogeneous Fredholm integral equation of the second kind is

$$\lambda \phi(x) = f(x) + \int_a^b K(x,y) \phi(y) dy, \quad x \in (a,b). \quad (A1.1)$$

The function  $f(x)$  is a known function,  $K(x,y)$  is called the kernel,  $\lambda$  is a parameter, the limits  $a$  and  $b$  are constants, and  $\phi(x)$  is the unknown function that is the solution to the integral equation. The homogeneous form of the equation is obtained by setting the function  $f(x)$  to zero:

$$\gamma_n u_n(x) = \int_a^b K(x,y) u_n(y) dy, \quad x \in (a,b). \quad (A1.2)$$

Here  $u_n(x)$  is an eigenfunction of the kernel and  $\gamma_n$  is an eigenvalue associated with the eigenfunction. The eigenfunctions and eigenvalues characterize the kernel. The eigenvalues form the spectrum of the kernel.

We will briefly state some of the basic properties of this class of equations. We assume that the kernels are continuous and linear. (We will later assume the kernel is complex-symmetric but this property is not required at this

time.) We now state a principle without proof, noting that the proof is covered in numerous textbooks on integral equations. (Ref 54)

This principle is the Alternative Principle. There are two classes of solutions for Eq(A1.1). The two classes depend on whether the parameter  $\lambda$  is in the spectrum of the kernel. If  $\lambda$  is not in the spectrum of  $K(x,y)$ , Eq(A1.1) has a unique, continuous solution for each continuous  $f(x)$ . The solution is

$$\phi(x) = f(x) + \int_a^b S(x,y;\lambda) f(y) dy, \quad (A1.3)$$

where  $S(x,y;\lambda)$  is the resolvent kernel given by

$$S(x,y;\lambda) = \sum_{k=0}^{\infty} \lambda^k K_k(x,y), \quad (A1.4)$$

where the iterated kernels,  $K_k(x,y)$ , are defined by

$$K_{k+1}(x,y) = \int_a^b K(x,u) K_k(u,y) du, \quad (A1.5)$$

with  $K(x,y) = K_0(x,y)$ . The kernel is restricted to be (i) any continuous function on  $a \leq x,y \leq b$  and (ii) a linear function. If  $\lambda$  is in the spectrum, then no solution exists unless  $f(x)$  is such that it is orthogonal to eigenfunctions of the transposed kernel,  $K^T(y,x)$ . Then no unique solution exists. The solutions are

$$\phi(x) = \psi(x) + \sum_{i=0}^{\infty} d_i u_i(x) \quad (A1.6)$$

where  $\Psi(x)$  is a particular solution and the eigenfunctions,  $u_i(x)$ , are associated with the eigenvalue at hand.

(The loaded cavity analysis of Chapter III draws an analogy to Eq(A1.1). We expect that the loaded cavity eigenvalue is not in the spectrum of the bare cavity kernel since it must have an exact magnitude of unity for above threshold conditions. Thus the first solution would be the analogous solution and suggests the loaded cavity integral equation may have a unique solution.)

We now show that the eigenfunctions of complex symmetric kernels obey an orthogonality relationship. This relation has been called "biorthogonality" in past articles on laser resonators. (Ref 55) A kernel is called complex symmetric if  $K(x,y) = K(y,x)$  for complex valued kernels. (If, for complex valued kernels,  $K(x,y) = K^*(y,x)$ , then the kernel is called hermitian and a different orthogonality relationship is obeyed by the eigenfunctions. This relationship will be discussed later.) We begin by obtaining the "first iterate" by multiplying Eq(A1.2) on both sides by  $K(z,x)$  and integrating over  $x$  from  $a$  to  $b$  and using Eq(A1.5) to define the iterated kernel:

$$\lambda_n^2 u_n(z) = \int_a^b dy K_1(z,y) u_n(y) \quad (A1.7)$$

We consider the inner product defined by

$$(u_n, u_m) \equiv \int_a^b dx u_n(x) u_m(x) \quad (A1.8)$$

Then, using Eq(A1.2) to replace the eigenfunctions, we obtain

$$(u_n, u_m) = \int_a^b dx \left[ \frac{1}{\gamma_n} \int_a^b K(x, y) u_n(y) dy \right] \left[ \frac{1}{\gamma_m} \int_a^b K(x, y') u_m(y') dy' \right] \quad (A1.9)$$

Now switch the order of the integration so that the kernels are isolated under an integral over  $x$  and use the assumption that the kernel is complex symmetric:

$$(u_n, u_m) = \frac{1}{\gamma_n \gamma_m} \int_a^b dy u_n(y) \int_a^b dy' u_m(y') \int_a^b dx K(y, x) K(x, y') \quad (A1.10)$$

The integral over  $x$  is just the iterated kernel used in Eq(A1.7) and then the integral over  $y$  is replaced by

$\gamma_m^2 u_m(y)$ , using Eq(A1.9). Then we have

$$(u_n, u_m) = \frac{\gamma_m}{\gamma_n} \int_a^b dy u_n(y) u_m(y) \quad (A1.11)$$

or, noting that the integral is the inner product defined in Eq(A1.8),

$$\left(1 - \frac{\gamma_m}{\gamma_n}\right) (u_n, u_m) = 0 \quad (A1.12)$$

Thus, if the eigenvalues are nondegenerate ( $\gamma_m \neq \gamma_n$ ), then the eigenfunctions are orthogonal (also called biorthogonal by Siegman in Ref 55) in the sense that

$$(u_n, u_m) = \int_a^b dx u_n(x) u_m(x) = \delta_{nm} \quad (\text{A1.13})$$

assuming the eigenfunctions are suitably normalized. (In fact, by setting  $n = m$ , one can use Eq(A1.13) to normalize the eigenfunctions of complex symmetric kernels.)

We now digress to discuss the orthogonality property that the eigenfunctions of hermitian kernels obey. The hermitian kernels are more well-behaved in that the eigenvalues are real and the eigenfunctions can be shown to form a complete set. Recall that a kernel is hermitian if  $K(x,y) = K^*(y,x)$ . We define the inner product for this class of kernels as

$$(u_n, u_m) \equiv \int_a^b dx u_n(x) u_m^*(x) \quad (\text{A1.14})$$

Again, using Eq(A1.2) to replace the eigenfunctions, and conjugating as necessary, we obtain

$$(u_n, u_m) = \int_a^b dx \left[ \frac{1}{\lambda_n} \int_a^b K(x,y) u_n(y) dy \right] \left[ \frac{1}{\lambda_m^*} \int_a^b K^*(x,y') u_m^*(y') dy' \right] \quad (\text{A1.15})$$

Regrouping the terms and using the hermitian property of the kernel, the conjugate of the first iterated kernel is:

$$(u_n, u_m) = \frac{1}{\gamma_n \gamma_m^*} \int_a^b dy u_n(y) \int_a^b dy' u_m^*(y') K_i^*(y, y') \quad (\text{A1.16})$$

Using the conjugate of Eq(A1.7); we find

$$(u_n, u_m) = \frac{\gamma_m^*}{\gamma_n} \int_a^b dy u_n(y) u_m^*(y) \quad (\text{A1.17})$$

The integral is just the inner product we started with, so the orthogonality property is

$$(u_n, u_m) = \int_a^b dy u_n(y) u_m^*(y) = \delta_{nm} \quad (\text{A1.18})$$

Again, we have assumed the eigenfunctions are suitably normalized. This result, Eq(A1.18), is the orthogonality property that is more frequently encountered, since many physical problems can be described by integral equations that have hermitian kernels. The bare cavity modes of the optical resonator is one case that cannot be so described and thus a different orthogonality relationship is applicable. This relationship is given in Eq(A1.13).

## Appendix 2. Derivation of Matrix Eigenvalue Problem for Strip Resonator

This appendix includes the derivation of the Horwitz standard form of the integral equation for the modes of a single-ended, strip resonator and the derivation of the matrix eigenvalue problem for the bare cavity modes using the linear prolate functions as a basis set. We begin with the integral equation that describes the modes of an aligned, strip resonator that does not contain gain. This equation can be obtained from the analysis of the loaded cavity contained in Appendix 4 if the gain term is set to zero. Also, this equation has appeared frequently in the literature. The equation is

$$\sigma u(x) = \sqrt{iF} \int_{-1}^1 dy e^{-i\pi F[g(x^2+y^2)-2xy]} u(y) \quad (A2.1)$$

Let

$$u(x) = h(x) e^{-i\pi F_{\text{eff}} x^2} \quad (A2.2)$$

where

$$F_{\text{eff}} = \frac{F}{2} \left( M - \frac{1}{M} \right) \quad (A2.3)$$

and

$$M = g + \sqrt{g^2 - 1} \quad (A2.4)$$

Substituting Eq(2.1) into Eq(A2.2) and collecting terms in the exponential functions, one obtains

$$\sigma h(x) e^{-i\pi(F_{eff} - F_g)} = \sqrt{iF} \int_{-1}^1 dy e^{-i\pi[(F_g + F_{eff})y^2 - 2Fxy]} h(y) \quad (A2.5)$$

By using Eq(A2.3) and Eq(A2.4), one can show that

$F_{eff} - F_g = -F/M$  and  $F_{eff} + F_g = F/M$ . Using these relationships and completing the square in the exponential function, Eq(A2.5) becomes

$$\sigma h(x) = \sqrt{iF} \int_{-1}^1 dy e^{-it(y - \frac{x}{M})^2} h(y) \quad (A2.6)$$

If we define  $t = \pi MF$  and  $\mu = \sigma\sqrt{M}$ , then Eq(A2.6) becomes the Horwitz standard form of the single-ended, aligned strip resonator:

$$\mu h(x) = \sqrt{\frac{it}{\pi}} \int_{-1}^1 dy e^{-it(y - \frac{x}{M})^2} h(y) \quad (A2.7)$$

The next derivation that will be done in this appendix is the derivation of the matrix eigenvalue problem using the linear prolate functions as a basis set. First, we transform the eigenfunction of Eq(A2.7). Let

$$h(x) = e^{itx^2} v(x) \quad (A2.8)$$

Then the integral equation is

$$\mu v(x) = e^{-it(1+\frac{1}{M^2})x^2} \sqrt{\frac{it}{\pi}} \int_{-1}^1 dy e^{i(\frac{2t}{M})xy} v(y) \quad (\text{A2.9})$$

Now define  $c = \frac{2t}{M}$  and expand the kernel and the eigenfunction in terms of the the linear prolate functions, i.e.,

$$e^{icxy} = \sum_{\ell=0}^{\infty} i^{\ell} \sqrt{\frac{2\pi}{c\gamma_{\ell}}} \psi_{\ell}(x) \psi_{\ell}(y) \quad (\text{A2.10})$$

and

$$v(x) = \sum_{\ell=0}^{\infty} b_{\ell} i^{-\frac{\ell}{2}} \gamma_{\ell}^{-\frac{3}{4}} \psi_{\ell}(x) \quad (\text{A2.11})$$

(Refer to Chapter 2 for a discussion of the linear prolate functions.) Both of these series are convergent. Using these series, the integral equation becomes

$$\mu \sum_{\ell=0}^{\infty} b_{\ell} i^{-\frac{\ell}{2}} \gamma_{\ell}^{-\frac{3}{4}} \psi_{\ell}(x) = \quad (\text{A2.12})$$

$$e^{-it(1+\frac{1}{M^2})x^2} \sum_{n,m=0}^{\infty} \sqrt{\frac{it}{\pi}} b_n i^{-\frac{n}{2}} \gamma_n^{-\frac{3}{4}} i^m \sqrt{\frac{2\pi}{c\gamma_m}} \psi_m(x) \int_{-1}^1 dy \psi_n(y) \psi_m(y) \quad .$$

Now

$$\int_{-1}^1 dy \psi_n(y) \psi_m(y) = \gamma_n \delta_{nm} \quad (\text{A2.13})$$

This result is used in the right hand side of Eq(A2.12). We now multiply Eq(A2.12) by  $\psi_m(x)$  and integrate over  $x$ . Using Eq(A2.13) again, one obtains

$$\mu b_m = \sum_{n=0}^{\infty} [\sqrt{iM} i^{\frac{n+m}{2}} (y_n y_m)^{-\frac{1}{4}} \int_{-1}^1 dx e^{-it(1+\frac{1}{M})x^2} \psi_n(x) \psi_m(x)] b_n \quad (A2.14)$$

This is the matrix eigenvalue problem for the bare cavity modes of an aligned, single-ended strip resonator where the linear prolate functions are used as a basis set. Formally, the problem is stated as

$$\mu b_m = \sum_{n=0}^{\infty} B_{mn} b_n \quad (A2.15)$$

where the matrix elements are

$$B_{nm} = \sqrt{iM} i^{\frac{n+m}{2}} (y_n y_m)^{-\frac{1}{4}} \int_{-1}^1 dx e^{-it(1+\frac{1}{M})x^2} \psi_n(x) \psi_m(x) \quad (A2.16)$$

Note that this matrix has retained the complex-symmetric nature of the original kernel in Eq(A2.1). The solution of the matrix eigenvalue problem gives the eigenvalues and the expansion coefficients. The modes are reconstructed using the relation

$$u(x) = e^{i\pi F_{2g} x^2} \sum_{n=0}^{\infty} b_n i^{-\frac{n}{2}} y_n^{-\frac{3}{4}} \psi_n(x) \quad (A2.18)$$

Note finally that this equation expresses the mode at fictitious plane halfway through the feedback mirror. To find the field just prior to the mirror, one multiplies the field by the conjugate of the mirror factor, i.e.,

$$M_1(x) = e^{\frac{i\pi(g-1)x^2}{\lambda L}} \quad (A2.19)$$

Appendix 3. Derivation of Green's Function for Paraxial Wave Equation (2-D)

We seek a solution to the equation

$$\frac{\partial^2 u}{\partial x^2} - 2ik \frac{\partial u}{\partial z} = -k^2 \chi u \quad (A3.1)$$

We construct an auxiliary equation for a Green's function where translational invariance has been assumed:

$$\frac{\partial^2}{\partial x^2} G(x-x', z-z') - 2ik \frac{\partial}{\partial z} G(x-x', z-z') = -4\pi \delta(x-x', z-z'). \quad (A3.2)$$

If the coordinates are interchanged, then Eq(A3.2) becomes

$$\frac{\partial^2}{\partial x^2} G(x'-x, z'-z) + 2ik \frac{\partial}{\partial z} G(x'-x, z'-z) = -4\pi \delta(x'-x, z'-z). \quad (A3.3)$$

Now, suppressing the coordinate dependence for a moment and letting  $u' = u(x', z')$ , the differential equation can be transformed into an integral equation by multiplying Eq(A3.1) by  $G$  and Eq(A3.3) by  $u$  and subtracting the two equations:

$$\int dx dz (G u_{xx} - u G_{xx}) - 2ik \int dx dz \frac{\partial (uG)}{\partial z} + \int dx dz G k^2 \chi u = 4\pi u'. \quad (A3.4)$$

Integrating by parts, the first term becomes

$$\int dx dz (G u_{xx} - u G_{xx}) = \int dx dz \frac{\partial}{\partial x} (G u_x - u G_x) \quad (A3.5)$$

The boundary conditions are chosen such that both  $u$  and  $G$

vanish on the surface. Note that this is analogous to the Kirchhoff radiation condition. Therefore, the first term in Eq(A3.4) is zero. Also, we chose the case where  $z' > z$ . Thus, the integral equation that is equivalent to the differential equation is

$$u(x', z') = \frac{i}{\lambda} \int_{-\infty}^{\infty} dx G(x'-x, z') u(x, 0) + \quad (A3.6)$$

$$+ \frac{1}{2\lambda} \int_0^{z'} dz \int_{-\infty}^{\infty} dx G(x'-x, z'-z) k \chi(x, z) u(x, z).$$

We now find an appropriate Green's function.

Consider the Fourier transform

$$G(\xi, \eta) = \frac{1}{2\pi} \iint_{-\infty}^{\infty} dw dv e^{-i(w\xi + v\eta)} g(w, v) \quad (A3.7)$$

where  $\xi = x' - x$  and  $\eta = z' - z$ , and substitute this into the differential equation

$$\frac{\partial^2}{\partial \xi^2} G(\xi, \eta) - 2ik \frac{\partial}{\partial \eta} G(\xi, \eta) = -4\pi \delta(\xi, \eta) \quad (A3.8)$$

Recall the integral form for the delta function:

$$\delta(\xi, \eta) = \frac{1}{(2\pi)^2} \iint_{-\infty}^{\infty} dw dv e^{-i(w\xi + v\eta)} \quad (A3.9)$$

Then we find that

$$g(w, v) = \frac{2}{w^2 + 2kv} \quad (A3.10)$$

so

$$G(\xi, \eta) = \frac{1}{\pi} \int_{-\infty}^{\infty} \int_{-\infty}^{\infty} dw dv \frac{e^{-i(w\xi + v\eta)}}{w^2 + 2kv} \quad . \quad (\text{A3.11})$$

Rewrite this equation as

$$G(\xi, \eta) = \frac{1}{2k\pi} \int_{-\infty}^{\infty} dw e^{-iw\xi} \int_{-\infty}^{\infty} dv \frac{e^{-i\eta v}}{v + \frac{w^2}{2k}} \quad . \quad (\text{A3.12})$$

We move the singularity to the origin by replacing  $v$  with  $y - \frac{w^2}{2k}$  . Then

$$G(\xi, \eta) = \frac{1}{2\pi k} \int_{-\infty}^{\infty} dw e^{-i(w\xi - \frac{\eta w^2}{2k})} \int_{-\infty}^{\infty} dy \frac{e^{-i\eta y}}{y} \quad . \quad (\text{A3.13})$$

The integral over  $y$  can be readily evaluated. Let

$$I = \int_{-\infty}^{\infty} dy \frac{e^{-i\eta y}}{y} \quad . \quad (\text{A3.14})$$

We let  $y = \lim_{\nu \rightarrow 0^+} y - i\nu$  to shift the pole slightly off-axis.

Then, with  $y' = y - i\nu$  ,

$$I = \lim_{\nu \rightarrow 0^+} e^{-\eta\nu} \int_{-\infty}^{\infty} dy' \frac{e^{-i\eta y'}}{y' + i\nu} \quad . \quad (\text{A3.15})$$

The residue is  $e^{-\eta\nu}$  , so, choosing a contour on the lower half plane, we find

$$I = -2\pi i \Theta(\eta) \quad (\text{A3.16})$$

where  $\Theta(\eta)$  is the step function.

Substituting this into the Green's function, Eq(A3.13), we have

$$G(\xi, \eta) = \frac{-i\Theta(\eta)}{k} \int_{-\infty}^{\infty} d\omega e^{-i(\omega\xi - \frac{\eta\omega^2}{2k})} \quad (A3.17)$$

If we assume  $\eta = \lim_{\mu \rightarrow 0^+} \eta - i\mu$ , then this integral can be evaluated (see Eq(A4.10) for the general form), and the Green's function is obtained:

$$G(\xi, \eta) = \lim_{\mu \rightarrow 0^+} \frac{-i\pi}{\sqrt{k(\eta - i\mu)}} e^{-\frac{ik\xi^2}{2(\eta - i\mu)}} \Theta(\eta) \quad (A3.18)$$

We choose  $\eta > 0$ , and taking the limit, then the Green's function can be written

$$G(\xi, \eta) = \sqrt{\frac{\lambda}{i\eta}} e^{-\frac{i\pi\xi^2}{\lambda\eta}} \quad (A3.19)$$

Thus, the two-dimensional propagator can be written as

$$u(x, z) = u_h(x, z) + u_i(x, z) \quad (A3.20)$$

where

$$u_h(x, z) = \sqrt{\frac{i}{\lambda z}} \int_{-\infty}^{\infty} dx' e^{-\frac{i\pi(x-x')^2}{\lambda z}} u(x', 0) \quad (A3.21)$$

and

$$u_i(x, z) = \frac{1}{2\sqrt{i\lambda}} \int_{-\infty}^z dz' \int_{-\infty}^{\infty} dx' \frac{e^{-\frac{i\pi(x-x')^2}{\lambda(z-z')}}}{\sqrt{z-z'}} k \chi(x', z') u(x', z') \quad (A3.22)$$

If we restrict the study to the case where the longitudinal mode is coincident with the line-center of the gain profile, then the susceptibility is purely imaginary, and, using the gain function,  $g_s(x, z) = k \chi''(x, z)$ , we have

$$u_i(x, z) = \frac{1}{z} \sqrt{\frac{i}{\lambda}} \int_0^z dz' \int_{-\infty}^{\infty} dx' \frac{e^{-\frac{i\pi(x-x')^2}{\lambda(z-z')}}}{\sqrt{z-z'}} g_s(x', z') u(x', z'). \quad (\text{A3.23})$$

This concludes the derivation of the two-dimensional propagator for the loaded strip resonator.

#### Appendix 4. Round Trip Equation for Loaded Strip Resonator

This appendix contains the derivation of the round trip integral equation using the propagator, Eq(A3.20), derived in Appendix 3. The resonator is modeled by an equivalent lens train which is shown in Figure A4.1. The various  $u_i$  shown on this figure are fields in the resonator that will be calculated. Each lens shown in the figure is modeled as a phase sheet. In the paraxial approximation, the spherical curvature is approximated by a parabola. (Ref 50) The phase factor for the lenses (which represent half of the phase effect of the mirror) is then

$$A_i(x) e^{-\frac{i\pi(q_i-1)x^2}{\lambda l}}$$

where the amplitude factor,  $A_i(x)$ , is used to both aperture the lens and include any transmission profiles (equivalent to the mirror reflectivity profile) that may be on the lens. Here, we assume the lenses are perfectly transmitting (i.e. the mirrors are perfectly reflecting) across their width,

$2a_i$ , and they are totally obscured outside this region. Thus

$$A_i(x) = \begin{cases} 1 & , \text{ if } |x| \leq a_i \\ 0 & , \text{ if } |x| > a_i \end{cases} \quad (\text{A4.1})$$

Let us now proceed with deriving the round trip equation.

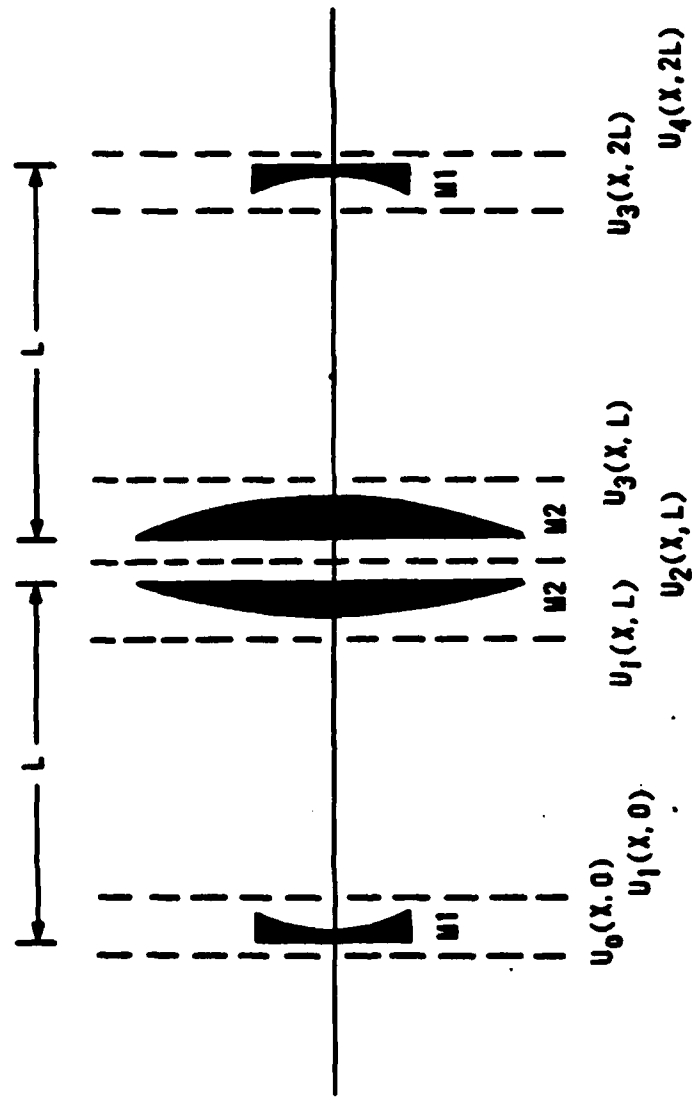


Figure A4.1 Lens Train Diagram.

We assume the field  $u_0(x,0)$  is known. Then the field just after the first half lens is

$$u_1(x,0) = A_1(x) e^{-\frac{i\pi(g_1-1)x^2}{\lambda L}} u_0(x,0) \quad (A4.2)$$

Now, using Eq(A3.20) as a propagator, we find  $u_1(x,L)$ :

$$u_1(x,L) = \sqrt{\frac{i}{\lambda L}} \int_{-a_1}^{a_1} dx' e^{-\frac{i\pi}{\lambda L}(x^2 - 2xx' + g_1 x'^2)} u_0(x',0) + \frac{1}{2} \sqrt{\frac{i}{\lambda}} \int_{-\infty}^{\infty} dx' \int_0^L dz' \frac{e^{-\frac{i\pi(x-x')^2}{\lambda(L-z')}}}{\sqrt{L-z'}} g_s(x',z') u_1(x',z') \quad (A4.3)$$

We multiply  $u_1(x,L)$  by the mirror factor twice to account for the two lenses that are equivalent to the full reflection off the back mirror. Thus

$$u_3(x,L) = [A_2(x)]^2 e^{-\frac{i2\pi}{\lambda L}(g_2-1)x^2} u_1(x,L) \quad (A4.4)$$

We hold off substituting for  $u_1$  for the moment to avoid unnecessarily complicating the development. The propagation from the back mirror up to the feedback mirror is

$$u_3(x,2L) = \sqrt{\frac{i}{\lambda L}} \int_{-a_2}^{a_2} dx'' e^{-\frac{i\pi}{\lambda L}[x^2 - 2xx'' + (2g_2-1)x''^2]} u_1(x'',L) + \frac{1}{2} \sqrt{\frac{i}{\lambda}} \int_{-\infty}^{\infty} dx'' \int_L^{2L} dz'' \frac{e^{-\frac{i\pi(x-x'')^2}{\lambda(2L-z'')}}}{\sqrt{2L-z''}} g_s(x'',z'') u_3(x'',z'') \quad (A4.5)$$

The final lens is included by

$$u_4(x, 2L) = A_1(x) e^{-\frac{i\pi(q_1-1)x^2}{\lambda L}} u_3(x, 2L) \quad (A4.6)$$

Now we substitute the expression for  $u_3(x, 2L)$  into Eq(A4.6) and then substitute the expression for  $u_1(x, L)$  into this result. The equation for  $u_4$  is then

$$\begin{aligned} u_4(x, 2L) = A_1(x) & \left\{ \frac{i}{\lambda L} \int_{-a_1}^{a_1} dx' e^{-\frac{i\pi q_1(x^2+x'^2)}{\lambda L}} u_0(x', 0) I_0(x, x') + \right. \\ & + \frac{i}{2\lambda\sqrt{L}} \int_{-\infty}^{\infty} dx' \int_0^L dz' \frac{e^{-\frac{i\pi q_1 x^2}{\lambda L}}}{\sqrt{L-z'}} g_2(x', z') u_1(x', z') I_1(x, x', z') + \quad (A4.7) \\ & \left. + \frac{1}{2} \sqrt{\frac{i}{\lambda}} \int_{-\infty}^{\infty} dx' \int_L^{2L} dz' \frac{e^{-\frac{i\pi}{\lambda} \left[ \frac{q_1-1}{L} x^2 + \frac{(x-x')^2}{2L-z'} \right]}}{\sqrt{2L-z'}} g_2(x', z') u_3(x', z') \right\} \end{aligned}$$

where

$$I_0(x, x') = \int_{-a_2}^{a_2} d\eta e^{-\frac{i\pi}{\lambda L} [2g_2 \eta^2 - 2\eta(x+x')]} \quad (A4.8)$$

and

$$I_1(x, x', z') = \int_{-a_2}^{a_2} d\eta \exp \left\{ -\frac{i\pi}{\lambda L} \left[ (2g_2-1)\eta^2 - 2x\eta + \frac{L(\eta^2 - 2x'\eta + x'^2)}{L-z'} \right] \right\} \quad (A4.9)$$

These last two integrals are singled out since neither the gain function nor the fields appear in them. These equations as written apply to double-ended strip resonators. However, resonators are usually designed so that the back mirror is large enough that all of the resonator mode is reflected off the mirror. In this case, we can let  $a_2 \rightarrow \infty$ . Then these

two integrals can be evaluated analytically. In this evaluation, we use the integral relation

$$\int_{-\infty}^{\infty} dx e^{-(ax^2 \pm bx)} = \sqrt{\frac{\pi}{a}} e^{\frac{b^2}{4a}} \quad (\text{A4.10})$$

which is valid for complex  $a$  and  $b$  as long as the real part of  $a$  is positive. (Ref 51) Using this relation, we can immediately evaluate Eq(A4.8):

$$I_0(x, x') = \sqrt{\frac{\lambda L}{2ig_2}} e^{\frac{i\pi}{2\lambda L g_2} (x^2 + 2xx' + x'^2)} \quad (\text{A4.11})$$

A similar but somewhat more lengthy evaluation of Eq(A4.9) yields

$$I_1(x, x'; z') = e^{-\frac{i\pi x'^2}{\lambda(L-z')}} \sqrt{\frac{\lambda}{iL_e(z')}} e^{\frac{i\pi}{\lambda} \frac{(x + \frac{x'}{L-z'})^2}{L_e(z')}} \quad (\text{A4.12})$$

where

$$L_e(z') \equiv \frac{2g_2 - 1}{L} + \frac{1}{L - z'} \quad (\text{A4.13})$$

If these last two equations are substituted into Eq(A4.7), we obtain the final round trip integral equation for the loaded cavity modes of a single-ended strip resonator. If we define a Fresnel number with  $F = a^2 / (2\lambda L g_2)$ , then this equation can be written as

$$\begin{aligned}
u_4(x, 2L) = A_1(x) & \left\{ \frac{\sqrt{iF}}{a_1} \int_{-a_1}^{a_1} dx' e^{-\frac{i\pi F}{a_1^2} [g(x^2+x'^2) - 2xx']} u_0(x', 0) + \right. \\
& + \frac{1}{2} \sqrt{\frac{i}{\lambda L}} \int_{-\infty}^{\infty} dx' \int_0^L dz' \frac{e^{-\frac{i\pi}{\lambda} \left[ \frac{g_1 x^2}{L} + \frac{x'^2}{L-z'} - \frac{\left(\frac{x}{L} + \frac{x'}{L-z'}\right)^2}{L_0(z')} \right]}}{\sqrt{L_0(z')(L-z')}} g_s(x', z') u_1(x', z') + \\
& \left. + \frac{1}{2} \sqrt{\frac{i}{\lambda}} \int_{-\infty}^{\infty} dx' \int_L^{2L} dz' \frac{e^{-\frac{i\pi}{\lambda} \left[ \frac{g_2 x^2}{L} + \frac{(x-x')^2}{2L-z'} \right]}}{\sqrt{2L-z'}} g_s(x', z') u_3(x', z') \right\}. \tag{A4.14}
\end{aligned}$$

This concludes the derivation of the round trip equation for the loaded strip resonator. We note that the integral equation for the bare cavity modes of the strip resonator is obtained by setting the gain function,  $g_s(x, z)$ , to zero. Then, if we scale the coordinates by the half width of the feedback mirror, we obtain

$$u_4(x, 2L) = \sqrt{iF} \int_{-1}^1 dx' e^{-i\pi F [g(x^2+x'^2) - 2xx']} u_0(x', 0). \tag{A4.15}$$

This integral equation is discussed in Chapter 2 and used in Appendix 2.

to order  $t^{-\frac{1}{2}}$ . Here the stationary phase point,  $x_0$ , is determined by the condition  $p'(x) = 0$ . This approximation assumes that the function  $q(x)$  is slowly varying as compared to the variations in the exponential term. The result in Eq(A5.2) becomes more accurate for large  $t$  and this result does not show the endpoint contributions which are of higher order in  $t$ . For further reading in the MOSP, the reader is referred to Appendix III of Ref 48.

Before we can apply Eq(A5.2) to the second term of Eq(A5.1), we must insure that  $q(x)$  is not rapidly varying. Since we have assumed a positive branch confocal unstable resonator (PBCUR), one leg is expanding and the other leg is collimated. For the collimated leg, the field  $u(x)$  has a slowly varying phase and Eq(A5.2) can be applied directly. However, the field in the expanding leg has a spherical curvature that must be moved into the exponential term before Eq(A5.2) can be applied. We deal with each case separately.

#### Collimated Leg Propagator

We consider the second term of Eq(A5.1):

$$u_2(x, z) = \frac{1}{2} \sqrt{\frac{i}{\lambda}} \int_0^z \frac{dz'}{\sqrt{z-z'}} \int_{-\infty}^{\infty} dx' e^{-\frac{i\pi(x-x')^2}{\lambda(z-z')}} g_s(x', z') u(x', z'). \quad (A5.3)$$

Here,  $g_s(x', z') u(x', z')$  is slowly varying compared to the exponential. The stationary phase point is  $x' = x$ . Using Eq(A5.2), Eq(A5.3) is approximated by

## Appendix 5. Method of Stationary Phase Applied to Two Dimensional Propagator

In this appendix, we will use the method of stationary phase (MOSP) on the two dimensional propagator, Eq(3.23), which is reproduced here:

$$\begin{aligned}
 u(x,z) = & \sqrt{\frac{i}{\lambda z}} \int_{-\infty}^{\infty} dx' e^{-\frac{i\pi}{\lambda z} (x-x')^2} u(x',0) + \\
 & + \frac{1}{2} \sqrt{\frac{i}{\lambda}} \int_{-\infty}^{\infty} dx' \int_0^z dz' \frac{e^{-\frac{i\pi}{\lambda} \frac{(x-x')^2}{(z-z')}}}{\sqrt{z-z'}} g_s(x',z') u(x',z').
 \end{aligned}
 \tag{A5.1}$$

The susceptibility that had been in Eq(3.23) has been replaced with the gain functions. This restriction is discussed at the beginning of Section C of Chapter III. The goal of this appendix is to use MOSP on the second integral in Eq(A5.1). This approximation is equivalent to ignoring diffraction of the stimulated radiation over the propagation length. The purpose is to include the stimulated radiation in a successively more complicated manner. The approximation also simplifies the numerical modelling of the loaded strip resonator.

According to the MOSP, a general integral can be approximated by

$$\int_a^b dx e^{-it_p(x)} q(x) \approx e^{-\frac{i\pi}{4}} q(x_0) e^{-it_p(x_0)} \sqrt{\frac{2\pi}{t_p''(x_0)}} \tag{A5.2}$$

$$u_1(x, z) \approx \frac{1}{2} \int_0^z dz' g_s(x, z') u(x, z') \quad (\text{A5.4})$$

and the collimated leg propagator is written as

$$u(x, z) = \sqrt{\frac{i}{\lambda z}} \int_{-\infty}^{\infty} dx' e^{-\frac{i\pi}{\lambda z}(x-x')^2} u(x', 0) + \frac{1}{2} \int_0^z dz' g_s(x, z') u(x, z'). \quad (\text{A5.5})$$

To show the utility of this approximation, we will obtain Beer's Law from this analysis. Note that the MOSP can be applied to the first term as well to obtain a geometric propagator for the collimated leg:

$$u(x, z) \approx u(x, 0) + \frac{1}{2} \int_0^z dz' g_s(x, z') u(x, z'). \quad (\text{A5.6})$$

If we now assume that the gain is small over the gain length,  $L$ , and replace the integral in the second term with a gain sheet as discussed in Chapter III, then we obtain

$$u(x, L) \approx \left[ 1 + \frac{L}{2} g_s(x, 0) \right] u(x, 0) \quad (\text{A5.7})$$

Now for small gain, the first term on the right hand side of Eq(A5.7) can be replaced by an exponential:

$$u(x, L) \approx e^{\frac{g_s(x, 0)L}{2}} u(x, 0) \quad (\text{A5.8})$$

This is Beer's Law which arises naturally from the theory developed in Chapter III. One sees the number of restrictions that need to be invoked to obtain this simple

but useful relationship.

### Expanding Leg Propagator

To model the expanding leg, we first remove the spherical curvature on the field. In the paraxial approximation, this curvature is represented by a quadratic phase term:

$$u(x, z) = e^{-\frac{i\pi x^2}{\lambda f}} v(x, z) \quad . \quad (\text{A5.9})$$

Then the second term of the two dimensional propagator is

$$u_i(x, z) = \frac{1}{2} \sqrt{\frac{i}{\lambda}} \int_0^z \frac{dz'}{\sqrt{z-z'}} \int_{-\infty}^{\infty} dx' e^{-\frac{i\pi}{\lambda} \left[ \frac{(x-x')^2}{z-z'} + \frac{x'^2}{f} \right]} v(x', z') q_s(x', z'). \quad (\text{A5.10})$$

Here,  $q(x') = v(x') g(x')$  and

$$p(x') = (x-x')^2 + x'^2 \left( \frac{z-z'}{f+z'} \right) \quad . \quad (\text{A5.11})$$

By setting the first derivative to zero, the stationary point may be found:

$$x'_0 = \frac{x}{1 + \frac{z-z'}{f+z'}} \quad , \quad (\text{A5.12})$$

and thus

$$p(x'_0) = x^2 \frac{\left( \frac{z-z'}{f+z'} \right)}{1 + \left( \frac{z-z'}{f+z'} \right)} \quad . \quad (\text{A5.13})$$

Applying Eq(A5.2), we obtain

$$u_1(x, z) = \frac{1}{2} \int_0^z dz' \frac{e^{-\frac{i\pi}{\lambda^2} \frac{x^2}{(1 + \frac{z-z'}{f+z'})}}}{\sqrt{1 + \frac{z-z'}{f+z'}}} v\left(\frac{x}{1 + \frac{z-z'}{f+z'}}, z'\right) g_s\left(\frac{x}{1 + \frac{z-z'}{f+z'}}, z'\right). \quad (\text{A5.14})$$

After some straightforward algebra, the final expression for the expanding leg propagator is

$$u(x, z) = \sqrt{\frac{i}{\lambda^2}} \int_{-\infty}^{\infty} dx' e^{-\frac{i\pi}{\lambda^2} (x-x')^2} u(x', 0) + \quad (\text{A5.15})$$

$$+ \frac{1}{2} \int_0^z dz' \sqrt{\frac{f+z'}{f+z-z'}} e^{-\frac{i\pi x^2 f(z-z')}{\lambda^2 (f+z-z')^2}} u\left(\frac{x(f+z')}{f+z-z'}, z'\right) g_s\left(\frac{x(f+z')}{f+z-z'}, z'\right).$$

These two propagators will be used to derive a round trip integral equation for the loaded strip resonator that will be used for a numerical model.

## Appendix 6. Matrix Eigenvalue Problem for Stable Strip Resonator

In this appendix, we derive a matrix eigenvalue problem (MEVP) for the case of the stable resonator, that is, for the case where  $0 < g < 1$ . The derivation parallels Appendix 2.

We begin with the integral equation for a empty strip resonator:

$$\sigma u(x) = \sqrt{iF} \int_{-1}^1 dy e^{-i\pi F [g(x^2+y^2) - 2xy]} u(y) . \quad (\text{A6.1})$$

This formulation is directly applicable to the stable resonator. The transformations in Appendix 2 introduce the magnification and the equivalent Fresnel number, which are quantities that are most applicable to the unstable resonator. If we examine Eq(A2.3) and Eq(A2.4) for the case where  $0 < g < 1$ , the magnification becomes a complex number of unit magnitude and the equivalent Fresnel number becomes a pure imaginary number. The quantities  $F$  and  $g$  remain more meaningful for the stable region.

Let  $c = 2\pi F$  and make the transformation

$$h(y) = e^{-i\pi F g y^2} u(y) . \quad (\text{A6.2})$$

Then Eq(A6.1) becomes

$$\sigma h(x) = \sqrt{iF} e^{-icgx^2} \int_{-1}^1 dy e^{icxy} h(y) . \quad (\text{A6.3})$$

We now expand the kernel and the eigenfunction in linear prolate functions:

$$e^{icxy} = \sum_{l=0}^{\infty} i^l \sqrt{\frac{2\pi}{c\gamma_l}} \psi_l(x) \psi_l(y) \quad , \quad (\text{A6.4})$$

$$h(x) = \sum_{m=0}^{\infty} b_m i^{-\frac{m}{2}} \gamma_m^{-\frac{3}{4}} \psi_m(x) \quad . \quad (\text{A6.5})$$

Substituting these expressions into Eq(A6.3), and using the orthogonality property of the linear prolate functions,

$$\int_{-1}^1 dx \psi_m(x) \psi_n(x) = \gamma_n \delta_{mn} \quad , \quad (\text{A6.6})$$

we obtain the MEVP

$$\sigma_k b_k = \sum_{l=0}^{\infty} B_{kl} b_l \quad (\text{A6.7})$$

where

$$B_{kl} = \sqrt{i} (\gamma_k \gamma_l)^{\frac{1}{4}} i^{\frac{l+k}{2}} \int_{-1}^1 dx e^{-icg x^2} \psi_l(x) \psi_k(x) \quad . \quad (\text{A6.8})$$

We consider two special cases. The first case is when  $g_1 = g_2 = 0$  which is the stable, confocal resonator. For this case,  $g = -1$ . In this case, the modes are known to be proportional to the linear prolate functions. (Ref 52) The eigenvalues should be real, according to Boyd and Gordon. In this special case, the matrix becomes

$$B_{kl} = \sqrt{i} (\gamma_k \gamma_l)^{-1/4} i^{\frac{l+k}{2}} \int_{-1}^1 dx e^{icx^2} \psi_l(x) \psi_k(x) . \quad (\text{A6.9})$$

The result does not show that the eigenfunctions are the linear prolate functions nor does it show the eigenvalues are real. In fact, they are not. The difference is a subtle one but worth noting. The resonator model developed here is for a single-ended resonator, while the case studied by Boyd and Gordon was a double-ended resonator.

The second special case is the case where  $g = 0$ . This case is for the stable resonators where  $g, g_2 = 0.5$ . Then the matrix becomes a diagonal matrix,

$$B_{kl} = \sqrt{i} i^l \sqrt{\gamma_l} \delta_{lk} \quad (\text{A6.10})$$

and the eigenvalues are

$$\sigma_k = \sqrt{i \gamma_k} i^k \quad (\text{A6.11})$$

and the eigenfunctions are

$$u_k(x) = i^{-\frac{k}{2}} \gamma_k^{-\frac{3}{4}} \psi_k(x) \quad (\text{A6.12})$$

A geometric analysis of this special case shows that the feedback mirror is confocal with its image in the back mirror. Thus, it is this case that more closely parallels the study done by Boyd and Gordon.

The parallel derivation of the MEVP for stable, strip resonators is presented for completeness. A numerical model could be readily developed from the unstable resonator model developed in Chapter II. A final note: the eigenfunctions of the stable resonator are only the Hermite-gaussian functions in the asymptotic limit where the feedback mirror becomes large. (Ref 25) Thus, for small feedback mirrors and for stable resonators, the derivation presented in this appendix would be an appropriate method.

## Appendix 7. Matrix Eigenvalue Problem for Resonators with Circular Mirrors

In this appendix, we derive a matrix eigenvalue problem for empty resonators that have circular mirrors. This derivation parallels the development for strip resonators. We begin by including some key results for the circular prolate functions, which are similar to the linear prolate functions discussed in detail in Chapter II. The reader is referred to the article by Frieden. (Ref 27)

The circular prolate functions are defined by an integral equation:

$$\int_0^{r_0} dr r J_N(\omega' r) \Phi_{N,n}(r) = (-1)^n \left(\frac{r_0}{\Omega}\right) \gamma_{N,n}^{1/2} \Phi_{N,n}\left(\frac{\omega' r_0}{\Omega}\right). \quad (\text{A7.1})$$

Letting  $r_0 = 1$ , so the space-bandwidth product,  $c$ , is defined by  $c = \Omega$ , and, letting  $\omega = \frac{\omega'}{c}$ , the integral equation becomes

$$(-1)^n \frac{\sqrt{\gamma_{N,n}}}{c} \Phi_{N,n}(\omega) = \int_0^1 dr r J_N(c\omega r) \Phi_{N,n}(r) \dots \quad (\text{A7.2})$$

The circular prolate functions also obey an orthogonality relation:

$$\int_0^1 dr r \Phi_{l,m}(r) \Phi_{l,n}(r) = \gamma_{l,n} \delta_{mn} \quad . \quad (\text{A7.3})$$

Now the modes of a resonator that has circular (or cylindrical) symmetry can be decomposed into radial and

azimuthal modes, just like the resonator with rectangular symmetry has modes that can be decomposed into the strip modes studied in Chapter II. Following Butts and Avizonis, we write the round trip integral equation for the radial modes: (Ref 21)

$$\sigma_2 f_\ell(x) = i^{\ell+1} 2t \int_0^1 dy y J_\ell\left(\frac{2t}{M} xy\right) e^{-it\left[y^2 + \frac{x^2}{M^2}\right]} f_\ell(y). \quad (\text{A7.4})$$

Each radial mode has an  $\exp(i\ell\phi)$  dependence. The variable  $t$  is  $\pi MF$  where  $M$  is the magnification and  $F$  is the Fresnel number used in Chapter II. We make the transformation

$$g_\ell(x) = e^{-itx^2} f_\ell(x), \quad (\text{A7.5})$$

and then expand  $g(x)$  in circular prolate functions:

$$g_\ell(x) = \sum_{n=0}^{\infty} a_n^\ell \Phi_{\ell,n}(x). \quad (\text{A7.6})$$

Then the integral equation becomes

$$\sigma_2 \sum_{n=0}^{\infty} a_n^\ell \Phi_{\ell,n}(x) = i^{\ell+1} 2t e^{-it\left(1 + \frac{1}{M^2}\right)x^2} \sum_{m=0}^{\infty} a_m^\ell d_m^\ell(x) \quad (\text{A7.7})$$

where

$$d_m^\ell(x) \equiv \int_0^1 dy y J_\ell(cx y) \Phi_{\ell,m}(y). \quad (\text{A7.8})$$

Using Eq(A7.1), Eq(A7.8) can be rewritten as

$$\mathcal{A}_m^l(x) = (-1)^m \frac{\sqrt{\gamma_{l,m}}}{c} \Phi_{l,m}(x) . \quad (\text{A7.9})$$

Then Eq(A7.7) becomes

$$\sigma_l \sum_{n=0}^{\infty} a_n^l \Phi_{l,n}(x) = i^{l+1} 2t e^{-it(1+\frac{1}{M^2})x^2} \sum_{m=0}^{\infty} a_m^l (-1)^m \frac{\sqrt{\gamma_{l,m}}}{c} \Phi_{l,m}(x) . \quad (\text{A7.10})$$

By multiplying by a circular prolate function of arbitrary index and integrating from 0 to 1, we obtain a matrix eigenvalue problem,

$$\sigma_l a_n^l = \sum_{m=0}^{\infty} B_{nm}^l a_m^l \quad (\text{A7.11})$$

where the matrix is

$$B_{nm}^l = i^{l+1} 2t (-1)^m \frac{\sqrt{\gamma_{l,m}}}{\gamma_{l,m}} \cdot \int_0^1 dx x e^{-it(1+\frac{1}{M^2})x^2} \Phi_{l,m}(x) \Phi_{l,n}(x) . \quad (\text{A7.12})$$

The derivation used here does not lead to a complex-symmetric matrix. Different expansion coefficients like those used in Appendix 2, Eq(A2.11), or Appendix 6, Eq(A6.5), would be needed in order to obtain a complex-symmetric matrix. Recall that the complex-symmetric matrix is necessary to retain the properties of the round trip integral equation.

This formulation is most applicable to unstable resonators. At present, a numerical code does not exist that solves this geometry, but the development of such a code would parallel the strip resonator code development discussed in Chapter II. The use of the circular prolate functions would have the same advantages that the linear prolate functions have, i.e., they should give the N-term best representation for the modes of the circular mirror resonator.

### Appendix B. Geometrical Optics Approximation to the Loaded Cavity Round Trip Integral Equation

In this appendix, the loaded cavity round trip integral equation is approximated using asymptotic methods. The equation we will approximate is Eq(3.26) which describes the loaded strip resonator. By letting the wavelength go to zero, a geometrical optics approximation to this equation will be obtained. We begin by reproducing Eq(3.26):

$$u_4(x, zL) = I_1 + I_2 + I_3 \quad (\text{A8.1})$$

where

$$I_1 = \sqrt{\frac{iF}{a_1^2}} \int_{-a_1}^{a_1} dy u_0(y, 0) e^{-i\pi \frac{F}{a_1^2} [g(x^2+y^2) - 2xy]} \quad (\text{A8.2})$$

$$I_2 = \frac{1}{2} \sqrt{\frac{i}{\lambda L}} \int_{-\infty}^{\infty} dy \int_0^L dz \frac{g_s(y, z) u_1(y, z)}{\sqrt{(L-z)L_e}} e^{-\frac{i\pi}{\lambda L} [g_s x^2 + \frac{L}{L-z} y^2 - \frac{L}{L_e} (\frac{x}{L} + \frac{y}{L-z})^2]} \quad (\text{A8.3})$$

and

$$I_3 = \frac{1}{2} \sqrt{\frac{i}{\lambda}} \int_{-\infty}^{\infty} dy \int_L^{2L} dz e^{-\frac{i\pi}{\lambda L} (g_s - 1)x^2} e^{-\frac{i\pi}{\lambda L} [\frac{L(x-y)^2}{2L-z}]} \frac{g_s(y, z) u_3(y, z)}{\sqrt{2L-z}} \quad (\text{A8.4})$$

where 
$$L_e = \frac{2g_s - 1}{L} + \frac{1}{L-z}$$

We restrict the approximation to the confocal resonator by using the following relations:

$$g_1 = \frac{M+1}{z} ; \quad g_2 = \frac{M+1}{2M} ; \quad g = \frac{M^2+1}{2M}$$

Then

$$L_c = \frac{ML + L - z}{ML(L-z)} \quad (A8.5)$$

and

$$\frac{L}{L_c} = \frac{ML^2(L-z)}{(M+1)L-z} \quad (A8.6)$$

The asymptotic approximation that is used is the method of stationary phase (MOSP), described in Appendix 5. Recall Eq(A5.2):

$$\int_a^b dy e^{-it_p(y)} q(y) \approx e^{-\frac{i\pi}{4}} q(y_0) e^{-it_p(y_0)} \sqrt{\frac{2\pi}{t_p''(y_0)}} \quad (A8.7)$$

We apply this equation to the term in Eq(A8.2), which is rewritten for the confocal resonator:

$$I_1 = \sqrt{\frac{iM}{\lambda L(M+1)}} \int_{-a_1}^{a_1} dy u_0(y,0) e^{-\frac{i\pi M}{\lambda L(M+1)} \left[ \left( \frac{M^2+1}{2M} \right) (x^2+y^2) - 2xy \right]} \quad (A8.8)$$

Now the field has a curvature on it due to the mirror. In order to accurately apply the MOSP, this curvature must be explicitly included in the exponential term. Thus

$$I_1(x,0) = Z_1^c(x,0) e^{-\frac{i\pi}{\lambda L} (g_1-1)x^2}$$

$$u_0(x,0) = u_0^c(x,0) e^{-\frac{i\pi}{\lambda L} \left( \frac{M-1}{2} \right) x^2} \quad (A8.9)$$

The superscript "c" denotes a collimated field. Then, after some straightforward algebra, the first term becomes

$$I_1^c(x,0) = \sqrt{\frac{iM}{\lambda L(M+1)}} e^{\frac{i\pi}{\lambda L} \left[ \left(\frac{M-1}{2}\right) - \frac{M^2+1}{2(M+1)} \right] x^2} \int_{-a_1}^{a_1} dy u_0^c(y,0) e^{-\frac{i\pi}{\lambda L} \left(\frac{M^2}{M+1}\right) y^2 - \frac{2My}{M+1}} \quad (A8.10)$$

Applying the method of stationary phase to the integral, we find

$$I_1^c(x,0) = \frac{1}{\sqrt{M}} u_0^c\left(\frac{x}{M}, 0\right) \quad (A8.11)$$

We now evaluate the second term. First we apply the confocal resonator constraints and transform the field to a collimated field. The result is

$$I_2^c = \frac{1}{2} \sqrt{\frac{i}{\lambda z}} \int_0^L dz \int_{-\infty}^{\infty} dy \frac{g_0(y,z) u_1(y,z)}{\sqrt{\frac{ML+L-z}{ML}}} \cdot e^{\frac{i\pi}{\lambda L} \left(\frac{M-1}{2}\right) x^2} e^{-\frac{i\pi}{\lambda L} \left[ \left(\frac{M+1}{2}\right) x^2 + \frac{L}{L-z} y^2 - \frac{ML^2(L-z)}{(M+1)L-z} \left(\frac{x}{L} + \frac{y}{L-z}\right)^2 \right]} \quad (A8.12)$$

Now the field  $u_1(x,z)$  contains an expanding spherical wave for the confocal resonator. This is modelled as

$$u_1(y,z) = u_1^c(y,z) e^{-\frac{i\pi y^2}{\lambda(f+z)}} = u_1^c(y,z) e^{-\frac{i\pi(M-1)y^2}{\lambda L[1+(M-1)z/L]}} \quad (A8.13)$$

where

$$f = \frac{L}{M-1} \quad , \quad (A8.14)$$

and

$$f + z = \frac{L + (M-1)z}{M-1} \quad (A8.15)$$

Using Eq(A8.13) and doing some algebra on the exponents, the  $y$  integral in Eq(A8.12) is rewritten as

$$d = \int_{-\infty}^{\infty} dy g_s(y, z) u_i^c(y, z) e^{-\frac{i\pi}{\lambda L} \left\{ \left[ \frac{M-1}{1+(M-1)\frac{z}{L}} + \frac{1}{M-1-\frac{z}{L}} \right] y^2 - \frac{2MLy}{(M-1)L-z} \right\}} \quad (A8.16)$$

We collect terms and rewrite Eq(A8.16) as

$$d = \int_{-\infty}^{\infty} dy g_s(y, z) u_i^c(y, z) e^{-\frac{i\pi}{\lambda L} [Ay^2 - Bxy]} \quad (A8.17)$$

where

$$A = \frac{M^2 L^2}{(Mz + L - z)(ML + L - z)}, \quad (A8.18)$$

and

$$B = \frac{2ML}{ML + L - z} \quad (A8.19)$$

We apply the MOSP on Eq(A8.17) and, after some lengthy algebra, obtain the final result for the second term:

$$I_2^c = \frac{1}{2} \int_0^L dz g_s \left( \frac{Mz + L - z}{ML} x, z \right) u_i^c \left( \frac{Mz + L - z}{ML} x, z \right) \sqrt{\frac{Mz + L - z}{ML}} \quad (A8.20)$$

The approximation of the third term is much simpler since the field  $u_3(x, z)$  is already collimated. We remove

### Vita

Mark Edward Rogers was born on 16 February 1954 in Milwaukee, Wisconsin. He graduated as valedictorian from Homestead High School in Mequon, Wisconsin in 1972 and attended the United States Air Force Academy, Colorado, from 1972 to 1976 where he graduated as a Distinguished Graduate and received a regular commission as a second lieutenant in the USAF. He majored in physics while at the USAF Academy. His first assignment was as an operations analyst at the Space and Missile Test Center where he worked on range support for future space programs and optical instrumentation analysis. In 1978, he entered the Master's Degree program in Engineering Physics, Laser/Optics, in residence at Wright-Patterson AFB, Ohio. His master's thesis was entitled "The Use of Complex Field Vectors in Diffraction Theory." He completed the program as a Distinguished Graduate and began a follow-on PhD program, also in Laser/Optics, but emphasizing the study of optical resonators for high energy lasers.

Captain Mark Rogers is married to the former Jan Maureen Warner of Brea, California and has three daughters, Jennifer, Julie and Gwendolyn.

Permanent Address : 10303 N. Greenview Dr  
Mequon, Wisconsin 53092

**END**

**FILMED**

**11-85**

**DTIC**